Application of Functional Metal-Organic Frameworks to Catalysis

Li, Jun

(Degree)
博士（学術）

(Date of Degree)
2015-03-25

(Date of Publication)
2017-03-25

(Resource Type)
doctoral thesis

(Report Number)
甲第6424号

(URL)
https://hdl.handle.net/20.500.14094/D1006424

博　士　論　文

Application of Functional Metal-Organic Frameworks to Catalysis

配位高分子の触媒反応への応用に関する研究

平成 27 年 1 月

神戸大学大学院工学研究科

李　君

博　士　論　文

Application of Functional Metal-Organic Frameworks to Catalysis

配位高分子の触媒反応への応用に関する研究

January, 2015

Department of Chemical Science and Engineering

Graduate School of Engineering

Kobe University

神戸大学大学院工学研究科

Jun LI

Acknowledgements

This dissertation is dedicated to all the people who have helped and supported me until now.

The studies described in the present doctoral dissertation have been carried out in the Cooperative Division (located at Kansai Center, National Institute of Advanced industrial Science and Technology (AIST)), Department of Chemical Science and Engineering, Graduate School of Engineering, Kobe University.

I would like to express my deepest gratitude to Professor Qiang Xu for his powerful guidance, inspiring ideas, constructive suggestions, valuable discussions, kind consideration, and for his carefully and critically reading of this dissertation.

I sincerely thank Professor Satoru Nishiyama and Professor Minoru Mizuhata for valuable supports and for critically reading of this dissertation.

I am deeply indebted to Dr. Qi-Long Zhu for his valuable discussion and valuable support.

I am grateful to Dr. Kengo Aranishi, Ms. Hitomi Fujii and all the other members in Professor Xu's group for their valuable discussions and valuable supports.

I am very thankful to Dr. Takeyuki Uchida, Dr. Hiroshi Shioyama, Dr. Naoko Fujiwara and all the other members in Kansai Center of AIST for valuable discussions and kind supports.

I thank for financial supports from AIST and Kobe University.

Finally, I appreciate my family for their constant supports and mental encouragements.

Jun LI

January 2015

Osaka, Japan

Abstract

This dissertation mainly contains two parts: one is the utilization of metal-organic framework (MOF) as a host matrice for immobilizing metal nanoparticles (MNPs) and the use of the fabricated MNP@MOF composites as catalysts for catalytic hydrogen generation from ammonia borane (AB), and the other is the utilization of MOF as a template/precursor for nanoporous carbon (NPC) material synthesis and the use of the resultant NPCs as supports of Pd electrocatalysts for methanol electrooxidation. Non-noble metal-based (AuCo) and non-noble bimetallic (CuCo) alloy nanoparticles were successfully encapsulated in the pores of MIL-101, a chromium-based MOF, which exhibit high catalytic activities for hydrolytic dehydrogenation of AB. Hierarchically porous carbon was synthesized by direct carbonization of assembled nanoparticles of zeolitic imidazolate framework (ZIF-8), which has been used as support for Pd electrocatalyst for methanol electrooxidation in alkaline media for the first time. The main research results of this dissertation are summarized as follows.

(i) Highly active AuCo alloy nanoparticles encapsulated in the pores of metal-organic frameworks for hydrolytic dehydrogenation of ammonia borane

Ultrafine AuCo alloy nanoparticles were successfully encapsulated in the pores of MIL-101 without aggregation on the external surfaces of the host framework by using the double solvents method combined with the overwhelming reduction approach, as demonstrated by transmission electron microscopic (TEM) and high-angle annular dark-field scanning TEM (HAADF-STEM) analyses. The ultrafine AuCo alloy NPs inside the mesoporous MIL-101 exhibit much higher catalytic activity for hydrolytic dehydrogenation of AB in comparison with their monometallic Au and Co counterparts. To the best of our knowledge, this obtained activity is the highest for supported Co and Co-based catalysts ever reported for hydrolytic dehydrogenation of aqueous AB.

(ii) Non-noble bimetallic CuCo nanoparticles encapsulated in the pores of metal-organic frameworks: synergetic catalysis in the hydrolysis of ammonia borane for hydrogen generation

Non-noble bimetallic CuCo alloy nanoparticles were successfully encapsulated in the pores of MIL-101 by using the double solvents method combined with the overwhelming reduction approach, which display remarkably enhanced catalytic activity for hydrolytic dehydrogenation of AB to generate a stoichiometric amount of hydrogen at room temperature for chemical hydrogen storage, which presents the first example of MOF-supported non-noble bimetallic catalysts for the hydrogen generation from hydrolysis of AB. The synergetic effect between copper and cobalt species plays an important role for the improved performance in the catalytic hydrolysis of AB.

(iii) Pd nanoparticles supported on hierarchically porous carbon derived from assembled nanoparticles of zeolitic imidazolate framework (ZIF-8) for methanol electrooxidation

We, for the first time, use the hierarchically porous carbons with both micro- and mesopores obtained from direct carbonization of assembled nanoparticles of ZIF-8 [$Zn(MeIM)_2$; MeIM = 2-methylimidazole] as support for Pd electrocatalysts for methanol electrooxidation in alkaline media. At the carbonization temperature of 1000 °C, the highest surface area (1105 m^2 g^{-1}) and the largest pore volume (0.95 cm^3 g^{-1}) of ZIF-8-derived carbon (ZC) are achieved. The Pd/ZC-1000 catalyst is the most active and electrochemically stable among the Pd catalysts supported on ZCs prepared at 800-1100 °C. Moreover, the catalytic activity of Pd/ZC-1000 is 5 times higher than that of Pd supported on the commercial carbon black Vulcan XC-72R at the same Pd loading. The ZC-1000 with unique physical properties and high electrochemical performance will be a promising catalyst support for the application of direct methanol fuel cell.

In summary, this dissertation focuses on the fabrication of a series of MOF-based materials, that is, the composites of metal nanoparticles with MOFs and MOF-derived carbons, and their applications as heterogeneous catalysts for hydrolytic dehydrogenation of ammonia borane and methanol electrooxidation.

Contents

Chapter 1

Introduction

Metal-organic frameworks (MOFs), also known as porous coordination polymers (PCPs) have been developed for around 20 years.[1] Starting from metal-organic coordination polymers developed by Robson et al.,[1-3] Yaghi and O'Keffee introduced the concept of the metal-organic frameworks,[4,5] which is an infinite network assembled by inorganic vertices/nodes (metal ions or clusters) and organic linkers/spacers (ligands). The two components are connected to each other by coordination bonds, together with other intermolecular interactions, to extend "infinitely" into one, two or three dimension networks with varieties of topologies (Fig. 1.1).[6] In order to well understand and describe topologies of MOF structures, Yaghi group firstly proposed the concepts of reticular chemistry and secondary building units and applied them with great success to design and description of highly porous and rigid MOF structures (Fig. 1.2).[7,8]

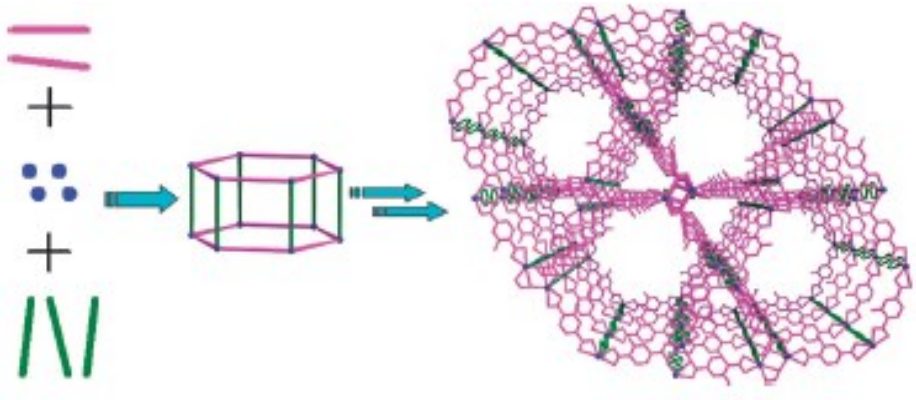

Fig. 1.1 A general scheme of MOF synthesis (from ref. 6).

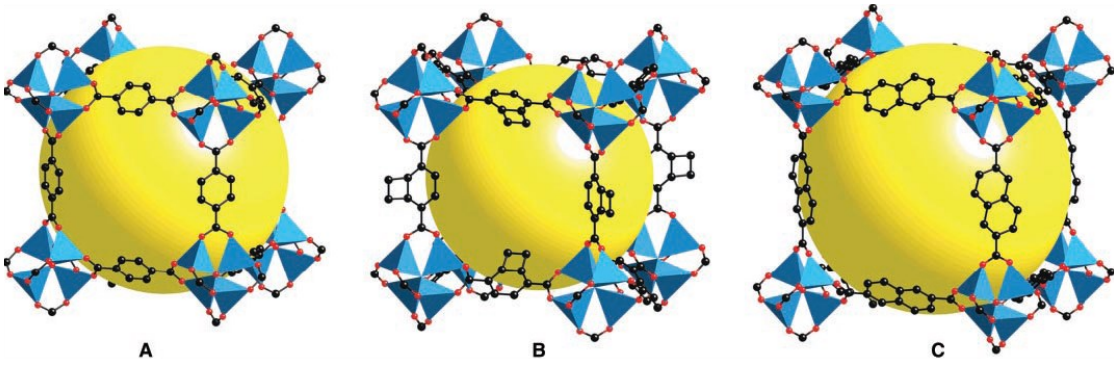

Fig. 1.2 A typical strategy for constructing MOF-5 (A), IRMOF-6 (B), and IRMOF-8 (C) by changing the links to increase the pore size using the same secondary building units (SBUs) (from ref. 8).

Emerging as a new class of porous crystalline materials, MOFs have shown high promising applications as functional physical or chemical materials.[9] A key structured feature in MOFs is their high porosity as well as large surface areas, which plays a crucial role in their functional properties, such as magnetism,[10] fluorescence,[11] thin films,[12] gas storage and separation,[13] catalysis,[14] sensing or recongnition,[15] proton conduction,[16] drug delivery,[17] and so on. In this context, we focus on the recent developments concerning the following two functional applications of MOFs: as supports/host matrices for metal nanoparticles (MNPs) and as templates/precursors for porous carbon material syntheses and applications.

1.1 MNP@MOF composites

Over the past years, MNPs have been broadly investigated due to their extremely small size and wide range of potential applications in industry,[18] information-storage,[19] biomedicine,[20] catalysis,[21] and so on. It is well known that MNPs have a much larger surface area to volume ratio than their bulk counterparts, which is the basis of their unique physicochemical properties, however, which results in the free MNPs having high surface energies and tending to aggregate.[22] To solve this contradiction, one of the efficient ways is utilization of porous materials, such as metal oxides, zeolites, mesoporous silica and activated carbons as supports for MNP immobilization, which allows the generation of specific surfactant-free active sites with the merits of controlling

particle nucleation and growth to a nanosize region in the confined void spaces and preventing particle aggregation.[23,24]

Given the similarity to zeolites, porous MOFs are a promising new class of matrice for hosting MNP catalysts due to their rationally designed framework structures with desired pore sizes, shapes and functionalities, and moderate electronic interaction between the MNPs and organic linkers, which is significantly important for controlling the limited growth of MNPs in their confined cavities and producing highly reactive MNPs for the final applications in heterogonous catalysis.[25] During the last five years, a number of examples for a range of metals like Cu, Ni, Ru, Pd, Au, Ag and Pt supported on MOFs have been reported.[26]

1.1.1 Preparation methods

In general, embedding MNPs in a MOF matrix is achieved by the impregnation of metal precursors followed by reduction or decomposition of the precursors to metal atoms. It has been reported that gas-, solid- and solution-phase loading methods have been well carried out with different metal precursors by different research groups.[26-38]

Gas-phase infiltration method or metal organic chemical vapor deposition (MOCVD) initially developed by Fischer and co-workers, in which volatile metal organic compounds, such as $(\eta^3\text{-}C_3H_5)Pd(\eta^5\text{-}C_5H_5)$, $(\eta^5\text{-}C_5H_5)Cu(PMe_3)$ and $(CH_3)Au(PMe_3)$, known as precursors were incorporated into the pores or channels of MOFs at an appropriate temperature depending on the vapor pressure of the metal precursor under a static vacuum by a sublimation process and subsequently reduced by hydrogen reduction or simple thermal decomposition. Since 2005, by using the highly porous MOF-5, MOF-177, ZIF-8 and ZIF-90, a series of MNP@MOF nanocomposites have been prepared. [27-29]

In contrast to gas-phase method, solid grinding is a very facile yet surprisingly effective method for depositing MNPs onto MOFs and was developed in 2008 by Haruta and co-workers.[30] So far, this method was especially developed for supporting nanosized gold clusters on different MOF (MIL-53(Al), MOF-5, HKUST-1, and so on) matrice.[30-32] In this method, desolvated MOF and volatile $Me_2Au(acac)$ (acac = acetylacetonate) were

grinded in a mortar for several minutes at room temperature without using any solvent. Like the MOCVD strategy, the chosen precursors are volatile and may be absorbed from the gas phase infiltrates into the cavities of MOFs during the grinding process, leading to well-distributed deposition of the precursor. Then the adsorbed species were treated with H_2 gas to form small MNPs.

Generally speaking, the gas- and solid-phase infiltration methods have the merit of allowing particularly high loading amount of metal precursors. However, on other hand, such high loading degree sometimes leads to agglomeration of MNPs as well as partial/full degradation of the frameworks. In addition, the limited number of volatile metal organic compounds restricts the applications of these metholds.

The simplest and most-used approach for the introduction of MNPs into MOFs is utilization of an aqueous solution of simple metal salts for liquid impregnation. Once the desolvated porous MOFs are soaked into the metal precursor solution, the precursors are infiltrated into the pores of MOFs by capillary force. After removal of solvents from the host framework, composites are reduced by a reducing agent, typically H_2 gas or $NaBH_4$, to obtain fine MNPs deposited in MOFs.

Zlotea *et al.* reported the deposition of Pd NPs with a mean size of 2.5 nm into a MOF, MIL-100(Al) ($[Cr_3F(H_2O)_3O(btc)_2]$, btc=1,3,5-benzenetricarboxylate) by using the tetrachloropalladinic acid solution for liquid impregnation.[33] In order to facilitate the infiltration of the metal precursors, it is necessary to improve the interactions between the metal precursors and MOF supports. Férey and coworkers have successfully encapsulated effective noble metals into the pores of MIL-101 by pre-grafting an amine, ethylenediamine (ED), on its coordinatively unsaturated Cr (III) center. After neutralization of the surface amine groups with an aqueous HCl solution, ionic reactions between the positively charged surface ammonium groups and anionic noble metal salts ($[PdCl_4]^{2-}$, $[PtCl_6]^{2-}$ and $[AuCl_4]^-$) took place by anionic exchange of the chloride anions (Fig. 1.3).[34] In a same way, we successfully immobilized bimetallic Au-Pd NPs in the ED-grafted MIL-101.[35]

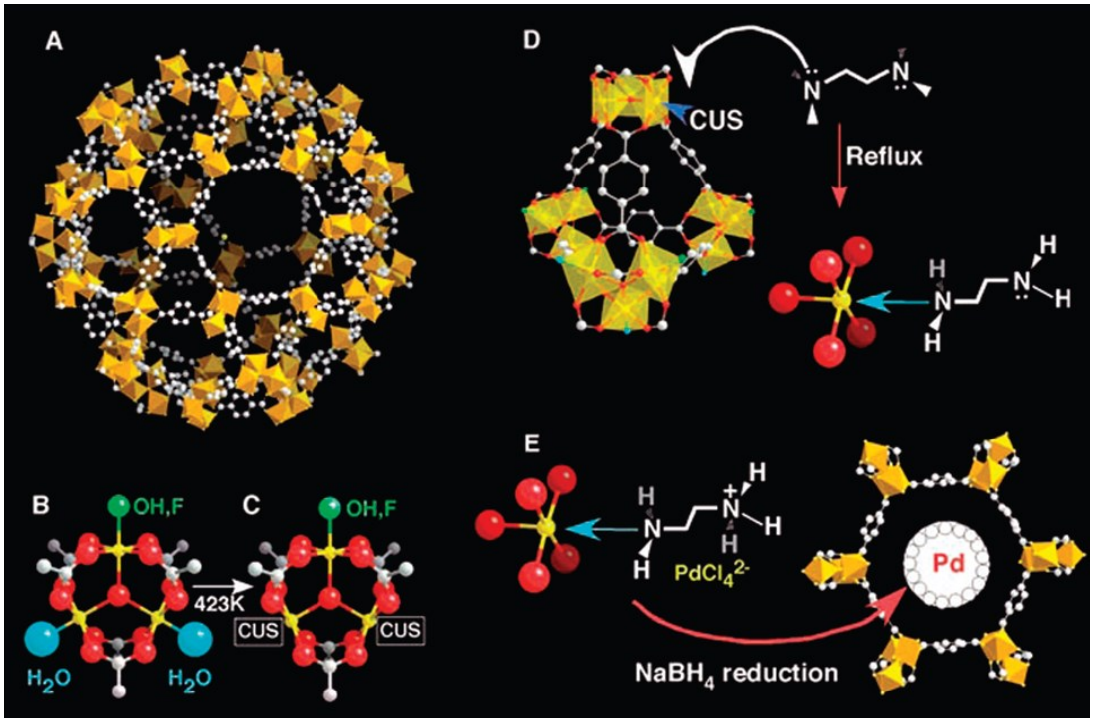

Fig. 1.3 Site-selective functionalization of MIL-101 with unsaturated metal sites: (a) perspective view of the mesoporous cage of MIL-101 with hexagonal windows; (b,c) evolution of coordinatively unsaturated sites from chromium trimers in mesoporous cages of MIL-101 after vacuum treatment; (d) surface functionalization of the dehydrated MIL-101 through selective grafting of amine molecules onto coordinatively unsaturated sites; (e) selective encapsulation of noble metals in the amine-grafted MIL-101 (from ref. 34).

Compared to this simple liquid impregnation method, the incipient wetness method, one of the impregnation techniques, can feasibly control the loading amount of metals in the MOFs. In this method, a defined concentration of metal precursor solution with a volume equal to the total pore volume of the MOF support is impregnated, and the pores are filled by the capillary force. With this method, the introduction of 1 wt% of Pd into MOF-5 was performed by using a solution of $[Pd(acac)_2]$ (acac = acetylacetonate) in $CHCl_3$ and subsequent thermal hydrogenolysis of the formed intermediate material.[36]

One of the inevitable drawbacks of this method is the metal precursor compounds and products can actually deposit on the external surface of MOFs to form the MNPs with aggregation on the external surface of MOFs. Therefore, the development of a general and facile method to incorporate fine MNPs within the pores of MOFs remains a real challenge. Recently, we have developed a double solvents method (DSM), which can

introduce noble metal precursors into the pores of MOF without deposition on the external surface of the framework. After the treatment with hydrogen at a relatively low temperature, ultrafine MNPs within the pores of the MOFs can been obtained (Fig. 1.4).[37-39] By using this method, ultrafine Pt, Pd, Au and Rh NPs were also successfully encapsulated into the pores of MIL-101 without aggregation on the external surface of the framework.[37,39]

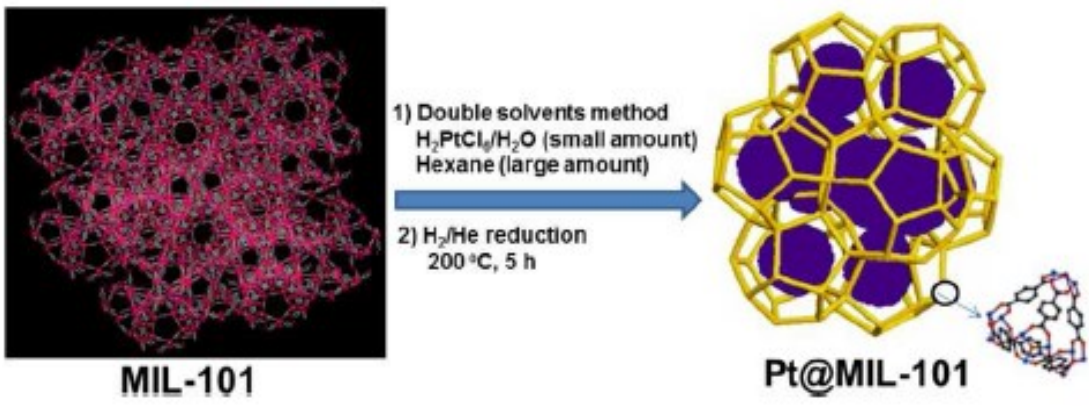

Fig. 1.4 Schematic representation of synthesis of Pt nanoparticles inside the MIL-101 matrix using double solvents method (from ref. 37).

In contrast to noble metals, non-noble metals need more drastic reduction conditions such as higher temperature for molecular H_2 reduction, however, the limited thermal stabilities of MOFs do not allow this. To solve this problem, a strategy combined DSM and the liquid-phase concentration-controlled reduction (CCR) approach has been developed by us to immobilize non-noble metal based alloy NPs to MIL-101 with size and location control.[38] This effective strategy represents a promising step toward the applications of porous MOFs as hosts for ultrafine non-noble metal NPs .

1.1.2 Use as catalysts for catalytic hydrogen generation from ammonia borane

Hydrogen has been considered as one of the best alternative energy carriers to satisfy the increasing demand for a sustainable and clean energy supply.[40] The development of effective hydrogen-storage materials is imperative but challenging for

establishing a hydrogen-based energy system.[41] Recently, liquid-phase chemical storage materials with high hydrogen contents, such as aqueous ammonia borane (NH_3BH_3, AB), hydrazine (N_2H_4) and formic acid (HCOOH, FA) with the hydrogen capacities of 19.6, 12.6 and 4.4 wt%, respectively, have become the promising candidates for chemical hydrogen storage applications.[42-47] Among them, AB has attracted much attention, which is not only due to its highest gravimetric hydrogen capacity (19.6 wt.%) and low molecular weight, but also because it is nontoxic, stable, environmental benign, and can safely handled under ambient conditions.[47]

So far various catalyst systems have been tested in the hydrolysis of AB and rapid hydrogen generation has been achieved by using noble metals such as Pt, Ru and Rh.[37,47c,48] In 2012, we reported ultrafine Pt NPs (1.8 ± 0.2 nm) successfully encapsulated into the pores of MIL-101 without aggregation on the external surfaces of framework by using a double solvents method combined with H_2 reduction.[37] The 2 wt% Pt@MIL-101 catalyst exhibited extremely high catalytic activity for hydrolysis of AB, over which the dehydrogenation reaction can be completed (H_2/AB = 3.0) within only 2.5 min at room temperature (($Pt/AB = 0.0029$ in molar ratio), giving a rate of ~1.0×10^4 $L_{H2}\, mol_{Pt}^{-1}\, min^{-1}$.

Although the noble metal catalysts show very high activities for hydrolysis of AB, the limited resource restricts their practical applications. Therefore, the development of cost-effective non-noble MNPs catalysts is very important. In 2012, we successfully prepared highly dispersed Ni NPs immobilized by ZIF-8, via chemical vapor deposition (CVD) and chemical liquid deposition (CLD) approaches followed by H_2 reduction, which presents the first example of MOF-supported metal catalysts for the hydrogen generation from hydrolysis of AB.[49] For the CVD-Ni/ZIF-8 with a small particle size of 2.7 ± 0.7 nm, the hydrolytic dehydrogenation of AB can be completed (H_2/AB = 3.0) in 13 min (Ni/AB = 0.019), giving a turnover frequency (TOF) value of 14.2 $mol_{H2}\, mol_{Ni}^{-1}\, min^{-1}$.

To improve the catalytic activity of non-noble metals, bimetallic alloy NPs as a class of very important nanomaterials have gained particular attention, which show a great enhancement in their specific physical and chemical properties owing to a synergetic effect.[44,50] The addition of a second metal is an important method for tailoring the

electronic and geometric structures of NPs to enhance their catalytic activities. Very recently, we reported successful preparation and excellent catalytic activity of the ultrafine non-noble metal-based AuNi alloy NPs (1.8 ± 0.2 nm) encapsulated in the pores of MIL-101.[38] The AuNi@MIL-101 with the Au/Ni atomic ratio of 7:93 is the most active owing to the synergistic effect between Au and Ni, giving a turnover frequency (TOF) value of 66.2 mol_{H2} mol_{cat}^{-1} min^{-1}, which is even higher than that of most Pt-, Rh and Ru-related catalysts.[48] The highly efficient catalyst brings light to new opportunities in applications of MOF-supported non-noble metal-based alloy NPs catalysts in the catalytic hydrolysis of aqueous AB.

1.2 Porous MOFs as templates/precursors for porous carbon syntheses

Due to the high surface area, large pore volume and good electrochemical properties, porous carbons have been one of the most important and conventional porous materials, especially in the applications of gaseous or liquid adsorptions, catalyst supports, and electrode materials for electric double layer capacitors (EDLCs) and fuel cells.[51-53] Porous carbons can be prepared via several methods, including carbonization of polymeric aerogels, activation (physical or chemical) of carbon materials, nanocasting with hard-templates and so on.[51-54] Recently, MOFs as a novel class of porous materials have gained particular attention due to high porosity, large surface area and chemical tunability. The various pore sizes and high thermal stability of MOFs make them feasible as templates/precursors to prepare porous carbons through thermal conversion.[55-66]

Generally, MOF-derived carbon materials can be fabricated by means of two methods.[56] One is employing MOFs as sacrificial templates and some organic compounds such as furfuryl alcohol (FA) or glucose impregnated in the pores of MOF as the carbon precursors. During the carbonization process, MOF frameworks are decomposed, while the precursors lead to the formation of the nanoporous carbon (NPC). Another approach is direct carbonization of MOFs which contain abundant organic species that could be used as carbon precursors.

In 2008, we, for the first time, obtained the NPC material by employing the MOF-5 as a sacrificial template and FA as the carbon source (Fig 1.5).[57] The NPC obtained at

1000 °C exhibits a high BET surface area (2872 m^2 g^{-1}) and the H_2 uptake as high as 2.6 wt% at 77 K and 1 bar, twice of that of MOF-5. Moreover, the as-synthesized NPC material exhibits excellent electrochemical performance as an electrode material for electrical double-layer capacitors (EDLCs) (electrolyte, 1.0 M H_2SO_4). It showed a capacitance of 204 F g^{-1} at a sweep rate of 5 mV s^{-1}, which is higher than those of carbon material synthesized from SBA-15. Even at a current density of 50 mA g^{-1}, the specific capacitance was maintained as high as 258 F g^{-1}.

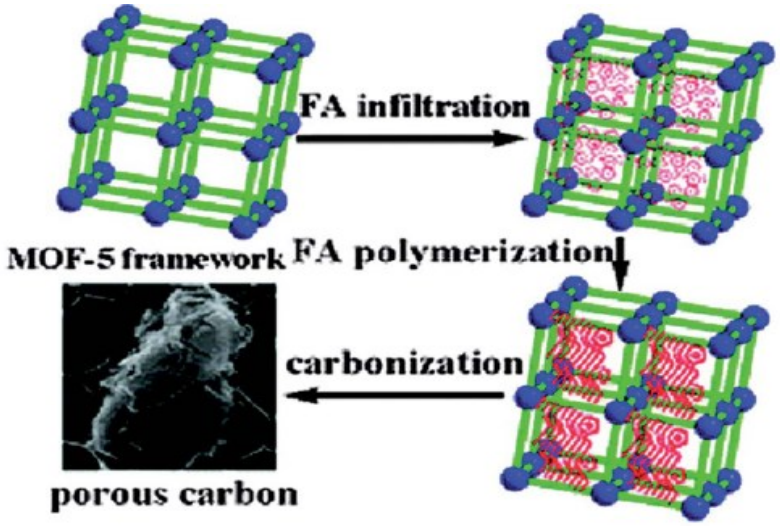

Fig. 1.5 A diagrammatic view of preparation of nanoporous carbon using MOF as a template (from ref. 57).

In 2010, Hu *et al.* prepared porous carbon materials through the direct carbonization of MOF-5 without or with additional carbon sources such as phenolic resin, carbon tetrachloride and ethylenediamine, and then the porous carbon materials were activated by KOH to further tune the pore structures.[58] The results of the electrochemical capacitance behavior of these carbon materials show that only the carbon materials obtained from MOF-5 with carbon tetrachloride and ethylenediamine after KOH activation exhibited the best capacitances of 271 and 156 F g^{-1} (at a current density of 250 mA g^{-1}) as well as the highest energy densities on a gravimetric basis of 9.4 and 31.2 W h kg^{-1} in aqueous and organic electrolytes, respectively.

As another types of templates and/or precursors, highly porous ZIF-8 and its

derivative IRZIF (isoreticular zeolitic imidazolate framework) series were extensively investigated in the last two years.[59,60] In 2011, we firstly utilized ZIF-8 as both a precursor and a template and furfuryl alcohol (FA) as the second carbon source to prepare the nanoporous carbon materials.[59] By changing the calcination temperature from 800 to 1000 °C, the surface areas of the resultant carbon materials increased from 2169 to 3405 m^2 g^{-1}. As shown in Fig. 1.6, both carbon-based electrodes displayed regular rectangular shapes without any redox peaks and the specific capacitance is about 200 F g^{-1} for both carbons at a current density of 50 mA g^{-1}. Recently, a series of carbon materials (C-68, C-69 and C-70) having increasing BET surface areas were prepared using IRZIFs (ZIF-68, ZIF-69 and ZIF-70) as templates and FA as the carbon source under thermolysis temperature at 1000 °C by Banerjee and co-workers.[60]

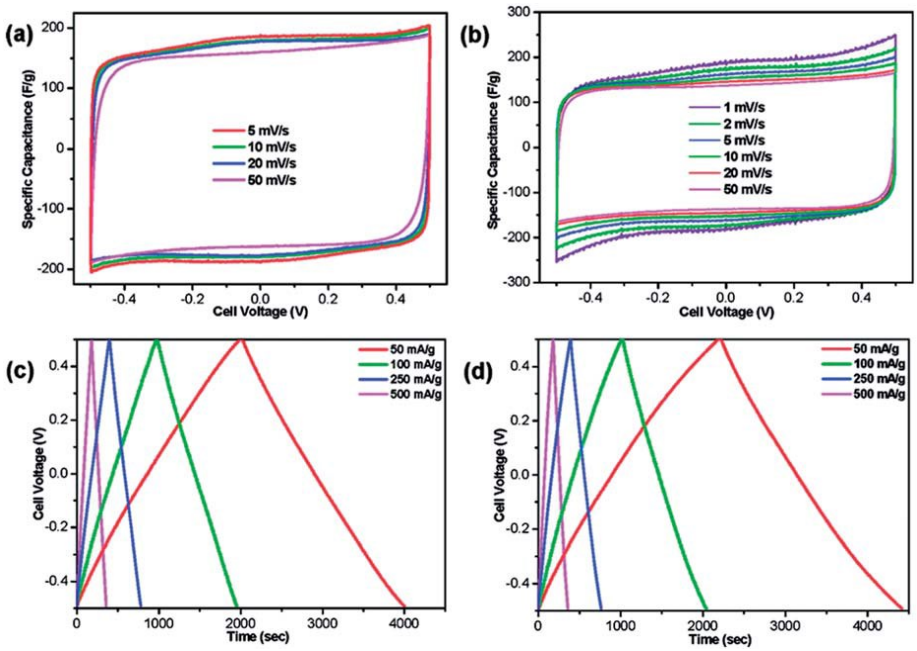

Fig. 1.6 (a and b) CVs at different scan rates and (c and d) galvanostatic charge–discharge profiles at different current densities for (a and c) C800 and (b and d) C1000 samples (from ref. 59).

Chen and co-workers reported the nitrogen-doped porous carbon nanopolyhedra (N-PCNPs) with high surface area (2221 m^2 g^{-1}) and narrow pore-size distributions (3.7 nm) through direct carbonization of lab-synthesized ZIF-8 nanopolyhedra without additional carbon sources.[61] Such N-PCNPs were employed to electrochemically detect

ascorbic acid (AA), dopamine (DA) and uric acid (UA) by modifying a glassy carbon electrode. The N-PCNPs/GC electrode exhibited the well-resolved oxidation peaks toward electrocatalytic oxidation of AA, DA and UA with the peak potentials at 40 mV, 188 mV and 312 mV, respectively, and could sense three analytes simultaneously with the detection limits (*S*/*N* = 3) of 740 nM, 11 nM and 21 nM for AA, DA and UA, respectively.

Al-based MOF is also an excellent candidate as a template/precursor to construct the nanostructured carbon material. In 2011, Yamauchi and co-workers used $\{Al(OH)(1,4\text{-NDC})\cdot 2H_2O\}_n$ (ref. 62) as a template/precursor with FA as an additional carbon source, which were carbonized at 1000 °C in an inert atmosphere to produce microporous carbon fibers.[63] The BET surface area of the carbon fibers increased from 178 to 513 $m^2\ g^{-1}$ upon increasing the loading amount of FA.

Besides these well-known MOFs, other MOFs such as $[Ni_3(btc)_2\cdot 12H_2O]$ (btc = benzene-1,3,5-tricarboxylato)[64] and Fe-based MOFs[65] have also been explored as templates and/or precursors to prepare carbon materials.

Although there are more and more reports on MOF-derived porous carbons, the applications of them are still in infancy. More excellent results in this area could be expected in near future.

1.3 Scope of the present work

This work emphasizes on exploiting the applications of MOFs as host matrices for immobilizing metal nanoparticles (MNPs) and as templates/precursors for nanoporous carbon (NPC) syntheses and the applications to catalysis.

(i) Highly active AuCo alloy nanoparticles encapsulated in the pores of metal-organic frameworks for hydrolytic dehydrogenation of ammonia borane

Ultrafine AuCo alloy nanoparticles were successfully encapsulated in the pores of MIL-101 without aggregation on the external surfaces of the host framework by using the double solvents method combined with the overwhelming reduction approach, as demonstrated by transmission electron microscopic (TEM) and high-angle annular dark-field scanning TEM (HAADF-STEM) analyses. The ultrafine AuCo alloy NPs

inside the mesoporous MIL-101 exhibit much higher catalytic activity for hydrolytic dehydrogenation of AB in comparison with their monometallic Au and Co counterparts. To the best of our knowledge, this obtained activity is the highest for supported Co and Co-based catalysts ever reported for hydrolytic dehydrogenation of aqueous AB. This part was described in chapter 2.

(ii) Non-noble bimetallic CuCo nanoparticles encapsulated in the pores of metal-organic frameworks: synergetic catalysis in the hydrolysis of ammonia borane for hydrogen generation

Non-noble bimetallic CuCo alloy nanoparticles were successfully encapsulated in the pores of MIL-101 by using the double solvents method combined with the overwhelming reduction approach, which display remarkably enhanced catalytic activity for hydrolytic dehydrogenation of AB to generate a stoichiometric amount of hydrogen at room temperature for chemical hydrogen storage, which presents the first example of MOF-supported non-noble bimetallic catalysts for the hydrogen generation from hydrolysis of AB. The synergetic effect between copper and cobalt species plays an important role for the improved performance in the catalytic hydrolysis of AB. This part was described in chapter 3.

(iii) Pd nanoparticles supported on hierarchically porous carbon derived from assembled nanoparticles of zeolitic imidazolate framework (ZIF-8) for methanol electrooxidation

To the best of our knowledge, the NPCs derived from MOFs as catalyst supports are rare reported in the studies of the fuel cells.[66] We, for the first time, use the hierarchically porous carbons with both micro- and mesopores obtained from direct carbonization of assembled nanoparticles of ZIF-8 [$Zn(MeIM)_2$; MeIM = 2-methylimidazole] as support for Pd electrocatalysts for methanol electrooxidation in alkaline media. At the carbonization temperature of 1000 °C, the highest surface area (1105 $m^2\ g^{-1}$) and the largest pore volume (0.95 $cm^3\ g^{-1}$) of ZIF-8-derived carbon (ZC) are achieved. The Pd/ZC-1000 catalyst is the most active and electrochemically among the Pd catalysts supported on ZCs prepared at 800-1100 °C. Moreover, the catalytic activity of Pd/ZC-1000 is 5 times higher than that of Pd supported on the commercial carbon black

Vulcan XC-72R at the same Pd loading. This part was described in chapter 4.

In summary, this dissertation focuses on the fabrication of a series of MOF-based materials, that is, the composites of metal nanoparticles with MOFs and MOF-derived carbons, and their applications as heterogeneous catalysts for hydrolytic dehydrogenation of ammonia borane and methanol electrooxidation.

References

1 B. F. Hoskins and R. Robson, *J. Am. Chem. Soc.,* **1989**, *111*, 5962.

2 B. F. Hoskins and R. Robson, *J. Am. Chem. Soc.,* **1990**, *112*, 1546.

3 R. S. Stuart and R. Robson, *Angew. Chem., Int. Ed.,* **1998**, *37*, 1461.

4 H. Li, M. Eddaoudi, M. O' Keeffe and O.M. Yaghi, *Nature,* **1999**, *402*, 276.

5 O. M. Yaghi, M. O' Keeffe, N. W. Ockwing, H. K. Chae, M. Eddaoudi and J. Kim, *Nature,* **2003**, *423*, 705.

6 H.-L. Jiang and Q. Xu, *Chem. Commun*., **2011**, *47*, 3351.

7 M. Eddaoudi, J. Kim, N. Rosi, D. Vodak, J. Wachter, M. O' Keeffe and O. M. Yaghi, *Science,* **2002**, *295*, 469.

8 N. L. Rosi, J. Eckert, M. Eddaoudi, D. T. Vodak, J. Kim, M. O'Keeffe and O. M. Yaghi, *Science,* **2003**, *300*, 1127.

9 (a) S. Kitagawa, R. Kitaura and S. Noro, Angew. *Chem., Int. Ed.,* **2004**, *43*, 2334; (b) G. Férey, *Chem. Soc. Rev.,* **2008**, *37*, 191; (c) J. R. Long and O. M. Yaghi, *Chem. Soc. Rev.,* **2009**, *38*, 1213.

10 (a) R.-Q. Zhong, R.-Q. Zou, M. Du, T. Yamada, G. Maruta, S. Takeda and Q. Xu, *Dalton Trans.,* **2008**, 2346; (b) M. Kurmoo, *Chem. Soc. Rev.,* **2009**, *38*, 1353; (c) L. Hou, W.-X. Zhang, J.-P. Zhang, W. Xue, Y.-B. Zhang and X.-M. Chen, *Chem. Commun.,* **2010**, *46*, 6311.

11 (a) R.-Q. Zou, Y. Yamada and Q. Xu, *Microporous Mesoporous Mater.,* **2006**, *91*, 233; (b) R.-Q. Zou, R.-Q. Zhong, L. Jiang, Y. Yamada, N. Kuriyama and Q. Xu, *Chem.–Asian J.,* **2006**, *1*, 536; (c) M. D. Allendorf, C. A. Bauer, R. K. Bhakta and R. J. T. Houk, *Chem. Soc. Rev.,* **2009**, *38*, 1330.

12 (a) D. Zacher, O. Shekhah, C. Wöll and R. A. Fischer, *Chem. Soc. Rev.,* **2009**, *38*,

1418; (b) R. Makiura, S. Motoyama, Y. Umemura, H. Yamanaka, O. Sakata and H. Kitagawa, *Nat. Mater.,* **2010**, *9*, 565.

13 (a) J. Y. Lee, L. Pan, S. P. Kelly, J. Jagiello, T. J. Emge and J. Li, *Adv. Mater.,* **2005**, *17*, 2703; (b) R.-Q. Zou, L. Jiang, H. Senoh, N. Takeichi and Q. Xu, *Chem. Commun.,* **2005**, 3526; (c) J.-R. Li, R. J. Kuppler and H.-C. Zhou, *Chem. Soc. Rev.,* **2009**, *38*, 1477; (d) H.-L. Jiang, N. Tsumori and Q. Xu, *Inorg. Chem.,* **2010**, *49*, 10001.

14 (a) M. Fujita, Y. J. Kwon, S. Washizu and K. Ogura, *J. Am. Chem. Soc.,* **1994**, *116*, 1151; (b) J. S. Seo, D. Whang, H. Lee, S. I. Jun, J. Oh, Y. J. Jeon and K. Kim, *Nature,* **2000**, *404*, 982; (c) L. Ma, C. Abney and W. Lin, *Chem. Soc. Rev.,* **2009**, *38*, 1248; (d) J. Y. Lee, O. K. Farha, J. Roberts, K. A. Scheidt, S. T. Nguyen and J. T. Hupp, *Chem. Soc. Rev.,* **2009**, *38*, 1450; (e) A. Corma, H. García and F. X. Llabrési Xamena, *Chem. Rev.,* **2010**, *110*, 4606.

15 (a) H.-L. Jiang, Y. Tastu, Z.-H. Lu and Q. Xu, *J. Am. Chem. Soc.,* **2010**, *132*, 5586; (b) B. Chen, S. Xiang and G. Qian, *Acc. Chem. Res.,* **2010**, *43*, 1115.

16 (a) M. Sadakiyo, T. Yamada and H. Kitagawa, *J. Am. Chem. Soc.,* **2009**, *131*, 9906; (b) S. Bureekaew, S. Horike, M. Higuchi, M. Mizuno, T. Kawamura, D. Tanaka, N. Yanai and S. Kitagawa, *Nat. Mater.,* **2009**, *8*, 831; (c) J. A. Hurd, R. Vaidhyanathan, V. Thangadurai, C. I. Ratcliffe, I. L. Moudrakovski and G. K. H. Shimizu, *Nat. Chem.,* **2009**, *1*, 705.

17 (a) P. Horcajada, C. Serre, M. Vallet-Regí , M. Sebban, F. Taulelle and G. Férey, *Angew. Chem., Int. Ed.,* **2006**, *45*, 5974; (b) K. M. L. Taylor-Pashow, J. D. Rocca, Z. Xie, S. Tran and W. Lin, *J. Am. Chem. Soc.,* **2009**, *131*, 14261.

18 (a) M. A. El-Sayed, *Acc. Chem. Res.,* **2001**, *34*, 257; (b) S. Chen and Y. Yang, *J. Am. Chem. Soc.,* **2002**, *124*, 5280.

19 (a) L. A. Peyser, A. E. Vinson, A. P. Bartko and R. M. Dickson, *Science,* **2001**, *291*, 103; (b) H. M. Chen, R.-S. Liu, H. Li and H. C. Zeng, *Angew. Chem.* **2006**, *118*, 2779; *Angew. Chem. Int. Ed.*, **2006**, *45*, 2713.

20 (a) R. Elghanian, J. J. Storhoff, R. C. Mucic, R. L. Letsinger and C. A. Mirkin, *Science,* **1997**, *277*, 1078; (b) T. A. Taton, C. A. Mirkin and R. L. Letsinger, *Science,* **2000**, *289*, 1757; (c) Y. W. Charles Cao, R. Jin and C. A. Mirkin, *Science,* **2002**, *297*, 1536; (d) S.-J. Park, T. A. Taton and C. A. Mirkin, *Science,* **2002**, *295*, 1503; (e) N. L.

Rosi, D. A. Giljohann, C. S. Thaxton, A. K. R. Lytton-Jean, M. S. Han and C. A. Mirkin, *Science,* **2006**, *312*, 1027.

21 (a) L. N. Lewis, *Chem. Rev.,* **1993**, *93*, 2693; (b) M. Valden, X. Lai and D. W. Goodman, *Science,* **1998**, *281*, 1647; (c) S.-W. Kim, M. Kim, W. Y. Lee and T. Hyeon, *J. Am. Chem. Soc.,* **2002**, *124*, 7642; (d) M. S. Chen and D. W. Goodman, *Science,* **2004**, *306*, 252; (e) S. Zhou, K. Mcllwrath, G. Jackson and B. Eichhorn, *J. Am. Chem. Soc.,* **2006**, *128*, 1780; (f) H. M. Chen, C. K. Chen, Y.-C. Chang, C.-W. Tsai, R.-S. Liu, S.-F. Hu, W.-S. Chang and K.-H. Chen, *Angew. Chem.,* **2010**, *122*, 6102.

22 Optical Properties of Metal Clusters (Eds.: U. Kreibig, M. Vollmer), Springer, New York, 1995.

23 R. J. White, R. Luque, V. L. Budarin, J. H. Clark and D. J. Macquarrie, *Chem. Soc. Rev.,* **2009**, *38*, 481.

24 M. Meilikhov, K. Yusenko, D. Esken, S. Turner, G. Van Tendeloo and R. A. Fischer, *Eur. J. Inorg. Chem.,* **2010**, 3701.

25 (a) M. Meilikhov, K. Yusenko, D. Esken, S. Turner, G. Van Tendeloo and R. A. Fischer, *Eur. J. Inorg. Chem.,* **2010**, 3701; (b) A. Dhakshinamoorthy and H. Garcia, *Chem. Soc. Rev.,* **2012**, *41*, 5262; (c) H. R. Moon, D.-W. Limb and M. P. Suh, *Chem. Soc. Rev.,* **2013**, *42*, 1807.

26 (a) Q.-L. Zhu and Q. Xu, *Chem. Soc. Rev.*, **2014**, *43*, 5468; (b) A. Aijaz and Q. Xu, *J. Phys. Chem. Lett.*, **2014**, *5*, 1400.

27 S. Hermes, M.-K. Schröter, R. Schmid, L. Khodeir, M. Muhler, A. Tissler, R. W. Fischer and R. A. Fischer, *Angew. Chem., Int. Ed.,* **2005**, *44*, 6237.

28 M. Muller, O. I. Lebedev and R. A. Fischer, *J. Mater. Chem.,* **2008**, *18*, 5274.

29 D. Esken, S. Turner, O. I. Lebedev, G. Van Tendeloo and R. A. Fischer, *Chem. Mater.,* **2010**, *22*, 6393.

30 T. Ishida, M. Nagaoka, T. Akita and M. Haruta, *Chem.–Eur., J.,* **2008**, *14*, 8456.

31 T. Ishida, N. Kawakita, T. Akita and M. Haruta, in *Stud. Surf. Sci. Catal.*, ed. M. D. E. M. Gaigneaux, S. Hermans, P. A. Jacobs, J. A. Martens and P. Ruiz, Elsevier, 2010, vol. 175, pp. 839–842.

32 T. Ishida, N. Kawakita, T. Akita and M. Haruta, *Gold Bull.,* **2009**, *42*, 267.

33 C. Zlotea, R. Campesi, F. Cuevas, E. Leroy, P. Dibandjo, C. Volkringer, T. Loiseau, G. Férey and M. Latroche, *J. Am. Chem. Soc.,* **2010**, *132*, 2991.

34 Y. K. Hwang, D. Y. Hong, J. S. Chang, S. H. Jhung, Y. K. Seo, J. Kim, A. Vimont, M. Daturi, C. Serre and G. Férey, *Angew. Chem., Int. Ed.,* **2008**, *47*, 4144.

35 X. Gu, Z.-H. Lu, H.-L. Jiang, T. Akita and Q. Xu, *J. Am. Chem. Soc.,* **2011**, *133*, 11822.

36 M. Sabo, A. Henschel, H. Frode, E. Klemm and S. Kaskel, *J. Mater. Chem.,* **2007**, *17*, 3827.

37 A. Aijaz, A. Karkamkar, Y. J. Choi, N. Tsumori, E. Rönnebro, T. Autrey, H. Shioyama and Q. Xu, *J. Am. Chem. Soc.,* **2012**, *134*, 13926.

38 Q.-L. Zhu, J. Li and Q. Xu, *J. Am. Chem. Soc.,* **2013**, *135*, 10210.

39 (a) M. Yadav, A. Aijaz and Q. Xu, *Funct. Mater. Lett.,* **2012**, *05*, 1250039; (b) M. Yadav and Q. Xu, *Chem. Commun.,* **2013**, *49*, 3327.

40 (a) P. P. Edwards, V. L. Kuznetsov, W. I. David and N. P. Brandon, *Energy Policy*, **2008**, *36*, 4356; (b) C. W. Hamilton, R. T. Baker, A. Staubitzc and I. Manners, *Chem. Soc. Rev.,* **2009**, *38*, 279; (c) H. M. Chen, C. K. Chen, R.-S. Liu, L. Zhang, J. Zhang and D. P. Wilkinson, *Chem. Soc. Rev.,* **2012**, *41,* 5654.

41 (a) L. Schlapbach and A. Züttel, *Nature,* **2001**, *414*, 353; (b) R. J. Keaton, J. M. Blacquiere and R. T. Baker, *J. Am. Chem. Soc.,* **2007**, *129*, 1844; (c) Z.-G. Huang and T. Autrey, *Energy Environ. Sci.,* **2012**, *5*, 9257.

42 H.-L. Jiang, S. K. Singh, J.-M. Yan, X.-B. Zhang and Q. Xu, *ChemSusChem,* **2010**, *3*, 541.

43 M. Yadav and Q. Xu, *Energy Environ. Sci.,* **2012**, *5*, 9698.

44 A. K. Singh and Q. Xu, *ChemCatChem,* **2013**, *5*, 652.

45 A. F. Dalebrook, W. Gan, M. Grasemann, S. Moret and G. Laurenczy, *Chem. Commun.,* **2013**, *49*, 8735.

46 Q.-L. Zhu, N. Tsumori and Q. Xu, *Chem. Sci.,* **2014**, *5*, 195.

47 (a) A. Gutowska, L. Li, Y. Shin, C.-M. Wang, X.-S. Li, J. C. Linehan, R. S. Smith, B. D. Kay, B. Schmid, W. Shaw, M. Gutowski and T. Autrey, *Angew. Chem., Int. Ed.,* **2005**, *44*, 3578; (b) M. Chandra and Q. Xu, *J. Power Sources,* **2006**, *156*, 190; (c) Q. Xu and M. J. Chandra, *J. Alloys Compd.,* **2007**, *446*, 729; (d) S.-K. Kim, W.-S. Han,

T.-J. Kim, T.-Y. Kim, S. W. Nam, M. Mitoraj, L. Piekos, A. Michalak, S. J. Hwang and S. O. Kang, *J. Am. Chem. Soc.,* **2010**, *132*, 9954; (e) U. Sanyal, U. B. Demirci, B. R. Jagirdar and P. Miele, *ChemSusChem,* **2011**, *4*, 1731; (f) S.-K. Kim, T.-J. Kim, T.-Y. Kim, G. Lee, J. T. Park, S. W. Nam and S. O. Kang, *Chem. Commun.,* **2012**, *48*, 2021.

48 H.-L. Jiang and Q. Xu, *Catal. Today,* **2011**, *170*, 56.

49 P.-Z. Li, K. Aranishi and Q. Xu, *Chem. Commun.,* **2012**, *48*, 3173.

50 H.-L. Jiang and Q. Xu, *J. Mater. Chem.,* **2011**, *21*, 13705.

51 (a) S. Flandrois and B. Simon, *Carbon,* **1999**, *37*, 165; (b) T. Kyotani, *Carbon,* **2000**, *38*, 269; (c) Z. Hu, M. P. Srinivasan and Y. Ni, *Adv. Mater.,* **2000**, *12*, 62; (d) R. Ryoo, S. H. Joo, M. Kruk and M. Jaroniec, *Adv. Mater.,* **2001**, *13*, 677; (e) J. Lee, J. Kim and T. Hyeon, *Adv. Mater.,* **2006**, *18*, 2073; (f) R. T. Yang and Y. Wang, *J. Am. Chem. Soc.,* **2009**, *131*, 4224; (g) B. Hu, K. Wang, L. Wu, S.-H. Yu, M. Antonietti and M.-M. Titirici, *Adv. Mater.,* **2010**, *22*, 813.

52 (a) C. G. Wu and T. Bein, *Science,* **1994**, *266*, 1013; (b) S. H. Joo, S. J. Choi, I. Oh, J. Kwak, Z. Liu, O. Terasaki and R. Ryoo, *Nature,* **2001**, *412*, 169; (c) S. Tanaka, N. Nishiyama, Y. Egashira and K. Ueyama, *Chem. Commun.,* **2005**, 2125; (d) C. Liang, Z. Li and S. Dai, *Angew. Chem., Int. Ed.,* **2008**, *47*, 3696.

53 (a) S. A. Johnson, E. S. Brigham, P. J. Ollivier and T. E. Mallouk, *Chem. Mater.,* **1997**, *9*, 2448; (b) K. Matsuoka, Y. Yamagishi, T. Yamazaki, N. Setoyama, A. Tomita and T. Kyotani, *Carbon,* **2005**, *43*, 855; (c) P.-X. Hou, T. Yamazakia, H. Orikasa and T. Kyotani, *Carbon,* **2005**, *43*, 2624; (d) Z. Yang, Y. Xia and R. Mokaya, *J. Am. Chem. Soc.,* **2007**, *129*, 1673; (e) Y. Xia, G. S. Walker, D. M. Grant and R. Mokaya, *J. Am. Chem. Soc.,* **2009**, *131*, 16493; (f) H. Itoi, H. Nishihara, T. Kogure and T. Kyotani, *J. Am. Chem. Soc.,* **2011**, *133*, 1165.

54 (a) T. Horikawa, J. Hayashi and K. Muroyama, *Carbon,* **2004**, *42*, 1625; (b) T. Matsuoka, H. Hatori, M. Kodama, J. Yamashita and N. Miyajima, *Carbon,* **2004**, *42*, 2329.

55 S. L. Li and Q. Xu, *Energy Environ. Sci.,* **2013**, *6*, 1656.

56 J.-K. Sun and Q. Xu, *Energy Environ. Sci*., **2014**, *7*, 2071.

57 B. Liu, H. Shioyama, T. Akita and Q. Xu, *J. Am. Chem. Soc.,* **2008**, *130*, 5390.

58 J. Hu, H. Wang, Q. Gao and H. Guo, *Carbon,* **2010**, *48*, 3599.

59 H. L. Jiang, B. Liu, Y. Q. Lan, K. Kuratani, T. Akita, H. Shioyama, F. Zong and Q. Xu, *J. Am. Chem. Soc.,* **2011**, *133*, 11854.

60 P. Pachfule, B. P. Biswal and R. Banerjee, *Chem.–Eur. J*., **2012**, *18*, 11399.

61 P. B. Gai, H. Zhang, Y. S. Zhang, W. Liu, G. B. Zhu, X. H. Zhang and J. H. Chen, *J. Mater. Chem. B,* **2013**, *1*, 2742.

62 A. Comotti, S. Bracco, P. Sozzani, S. Horike, R. Matsuda, J. X. Chen, M. Takata, Y. Kubota and S. Kitagawa, *J. Am. Chem. Soc.,* **2008**, *130*, 13664.

63 L. Radhakrishnan, J. Reboul, S. Furukawa, P. Srinivasu, S. Kitagawa and Y. Yamauchi, *Chem. Mater.,* **2011**, *23*, 1225.

64 L. Y. Chen, J. F. Bai, C. Z. Wang, Y. Pan, M. Scheer and X. Z. You, *Chem. Commun.,* **2008**, 1581.

65 (a) H. K. Youn, J. Kim and W. S. Ahn, *Mater. Lett.,* **2011**, *65*, 3055; (b) P. P. Su, L. Jiang, J. Zhao, J. W. Yan, C. Li and Q. H. Yang, *Chem. Commun.,* **2012**, *48*, 8769.

66 (a) F. Afsahi, H. V.-Thang, S. Mikhailenko and S. Kaliaguine, *J. Power Sources*, **2013**, *239*, 415; (b) J. Liu, H. Wang, C. Wu, Q.-L. Zhao, X.-Y. Wang and L.-H. Yi, *Int. J. Hydrogen Energ.*, **2014**, *39*, 6729.

Chapter 2

Highly active AuCo alloy nanoparticles encapsulated in the pores of metal-organic frameworks for hydrolytic dehydrogenation of ammonia borane

Ultrafine AuCo alloy nanoparticles were successfully encapsulated in the pores of MIL-101 without aggregation on the external surfaces of the host framework by using the double solvents method combined with the overwhelming reduction approach, as demonstrated by transmission electron microscopic (TEM) and high-angle annular dark-field scanning TEM (HAADF-STEM) analyses. The ultrafine AuCo alloy NPs inside the mesoporous MIL-101 exhibit much higher catalytic activity for hydrolytic dehydrogenation of AB in comparison with their monometallic Au and Co counterparts. To the best of our knowledge, this obtained activity is the highest for supported Co and Co-based catalysts ever reported for hydrolytic dehydrogenation of aqueous AB.

2.1 Introduction

The search for safe and efficient hydrogen storage materials remains one of the most difficult challenges for the transformation to a hydrogen-powered society as a long-term solution to the current energy problems.[1] Ammonia borane (NH_3BH_3, AB) has a hydrogen capacity as high as 19.6 wt%, exceeding that of gasoline and making it an attractive candidate for chemical hydrogen storage applications.[2] So far various catalyst systems have been tested for hydrogen generation from the hydrolysis of AB,[3] among which platinum based catalysts show the highest activities,[3d] while the limited resource of platinum restricts their practical applications. Therefore, the development of efficient and economical catalysts and further improvement of the kinetic properties by controlling the particle size of acquired non-noble metal or non-noble metal-based catalysts are very important.[4]

Due to large surface area, high porosity and chemical tunability, metal-organic frameworks (MOFs) have emerged as a new class of very promising functional porous

materials,[5] especially in the applications of gas storage and separation, sensing, optics, and drug delivery.[6] By serving as unique host matrices, the MOFs could be applied for heterogeneous catalysis by encapsulating metal nanoparticles (MNPs) within the frameworks.[7] Loading of MNPs inside the porous matrices of MOFs is of current interest. General synthetic methods to embed MNPs in a MOF matrix entail the impregnation of metal precursors with several approaches, for example metal organic chemical vapor deposition, solid grinding, and conventional solution infiltration, followed by reduction of the metal precursors to metal atoms.[7,8] However, with these methods, it seems difficult to completely avoid the precursor compounds and product aggregation on the external surface of MOFs. Therefore, the development of a general and facile method to incorporate fine metal nanoparticles within the pores of MOFs remains a real challenge. Currently, we have developed a double solvents method (DSM) which introduced noble metal precursors into the pores of MOF without MNP aggregation on the external surface of the framework after the precursors were treated by the hydrogen reduction at a relatively low temperature.[3d] However, the hydrogen reduction method is not suited for non-noble metal precursors because of contradictions between the high reduction temperatures of non-noble metals and the limited thermal stabilities of MOFs. To solve this problem, very recently, we exploited an overwhelming reduction (OWR) approach in solution at room temperature, which can encapsulate the metal NPs, especially the non-noble metal-based NPs, within the pores of MOFs with the sufficient reduction of the metal precursors.[9]

In this work, the ultrafine AuCo alloy NPs were successfully encapsulated in the pores of MOF without aggregation on the external surfaces of the host framework by using the DSM in combination with the OWR approach, which exhibit remarkably enhanced catalytic activity for hydrolytic dehydrogenation of AB in comparison with their monometallic Au and Co counterparts.

2.2 Experimental section

2.2.1 Materials and general methods

Chromic nitrate nonahydrate ($Cr(NO_3)_3 \cdot 9H_2O$, Sigma-Aldrich, 99%), hydrogen

tetrachloroaurate (III) tetrahydrate ($HAuCl_4 \cdot 4H_2O$, Wako Pure Chemical Industries, Ltd., >99%), cobalt (II) chloride hexahydrate ($CoCl_2 \cdot 6H_2O$, Wako Pure Chemical Industries, Ltd., >99%), ammonium fluoride (NH_4F, Kishida Chem. Co., >97%), sodium borohydride ($NaBH_4$, Aldrich, 99%), aqueous hydrofluoric acid (HF, Kishida Chemical Co. Ltd., 46%), ammonia borane (NH_3BH_3, JSC Aviabor, >97%), terephthalic acid ($HOOCC_6H_4COOH$, Tri Chemical Laboratories Inc., 99%), anhydrous n-hexane (Sigma-Aldrich) and ethanol (C_2H_5OH, Kishida Chem. Co., >99.8%) were used as received. All reagents were commercial and used without further purification. De-ionized water with the specific resistance of 18.2 MΩ·cm was obtained by reversed osmosis followed by ion-exchange and filtration (RFD 250NB, Toyo Seisakusho Kaisha, Ltd., Japan). The surface area measurements were performed with N_2 adsorption/desorption isotherms at liquid nitrogen temperature (77 K) after dehydration under vacuum at 150 °C for 12 h using automatic volumetric adsorption equipment (Belsorp-max). The pore volume was calculated by a single point method at P/P_0=0.99. Powder X-ray diffraction (PXRD) measurements were carried out on a Rigaku RINT-2000 X-ray diffractometer with Cu Kα source (40 kV, 40 mA). Transmission electron microscope (TEM, TECNAI G^2 F20) equipped with energy dispersed X-ray detector (EDX) was applied for the detailed microstructure and composition information for the prepared samples. X-ray photoelectron spectroscopic (XPS) measurements were performed on a Shimadzu ESCA-3400 X-ray photoelectron spectrometer using an Mg Kα source (10 kV, 10 mA). The Ar sputtering experiments were carried out under the conditions of background vacuum of 3.2×10^{-6} Pa, sputtering acceleration voltage of 2 kV and sputtering current of 10 mA.

2.2.2 Synthesis of MIL-101

MIL-101 was synthesized according the reported procedure.[10] Terephthalic acid (1.661 g, 10.0 mmol), $Cr(NO_3)_3 \cdot 9H_2O$ (4.002 g, 10.0 mmol), aqueous HF (0.5 mL, 46 wt%) and de-ionized water (70 mL) were mixed in a 100 mL Teflon-liner autoclave and heated at 220 °C for 8 h. After cooling, the resulting green powder of MIL-101 with formula $Cr_3F(H_2O)_2O[(O_2C)C_6H_4(CO_2)]_3 \cdot nH_2O$ ($n \approx 25$) were filtered off using two glass

filters with pore sizes between 40 and 100 μm to remove the unreacted crystals of terephthalic acid, and subsequently centrifuged and further purified by solvothermal treatment in ethanol at 80 °C for 24 h. In order to eliminate the terephthalic acid inside the pores of MIL-101, the resulting green solid was soaked in NH_4F (1.0 M) solution at 70 °C for 24 h and immediately filtered, washed with hot water several times, and finally dried overnight at 150 °C under vacuum for further use.

2.2.3 Preparation of Au@MIL-101, Co@MIL-101 and AuCo@MIL-101

The double solvents method was used in this work to encapsulate Au^{3+} and/or Co^{2+} precursors.[3d] Typically, 100 mg of green MIL-101 powder with a pore volume of 1.72 $cm^3\ g^{-1}$ as determined by N_2 sorption isotherm activated by heating at 150 °C for 12 h under dynamic vacuum was suspended in 20 mL of dry n-hexane as hydrophobic solvent and the green suspension was sonicated for 15 min until it became homogeneous. After stirring for 2 h, 0.15 mL of aqueous $HAuCl_4 \cdot 4H_2O$ and/or $CoCl_2 \cdot 6H_2O$ solution with desired concentrations as the hydrophilic solvent was added dropwise over a period of 15 min with constant vigorous stirring, and then the resulting solution was continuously stirred for 2 h. After filtration, the green powder was dried in air at room temperature. These synthesized samples were further dried overnight at 150 °C under vacuum. The molar ratio of $Au^{3+}/(Au^{3+}+Co^{2+})$ were varied with several values (0, 0.015, 0.03, 0.06, 0.075, 0.09, 0.125, 0.25 and 1.00), while the molar contents of $(Au^{3+}+Co^{2+})$ added to 100 mg MIL-101 matrix were kept to be 0.034 mmol. After dehydration of the $Au^{3+}Co^{2+}$@MIL-101 with different molar ratios of Au^{3+} to Co^{2+}, an overwhelming reduction approach[9] was carried out by using 3.5 mL freshly prepared 0.6 M aqueous $NaBH_4$ solution while vigorous shaking (220 rpm), resulting in the generation of catalysts as a dark green suspension. Finally, the synthesized samples were collected by centrifuging, and used for the catalytic reactions.

2.2.4 Catalytic hydrolysis of ammonia borane

The hydrolysis of ammonia borane (NH_3BH_3, AB) can be briefly expressed as the

formula: $NH_3BH_3 + 4H_2O \rightarrow NH_4^+ + B(OH)_4^- + 3H_2$. Reaction apparatus for measuring the hydrogen evolution from the aqueous AB solution is the same as previously reported.[2b] Typically, a mixture of catalyst (50 mg) and distilled water (4.8 mL) was placed in a two-necked round-bottomed flask (30 mL), which was placed in a water bath at room temperature under ambient atmosphere. In order to measure the volume of hydrogen, a gas burette filled with water was connected to the reaction flask. When aqueous AB solution (1 mmol in 200 μL water) was injected into the mixture using a syringe, the reaction started. The volume of the evolved hydrogen gas was monitored by recording the displacement of water in the gas burette and the reaction was completed when there was no more gas generation. Moreover, corresponding to 50 mg catalysts, the molar ratios of (Au+Co)/AB were theoretically fixed at 0.017 for all the catalytic reactions.

After the hydrogen generation reaction was completed, another aliquot of AB (1.0 mmol in 200 μL water) was added into the reaction system and the released gas was monitored by the gas burette. After the reaction, the as-synthesized AuCo@MIL-101 was separated from the reaction solution by centrifugation and dried under vacuum at room temperature. The obtained sample after hydrolysis of AB was used for PXRD and TEM analyses.

2.3 Results and discussion

2.3.1 Preparation

MIL-101, a chromium-based MOF with themolecular formula $Cr_3F(H_2O)_2O[(O_2C)C_6H_4(CO_2)]_3 \cdot nH_2O$ (where n is ~25), was chosen as a host matrix for this study to encapsulate metallic particles not only because of its higher stability than most of MOFs in water or high temperature, but also its large cavity sizes (2.9 to 3.4 nm) and window sizes (1.2 to 1.4 nm), large surface area, and hybrid pore surface, which may facilitate the encapsulation of MNPs and the adsorption of catalytic substrate AB and reductant $NaBH_4$ into the pores.[10] The double solvents method (DSM) was used in this work for avoiding the deposition of the precursors on the outer surface of MIL-101.[3d] In this method, the aqueous precursor solution as a hydrophilic solvent with a volume set

equal to or less than the pore volume of the adsorbent can be absorbed within the hydrophilic adsorbent pores of MIL-101, which was suspended in a large amount of n-hexane. Since the inner surface area of MIL-101 is much larger than the outer surface area, the small amount of aqueous precursor solution can readily go inside the hydrophilic pores, and the deposition of metal precursors on the outer surface can be minimized. After drying the metal precursor/MOF composite, the overwhelming reduction (OWR) approach was used to reduce the precursors.[9] In this approach, a pore-volume amount of $NaBH_4$ solution with a high concentration (0.6 M) incorporated into the pores by capillary force can reduce the metal precursors deposited in the pores of MIL-101 completely, and the aggregation of MNPs on the external surfaces of MOF will be avoided.

2.3.2 Characterization

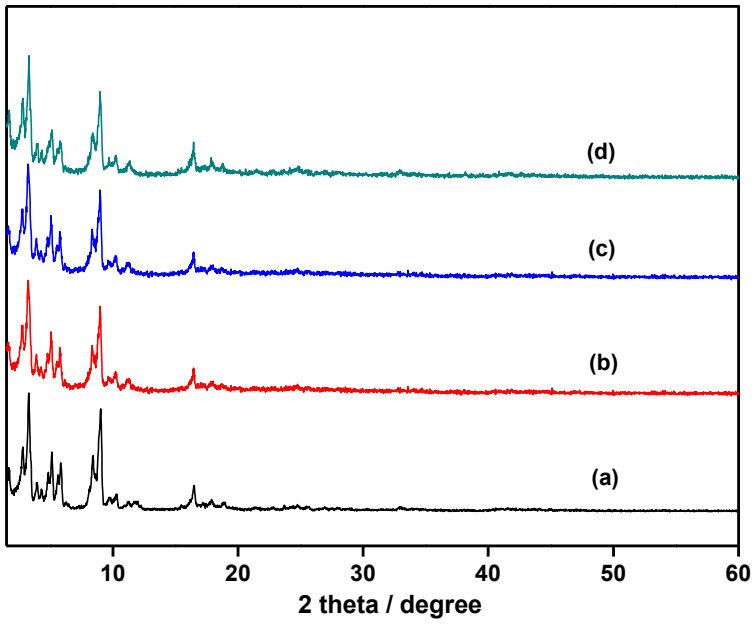

Fig. 2.1 Powder XRD patterns of (a) as-synthesized MIL-101, (b) AuCo@MIL-101 (Au/Co = 6:94), (c) Co@MIL-101 and (d) Au@MIL-101.

The powder X-ray diffraction (PXRD) patterns of all the prepared samples exhibited

that the main diffractions were well consistent with those of pristine MIL-101 reported by Férey *et al.*,[10] suggesting that the framework of MIL-101 was maintained well in the whole process of catalyst preparation (Fig. 2.1). In addition, no diffractions were detected for MNPs in M@MIL-101, suggesting the formation of very small MNPs.

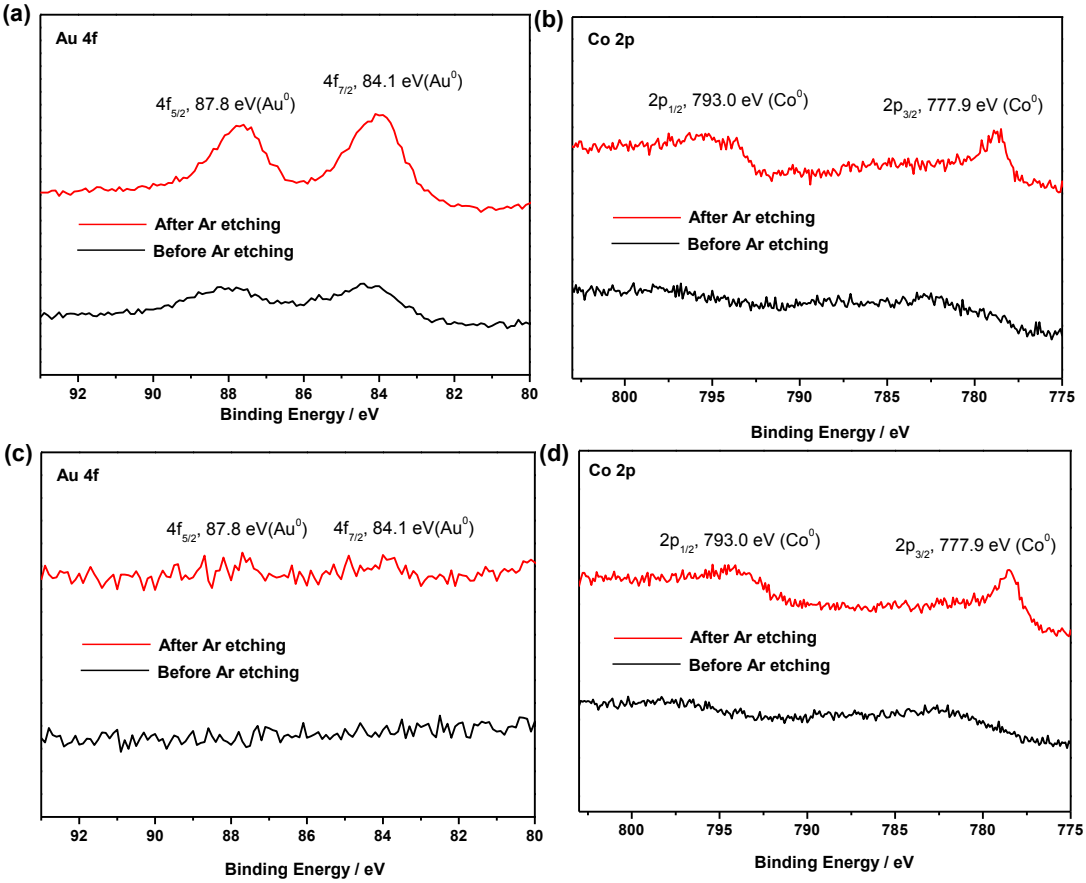

Fig. 2.2 XPS spectra for (a) Au@MIL-101, (b) Co@MIL-101 and (c, d) AuCo@MIL-101 (Au/Co = 6:94) before and after Ar etching for 60 min (Au $4f_{7/2}$ and $4f_{5/2}$ peaks, and Co $2p_{3/2}$ and $2p_{1/2}$ peaks).

X-Ray photoelectron spectroscopy (XPS) with Ar etching was applied to Au@MIL-101, Co@MIL-101 and AuCo@MIL-101 at the Au 4f and Co 2p levels. After Ar etching for 60 min, well-defined peaks corresponding to both metallic Au and Co species can be detected, indicating that both elements are in their zero-valent states. The observed Co $2p_{3/2}$ and Co $2p_{1/2}$ binding energies at 777.9 and 793.0 eV correspond to Co^0, and the Au $4f_{7/2}$ and Au $4f_{5/2}$ binding energies at 84.1 and 87.8 eV correspond to Au^0.

However, before Ar sputtering, peaks were observed for Co@MIL-101 and AuCo@MIL-101 with binding energies at 781.2 and 795.8 eV corresponding to Co $2p_{3/2}$ and Co $2p_{1/2}$, respectively, of CoO formed during the exposure of samples to air, which were readily removed by Ar etching. The metallic Au and Co peak intensities changed synchronously during the Ar etching in AuCo@MIL-101, indicating the homogeneity of the AuCo alloy particles (Fig. 2.2). The intensities of Au 4f peaks were weak (Fig. 2.2c) due to the low Au content of AuCo@MIL-101 (Au/(Au + Co) = 0.06 (molar ratio)).

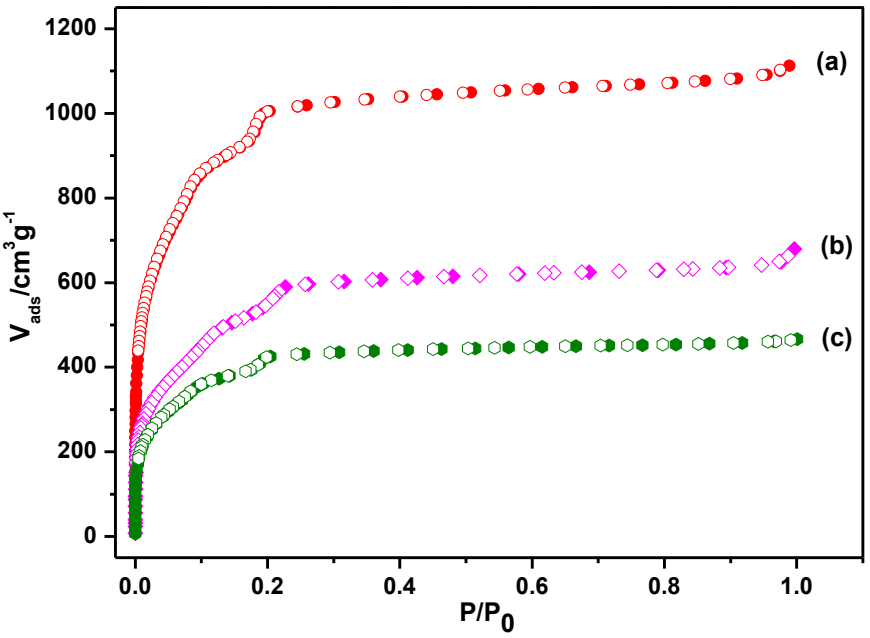

Fig. 2.3 N_2 sorption isotherms of (a) as-synthesized MIL-101, (b) AuCo@MIL-101 (Au/Co = 6:94) and (c) $Au^{3+}Co^{2+}$@MIL-101 at 77 K. The BET surface areas of the three samples are 3452, 1930 and 1455 m^2/g, respectively. Filled and open symbols represent adsorption and desorption branches, respectively.

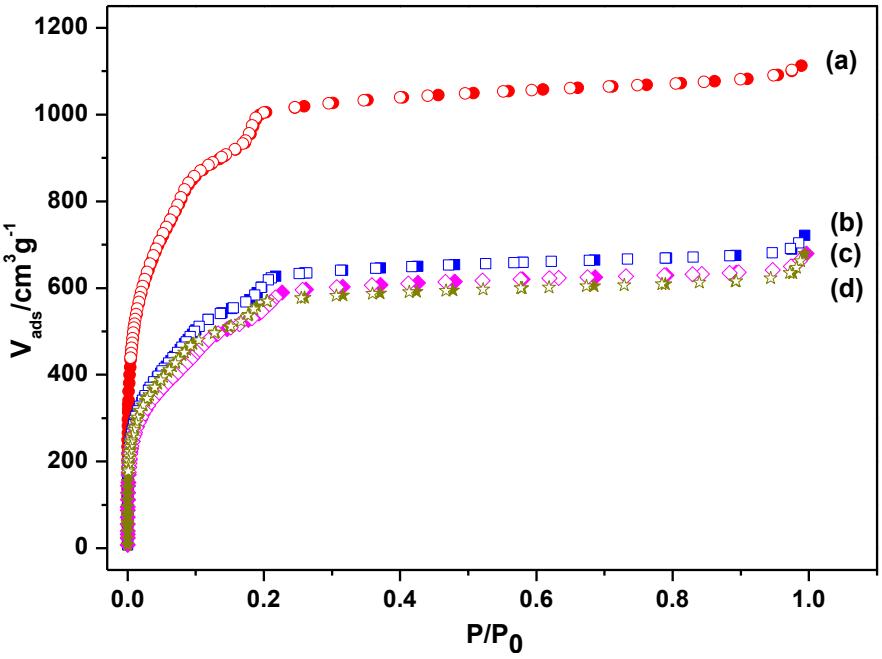

Fig. 2.4 N_2 sorption isotherms of (a) MIL-101, (b) Co@MIL-101, (c) AuCo@MIL-101 (Au/Co = 6 : 94) and (d) Au@MIL-101. Filled and open symbols represent adsorption and desorption branches, respectively.

The surface area decreased obviously after $HAuCl_4$ and/or $CoCl_2$ loading, while the reduction of Au^{3+} and Co^{2+} by $NaBH_4$ solution resulted in increase of surface area (Fig. 2.3). The BET surface areas of MIL-101, Co@MIL-101, Au@MIL-101 AuCo@MIL-101 and $Au^{3+}Co^{2+}$@MIL-101 are 3452, 2080, 1920, 1930 and 1455 $m^2\ g^{-1}$, respectively. Appreciable decreases in N_2 sorption compared with pristine MIL-101 were observed for all the samples (Fig. 2.4), indicating that MNPs were highly dispersed in the framework of MIL-101.

The uniformity of the AuCo alloy NPs in the MIL-101 framework was displayed by the TEM, high-angle annular dark-field scanning TEM (HAADF-STEM) and energy-dispersive X-ray spectroscopy (EDX) analyses (Fig. 2.5 and 2.6). Both TEM and HAADF-STEM images exhibited that the average sizes of the AuCo alloy NPs were 1.8 ± 0.2 nm (Fig. 2.7), which are small enough to be encapsulated in the two mesoporous cavities of MIL-101, and no big particle aggregation occurred, which is in good agreement with PXRD observations, providing evidence that the highly dispersed AuCo alloy NPs have been effectively encapsulated into the pores of MIL-101 with small sizes.

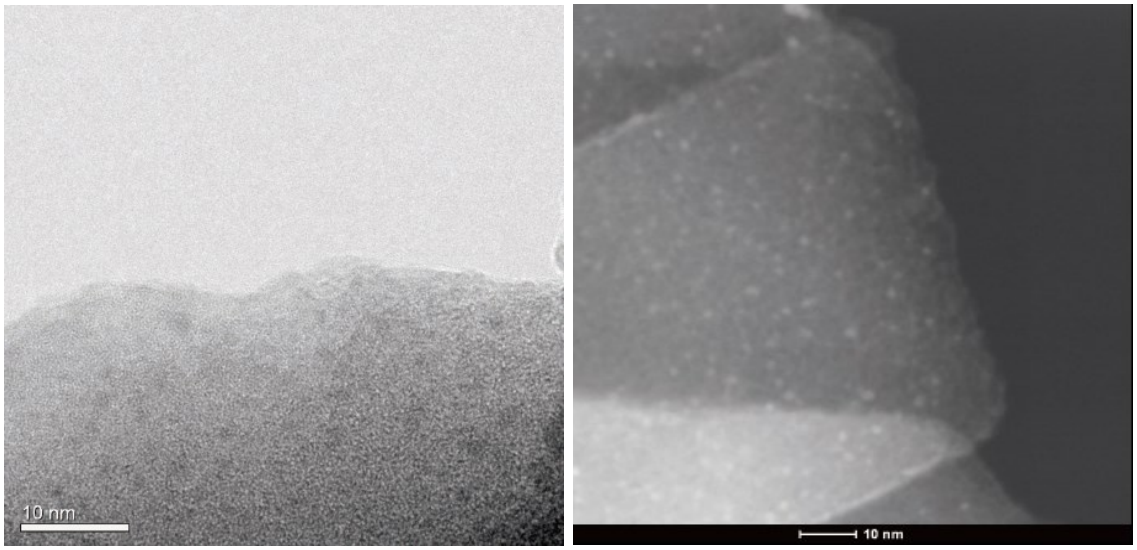

Fig. 2.5 TEM and HAADF-STEM images of AuCo@MIL-101 (Au/Co = 6:94).

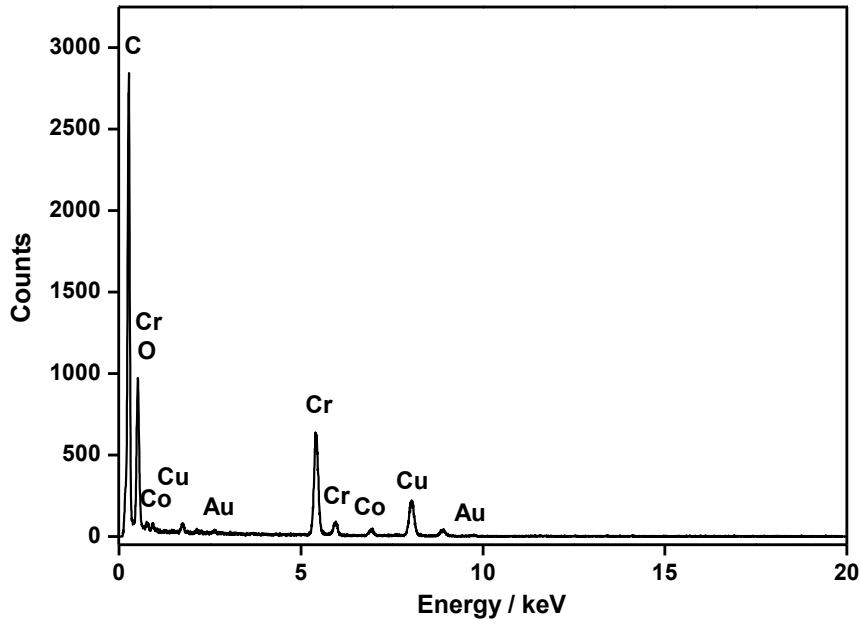

Fig. 2.6 EDX spectrum for the as-synthesized AuCo@MIL-101 (Au/Co = 6:94). The copper signal originates from Cu grid.

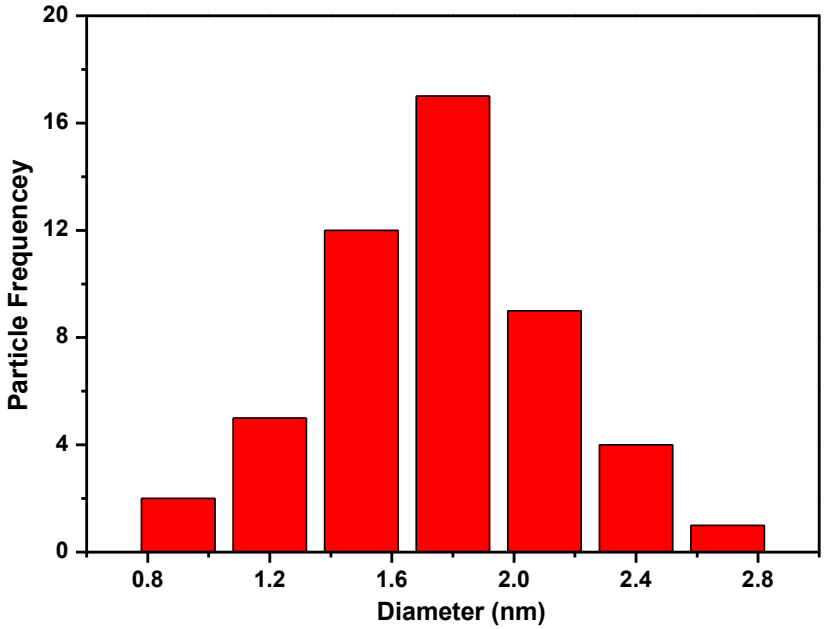

Fig. 2.7 Size distribution of AuCo alloy nanoparticles in AuCo@MIL-101 sample (Au/Co = 6:94).

2.3.3 Catalytic activity and durability

The catalytic activities on hydrolysis of aqueous AB were tested for the prepared samples. Among the samples of M@MIL-101 with various Au/Co compositions, the AuCo@MIL-101 catalysts exhibits much higher catalytic activity for hydrolysis of AB compared with its monometallic counterparts, indicating a synergetic effect between the binary components (Fig. 2.8a). Under our evaluation conditions, the AuCo@MIL-101 with the Au/Co atomic ratio of 6 : 94 is the most active, over which the AB hydrolysis reaction can be completed (H_2/AB = 3.0) in 7.5 min with a 72 mL H_2 release at room temperature ((Au+Co)/AB = 0.017 in molar ratio), giving a turnover frequency (TOF) value of 23.5 mol_{H2} mol_{cat}^{-1} min^{-1} (Fig. 2.8b and c). To the best of our knowledge, this obtained activity is the highest for supported Co and Co-based catalysts ever reported for hydrolytic dehydrogenation of aqueous AB.[4a,11] Reasonably, the remarkably high catalytic activity is attributed to the synergetic effect between Au and Co.

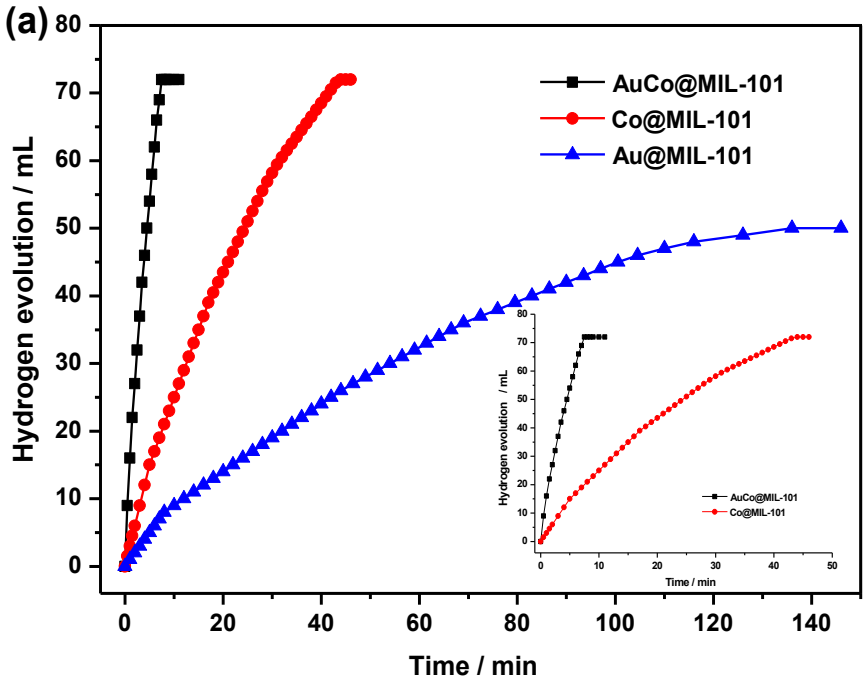
(a)
Hydrogen evolution / mL
Time / min
AuCo@MIL-101
Co@MIL-101
Au@MIL-101
0
10
20
30
40
50
60
70
80
0
20
40
60
80
100
120
140

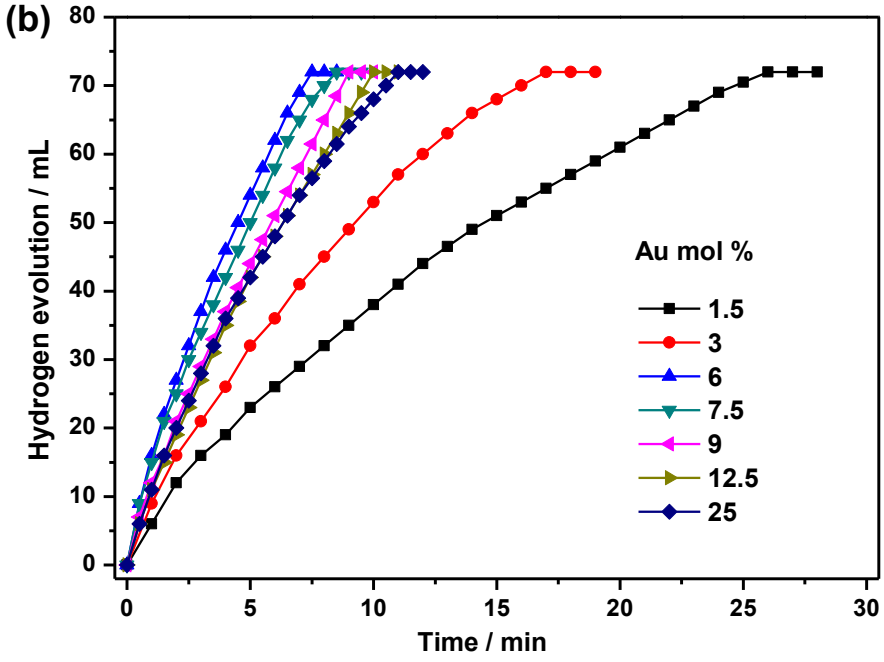
(b)
Hydrogen evolution / mL
Time / min
Au mol %
1.5
3
6
7.5
9
12.5
25
0
10
20
30
40
50
60
70
80
0
5
10
15
20
25
30

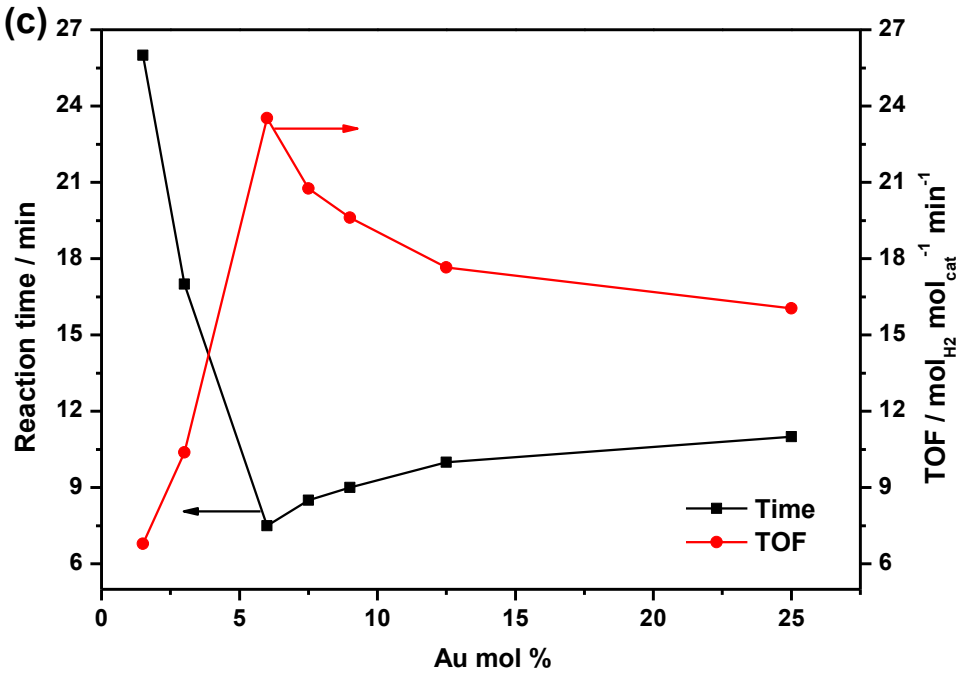

Fig. 2.8 (a) Plots of time vs volume of hydrogen generated from AB (1 mmol in 5 mL water) hydrolysis at room temperature catalyzed by the Au@MIL-101, Co@MIL-101, and AuCo@MIL-101 catalysts (50 mg, Au/Co = 6:94), (b) Plots of time versus volume of hydrogen generated from AB (1.0 mmol, 5 mL) by AuCo@MIL-101 catalysts with different Au molar contents ((Au+Co)/AB = 0.017), and (c) plots of time for reaction completion and the corresponding TOF value versus Au molar content in AuCo@MIL-101 ((Au+Co)/AB=0.017).

The durability/stability is the key point for the practical application of catalysts. We tested the durability of AuCo@MIL-101 by adding additional equivalents (1.0 mmol, 200 mL) of AB under an ambient atmosphere. As shown in Fig. 2.9, the activity of the as-prepared AuCo@MIL-101 catalyst has no significant decrease in catalytic activity even after five-time recycle of hydrolysis reactions, indicating the high durability in AB hydrolysis. There is no significant change in the morphologies of AuCo NPs with retention of the MIL-101 framework after catalysis showed by PXRD (Fig. 2.10) and TEM (Fig. 2.11) measurements, which further confirms the merit of the confinement effect of the MOF matrice.

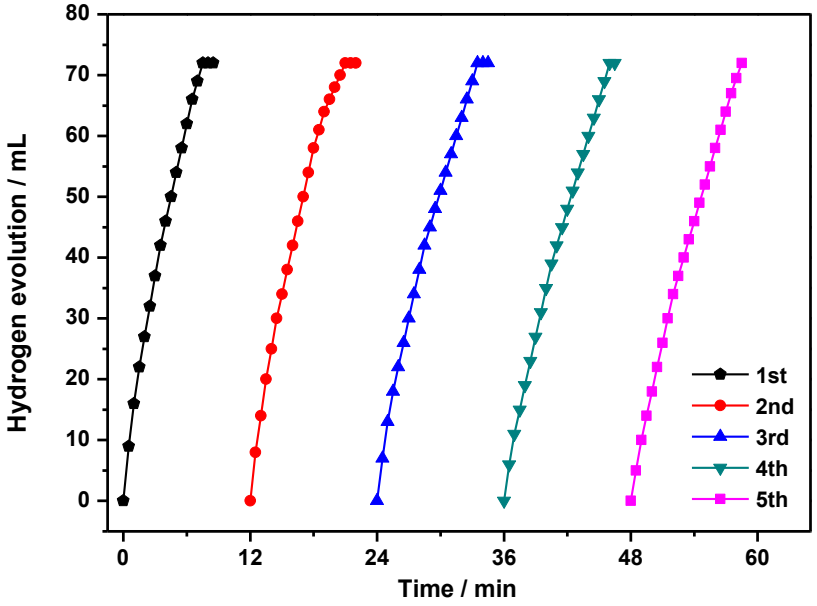

Fig. 2.9 Durability characterization of AuCo@MIL-101 in five runs for hydrogen generation from hydrolysis of aqueous AB solution (1.0 mmol, Au/Co = 6:94, (Au+Co)/AB＝0.017).

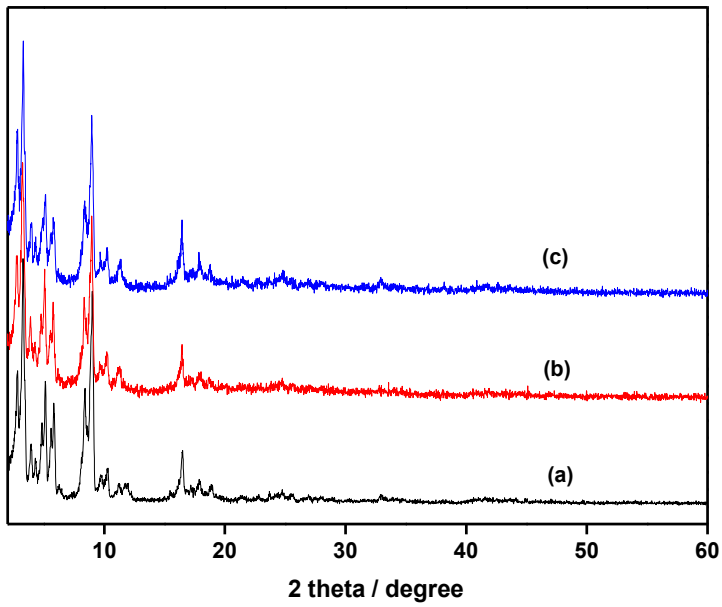

Fig. 2.10 Powder XRD patterns of (a) as-synthesized MIL-101 and AuCo@MIL-101 (Au/Co = 6:94) (b) before and (c) after the catalytic hydrolysis of AB.

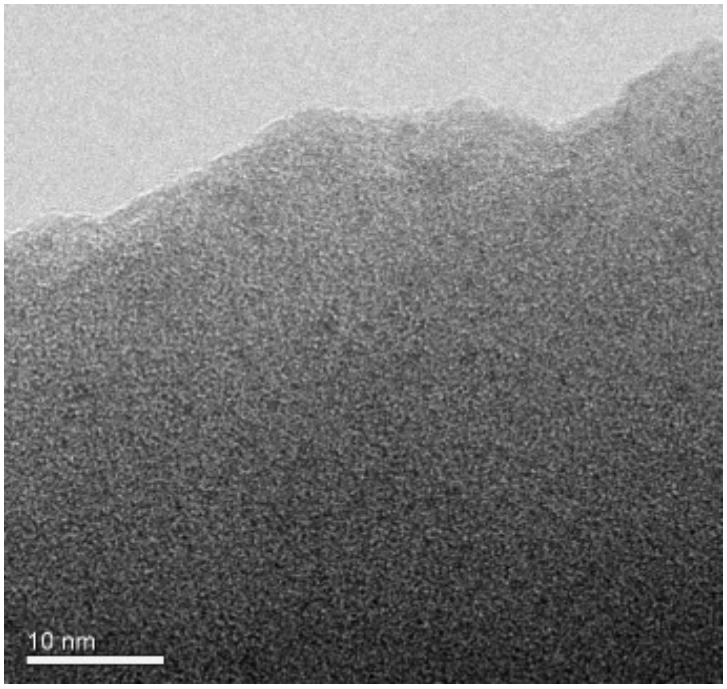

Fig. 2.11 TEM image of AuCo@MIL-101 after AB hydrolysis (Au/Co = 6:94).

2.4 Conclusion

In summary, we have successfully encapsulated the ultrafine AuCo alloy NPs in the pores of MIL-101 by using the DSM in combination with the OWR approach, which display excellent catalytic activity for hydrolytic dehydrogenation of aqueous AB, surpassing over their monometallic Au and Co counterparts. The present results not only bring light to new opportunities in the fabrication of ultrafine non-noble metal-based NPs as high performance heterogeneous catalysts throughout the interior pores of MOFs, but also represent a promising step toward developing AB as a viable on-board hydrogen storage and supply material.

References

1 (a) L. Schlapbach and A. Züttel, *Nature*, **2001**, *414*, 353; (b) R. J. Keaton, J. M. Blacquiere and R. T. Baker, *J. Am. Chem. Soc.*, **2007**, *129*, 1844; (c) C.W. Hamilton, R. T. Baker, A. Staubitz and I. Manners, *Chem. Soc. Rev.*, **2009**, *38*, 279; (d) Z.-G. Huang and T. Autrey, *Energy Environ. Sci.*, **2012**, *5*, 9257; (e) Q.-L. Zhu, N. Tsumori and Q. Xu, *Chem. Sci.*, **2014**, *5*, 195.

2 (a) A. Gutowska, L. Li, Y. Shin, C.-M. Wang, X.-S. Li, J. C. Linehan, R. S. Smith, B. D. Kay, B. Schmid, W. Shaw, M. Gutowski and T. Autrey, *Angew. Chem., Int. Ed.*, **2005**, *44*, 3578; (b) M. Chandra and Q. Xu, *J. Power Sources*, **2006**, *156*, 190; (c) S.-K. Kim, W.-S. Han, T.-J. Kim, T.-Y. Kim, S. W. Nam, M. Mitoraj, L. Piekos, A. Michalak, S. J. Hwang and S. O. Kang, *J. Am. Chem. Soc.*, **2010**, *132*, 9954; (d) S.-K. Kim, T.-J. Kim, T.-Y. Kim, G. Lee, J. T. Park, S. W. Nam and S. O. Kang, *Chem. Commun*., **2012**, *48*, 2021; (e)M. Yadav and Q. Xu, *Energy Environ. Sci.*, **2012**, *5*, 9698.

3 (a) J.-M. Yan, X.-B. Zhang, S. Han, H. Shioyama and Q. Xu, *Angew. Chem., Int. Ed.*, **2008**, *47*, 2287; (b) Ö. Metin, S. Ö zkar and S. Sun, *Nano Res.*, **2010**, *3*, 676; (c) P.-Z. Li, A. Aijaz and Q. Xu, *Angew. Chem., Int. Ed.*, **2012**, *51*, 6753; (d) A. Aijaz, A. Karkamkar, Y. J. Choi, N. Tsumori, E. Rönnebro, T. Autrey, H. Shioyama and Q. Xu, *J. Am. Chem. Soc.*, **2012**, *134*, 13926.

4 (a) J.-M. Yan, X.-B. Zhang, T. Akita, M. Haruta and Q. Xu, *J. Am. Chem. Soc*., **2010**, *132*, 5326; (b) J.-M. Yan, X.-B. Zhang, H. Shioyama and Q. Xu, *J. Power Sources*, **2010**, *195*, 1091; (c) U. Sanyal, U. B. Demirci, B. R. Jagirdar and P. Miele, *ChemSusChem*, **2011**, *4*, 1731.

5 (a) M. Eddaoudi, J. Kim, N. Rosi, D. Vodak, J. Wachter, M. O'Keeffe and O. M. Yaghi, *Science*, **2002**, *295*, 469; (b) J.-P. Zhang, X.-C. Huang and X.-M. Chen, *Chem. Soc. Rev*., **2009**, *38*, 2385; (c) G. Férey and C. Serre, *Chem. Soc. Rev.*, **2009**, *38*, 1380; (d) D. Yuan, D. Zhao, D. Sun and H.-C. Zhou, *Angew. Chem., Int. Ed.*, **2010**, *49*, 5357; (e) B. Chen, S. Xiang and G. Qian, *Acc. Chem. Res*., **2010**, *43*, 1115; (f) H.-L. Jiang and Q. Xu, *Chem. Commun.*, **2011**, *47*, 3351; (g) D. Zhao, D. J. Timmons, D. Yuan and H.-C. Zhou, *Acc. Chem. Res*., **2011**, *44*, 123; (h) T. Wu, L. Wang, X. Bu, V.

Chau and P. Feng, *J. Am. Chem. Soc.*, **2012**, *134*, 4517; (i) S. Sen, N. N. Nair, T. Yamada, H. Kitagawa and P. K. Bharadwaj, *J. Am. Chem. Soc.*, **2012**, *134*, 19432.

6 (a) R. Matsuda, R. Kitaura, S. Kitagawa, Y. Kubota, R. V. Belosludov, T. C. Kobayashi, H. Sakamoto, T. Chiba, M. Takata, Y. Kawazoe and Y. Mita, *Nature*, **2005**, *436*, 238; (b) S. Ma and H.-C. Zhou, *J. Am. Chem. Soc.*, **2006**, *128*, 11734; (c) S. K. Ghosh, S. Bureekaew and S. Kitagawa, *Angew. Chem., Int. Ed.*, **2008**, *47*, 3403; (d) L. Ma, A. Jin, Z. Xie and W. Lin, *Angew. Chem., Int. Ed.*, **2009**, *48*, 9905; (e) J. Lee, O. K. Farha, J. Roberts, K. A. Scheidt, S. T. Nguyen and J. T. Hupp, *Chem. Soc. Rev.*, **2009**, *38*, 1450; (f) H.-L. Jiang, Y. Tatsu, Z.-H. Lu and Q. Xu, *J. Am. Chem. Soc.*, **2010**, *132*, 5586; (g) Y. He, S. Xiang and B. Chen, *J. Am. Chem. Soc.*, **2011**, *133*, 14570; (h) S. Motoyama, R. Makiura, O. Sakata and H. Kitagawa, *J. Am. Chem. Soc.*, **2011**, *133*, 5640; (i) G. Akiyama, R. Matsuda, H. Sato, M. Takata and S. Kitagawa, *Adv. Mater.*, **2011**, *23*, 3294; (j) A. Shigematsu, T. Yamada and H. Kitagawa, *J. Am. Chem. Soc.*, **2012**, *134*, 13145; (k) M. M.Wanderley, C. Wang, C.-D. Wu and W. Lin, *J. Am. Chem. Soc*., **2012**, *134*, 9050.

7 (a) A. Henschel, K. Gedrich, R. Kraehnert and S. Kaskel, *Chem. Commun*., **2008**, 4192; (b) Y. K. Park, S. B. Choi, H. J. Nam, D. Jung, H. C. Ahn, K. Choi, H. Furukawa and J. Kim, *Chem. Commun.,* **2010**, *46*, 3086; (c) H.-L. Jiang, T. Akita, T. Ishida, M. Haruta and Q. Xu, *J. Am. Chem. Soc.*, **2011**, *133*, 1304; (d) G. Lu, S. Li, Z. Guo, O. K. Farha, B. G. Hauser, X. Qi, Y. Wang, X. Wang, S. Han, X. Liu, J. S. DuChene, H. Zhang, Q. Zhang, X. Chen, J. Ma, S. C. J. Loo, W. D.Wei, Y. Yang, J. T. Hupp and F. Huo, *Nat. Chem*., **2012**, *4*, 310; (e) A. Dhakshinamoorthy and H. Garcia, *Chem. Soc. Rev.*, **2012**, 41, 5262; (f) C. Wang, K. E. deKrafft and W. Lin, *J. Am. Chem. Soc*., **2012**, *134,* 7211; (g) H. R. Moon, D.-W. Lim and M. P. Suh, *Chem. Soc. Rev.*, **2013**, *42*, 1807; (h) S.-L. Li and Q. Xu, *Energy Environ. Sci*., **2013**, *6*, 1656; (i) Q.-L. Zhu and Q. Xu, *Chem. Soc. Rev.*, **2014**, *43*, 5468.

8 (a) S. Hermes, M.-K. Schröter, R. Schmid, L. Khodeir, M. Muhler, A. Tissler, R. W. Fischer and R. A. Fischer, *Angew. Chem., Int. Ed.*, **2005**, *44*, 6237; (b) S. Proch, J. Herrmannsdörfer, R. Kempe, C. Kern, A. Jess, L. Seyfarth and J. Senker, *Chem. – Eur. J.*, **2008**, *14*, 8204; (c) X. Gu, Z.-H. Lu, H.-L. Jiang, T. Akita and Q. Xu, *J. Am. Chem. Soc.*, **2011**, *133*, 11822.

9 Q.-L. Zhu, J. Li and Q. Xu, *J. Am. Chem. Soc*., **2013**, *135*, 10210.

10 G. Férey, C. Mellot-Draznieks, C. Serre, F. Millange, J. Dutour, S. Surblé and I. Margiolaki, *Science*, **2005**, *309*, 2040.

11 (a) H.-L. Jiang and Q. Xu, *Catal. Today*, **2011**, *170*, 56; (b) Ö. Metin and S. Ö zkar, *Int. J. Hydrogen Energy*, **2011**, *36*, 1424; (c) Z.-H. Lu, H.-L. Jiang, M. Yadav, K. Aranishi and Q. Xu, *J. Mater. Chem.*, **2012**, *22*, 5065.

Chapter 3

Non-noble bimetallic CuCo nanoparticles encapsulated in the pores of metal-organic frameworks: synergetic catalysis in the hydrolysis of ammonia borane for hydrogen generation

Non-noble bimetallic CuCo alloy nanoparticles were successfully encapsulated in the pores of MIL-101 by using the double solvents method combined with the overwhelming reduction approach, which display remarkably enhanced catalytic activity for hydrolytic dehydrogenation of ammonia borane (AB) to generate a stoichiometric amount of hydrogen at room temperature for chemical hydrogen storage, which presents the first example of MOF-supported non-noble bimetallic catalysts for the hydrogen generation from hydrolysis of AB. The synergetic effect between copper and cobalt species plays an important role for the improved performance in the catalytic hydrolysis of AB.

3.1 Introduction

Hydrogen has been considered as one of the best alternative energy carriers to satisfy the increasing demand for a sustainable and clean energy supply.[1] The development of effective hydrogen-storage materials is imperative but challenging for establishing a hydrogen-based energy system.[2] Ammonia borane (NH_3BH_3, AB) has become an attractive candidate for chemical hydrogen storage applications due to its high gravimetric hydrogen capacity (19.6 wt.%) and low molecular weight (30.86 g mol^{-1}).[3] However, one of the major obstacles for the practical application of this system is to develop low-cost and highly efficient catalysts for improving the kinetic properties under moderate conditions.[4]

So far various catalyst systems have been tested in the hydrolysis of AB and rapid hydrogen generation has been achieved by using noble metals such as Pt, Ru and Rh, while the limited resource restricts their practical applications.[5] Alternatively, cost-effective non-noble metals such as Co, Ni, Fe, have been developed.[6,7] However,

these materials tend to be fairly unstable in solution and air atmospheres due to magnetism-induced agglomeration and easy oxidation. To circumvent the drawback, several strategies, including fabricating non-noble metal based alloys[8] or core-shell[9] nanoparticls (NPs), and structured Co-B film catalysts[10], have been explored. Although great efforts have been made in this field, development of high-performance catalysts towards AB dehydrogenation with high activity and desired durability simultaneously remains a huge challenge.

In the design and fabrication of highly efficient catalysts for AB dehydrogenation, the dispersion and stabilization of active metal nanoparticls (MNPs) are two key factors. Metal-organic frameworks (MOFs) synthesized by assembling metal ions with organic ligands have emerged as a new class of porous materials due to their high porosity, large surface area and chemical tenability.[11] Given the similarity to zeolites, depositing MNPs to MOFs could afford heterogeneous catalysts.[12] It is expected that the crystalline porous structures of MOF limit the migration and aggregation of the active components and thus enhance the long-term stability. There were some reports of MOF-supported non-noble metal NPs as catalysts for heterogeneous reactions, while it was difficult to completely avoid MNPs aggregation on the external surface of MOFs.[13] Therefore, it is a big challenge to develop a general and facile method to incorporate fine MNPs within the pores of MOFs. Very recently, we exploited an approach via overwhelming reduction (OWR) approach combined with a double solvents method (DSM), which can encapsulate the non-noble metal-based NPs (AuNi and AuCo) in the pores of MOF without MNPs aggregation on the external surface of framework.[14]

In this work, we report successful preparation and excellent catalytic activity of the ultrafine CuCo alloy NPs encapsulated in the pores of MOF without aggregation on the external surfaces of host framework by using the DSM in combination with the OWR approach, which presents the first example of MOF-supported non-noble bimetallic catalysts for the hydrogen generation from hydrolysis of AB.

3.2 Experimental section

3.2.1 Materials and general methods

Vulcan XC-72R (Carbon, specific surface area = 240 m^2 g^{-1}, Cabot Corp., USA), anhydrous n-hexane (Sigma-Aldrich), terephthalic acid ($HOOCC_6H_4COOH$, Tri Chemical Laboratories Inc., 99%), ethanol (C_2H_5OH, Kishida Chem. Co., >99.8%), ammonia borane (NH_3BH_3, JSC Aviabor, >97%), sodium borohydride ($NaBH_4$, Aldrich, 99%), ammonium fluoride (NH_4F, Kishida Chem. Co., >97%), aqueous hydrofluoric acid (HF, Kishida Chemical Co. Ltd., 46%), cobalt (II) chloride hexahydrate ($CoCl_2 \cdot 6H_2O$, Wako Pure Chemical Industries, Ltd., >99%), copper (II) nitrate trihydrate ($Cu(NO_3)_2 \cdot 3H_2O$, Kishida Chem. Co., >99.5%) and chromic nitrate nonahydrate ($Cr(NO_3)_3 \cdot 9H_2O$, Sigma-Aldrich, 99%) were used as received. All reagents were commercial and used without further purification. De-ionized water with the resistivity of 18.2 MΩ·cm was obtained by reversed osmosis followed by ion-exchange and filtration (RFD 250NB, Toyo Seisakusho Kaisha, Ltd., Japan). Powder X-ray diffraction (PXRD) measurements were carried out on a Rigaku UItima IV X-ray diffractometer with Cu Kα source (40 kV, 40 mA). The surface area measurements were performed with N_2 adsorption/desorption isotherms at liquid nitrogen temperature (77 K) after dehydration under vacuum at 150 °C for 12 h using automatic volumetric adsorption equipment (Belsorp-max). The pore volume was calculated by a single point method at P/P_0=0.99. Transmission electron microscope (TEM, TECNAI G^2 F20) equipped with energy dispersed X-ray detector (EDX) was applied for the detailed microstructure and composition information for the prepared samples. X-ray photoelectron spectroscopic (XPS) measurements were performed on a Shimadzu ESCA-3400 X-ray photoelectron spectrometer using an Mg Kα source (10 kV, 10 mA). The Ar sputtering experiments were carried out under the conditions of background vacuum of 3.2×10^{-6} Pa, sputtering acceleration voltage of 2 kV and sputtering current of 10 mA.

3.2.2 Synthesis of MIL-101

MIL-101 was synthesized according the reported procedure.[15] $Cr(NO_3)_3 \cdot 9H_2O$

(4.002 g, 10.0 mmol), terephthalic acid (1.661 g, 10.0 mmol), aqueous HF (0.5 mL, 46 wt%) and de-ionized water (70 mL) were mixed in a 100 mL Teflon-liner autoclave, which was held in an oven at 220 °C for 8 h. After natural cooling, the resulting green powder of MIL-101 with formula $Cr_3F(H_2O)_2O[(O_2C)C_6H_4(CO_2)]_3 \cdot nH_2O$ ($n \approx 25$) were filtered off using two glass filters with pore sizes between 40 and 100 μm to remove the unreacted crystals of terephthalic acid, and subsequently centrifuged and further purified by solvothermal treatment in ethanol at 80 °C for 24 h. In order to eliminate the terephthalic acid inside the pores of MIL-101, the resulting green solid was soaked in NH_4F (1.0 M) solution at 70 °C for 24 h and immediately filtered, washed with hot water several times, and finally dried at 150 °C under vacuum for 12 h.

3.2.3 Preparation of Cu@MIL-101, Co@MIL-101 and CuCo@MIL-101

The double solvents method was used in this work to encapsulate Cu^{2+} and/or Co^{2+} precursors.[5f] Typically, 100 mg of green MIL-101 powder with a pore volume of 1.72 $cm^3\ g^{-1}$ as determined by N_2 sorption isotherm activated by heating at 150 °C for 12 h under dynamic vacuum was suspended in 20 mL of dry n-hexane as hydrophobic solvent and the green suspension was sonicated for 15 min until it became homogeneous. After stirring for 2 h, 0.15 mL of aqueous $Cu(NO_3)_2 \cdot 3H_2O$ and/or $CoCl_2 \cdot 6H_2O$ solution with desired concentrations as the hydrophilic solvent was added dropwise over a period of 15 min with constant vigorous stirring, and then the resulting solution was continuously stirred for 2 h. After filtration, the green powder was dried in air at room temperature. These synthesized samples were then dried overnight at 150 °C under vacuum. The molar ratio of Cu^{2+}:(Cu^{2+}+Co^{2+}) were varied with several values (0, 0.1, 0.2, 0.3, 0.4, 0.5, 0.7, 0.8 and 1.00), while the molar contents of (Cu^{2+}+Co^{2+}) added to 100 mg MIL-101 matrix were kept to be 0.034 mmol. After dehydration of the $Cu^{2+}Co^{2+}$@MIL-101 with different molar ratios of Cu^{2+} to (Cu^{2+}+Co^{2+}), an overwhelming reduction approach[14] was carried out by using 5 mL freshly prepared 0.6 M aqueous $NaBH_4$ solution while vigorous stirring, resulting in the generation of catalysts as a dark green suspension. Finally, the synthesized samples were collected by centrifuging, and used for the catalytic reactions.

3.2.4 Preparation of CuCo/XC-72R and CuCo/MIL-101

For comparison, CuCo/XC-72R and CuCo/MIL-101 catalysts were prepared. 100 mg of XC-72R carbon powder or activated MIL-101 was dispersed in 4.5 mL of aqueous $Cu(NO_3)_2 \cdot 3H_2O$ and $CoCl_2 \cdot 6H_2O$ solution. The molar ratio of Cu^{2+}:(Cu^{2+}+Co^{2+}) were fixed at 0.3, while the molar contents of (Cu^{2+}+Co^{2+}) added to 100 mg XC-72R or MIL-101 were kept to be 0.034 mmol. The resulted aqueous suspension was further homogenized under sonication for 0.5 hr. Then, 20 mg of $NaBH_4$ dissolved in 0.50 mL water was added to the above obtained solution with vigorous shaking. The mixture was further shaked for 0.5 hr at room temperature to fully deposit the metallic nanoparticles onto the support. Finally, the desired catalyst was collected by centrifuging and used for the catalytic reaction.

3.2.5 Catalytic hydrolysis of ammonia borane

The catalytic hydrolysis of AB was performed following our procedure reported previously.[4] Typically, a mixture of catalyst (100 mg) and distilled water (5 mL) was placed in a two-necked round-bottomed flask (30 mL), which was placed in a water bath at room temperature under ambient atmosphere. In order to measure the volume of hydrogen, a gas burette filled with water was connected to the reaction flask. When aqueous AB solution (1 mmol in 200 μL water) was injected into the mixture using a syringe, the reaction started. The volume of the evolved hydrogen gas was monitored by recording the displacement of water in the gas burette and the reaction was completed when there was no more gas generation.

For the durability test, catalytic reactions were repeated by injecting another aliquot of AB (1.0 mmol in 200 μL water) into the mixture after the previous cycle. After the reaction, the as-synthesized CuCo@MIL-101 was separated from the reaction solution by centrifuging and washed with de-ionized water and then dried under vacuum at room temperature for the PXRD and TEM analyses.

3.3 Results and discussion

3.3.1 Preparation

Chromium (III) terephthalate MIL-101 with molecular formula $Cr_3F(H_2O)_2O[(O_2C)C_6H_4(CO_2)]_3 \cdot nH_2O$ ($n \approx 25$), was chosen as a host matrix for this study to encapsulate metallic particles not only because of its higher stability than most of MOFs in water or high temperature, but also its large cavity sizes (2.9 to 3.4 nm) and window sizes (1.2 to 1.4 nm), large surface area, and hybrid pore surface, which may facilitate the encapsulation of MNPs and the adsorption of catalytic substrate AB and reductant $NaBH_4$ into the pores.[15] The double solvents method (DSM) was carried out in this work to impregnate the metal precursors ($Cu(NO_3)_2$ and/or $CoCl_2$) into the preactivated MIL-101 in order to avoid the precursors deposition on the outer surface of MOF.[5f] This method is based on a hydrophilic solvent containing the metal precursors and a hydrophobic solvent suspending the adsorbent, the former with a volume set equal to or less than the pore volume of the adsorbent, which can be readily adsorbed within the hydrophilic pores of adsorbent by the capillary force. Then, the overwhelming reduction (OWR) approach was used to reduce the precursors after the metal precursor/MOF composite was dried.[14] In this approach, a pore-volume amount of $NaBH_4$ solution with a high concentration (0.6 M) incorporated into the pores by capillary force can reduce the metal precursors deposited in the pores of MIL-101 completely, and the aggregation of MNPs on the external surfaces of MOF will be avoided.

3.3.2 Characterization

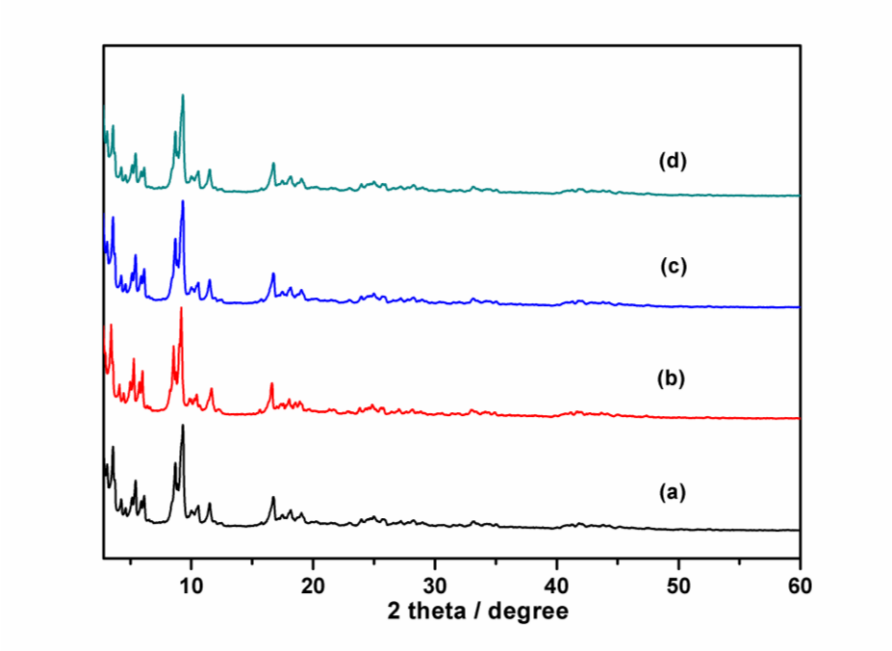

Fig. 3.1 Powder XRD patterns of (a) as-synthesized MIL-101, (b) CuCo@MIL-101 (Cu/Co = 3:7), (c) Co@MIL-101 and (d) Cu@MIL-101.

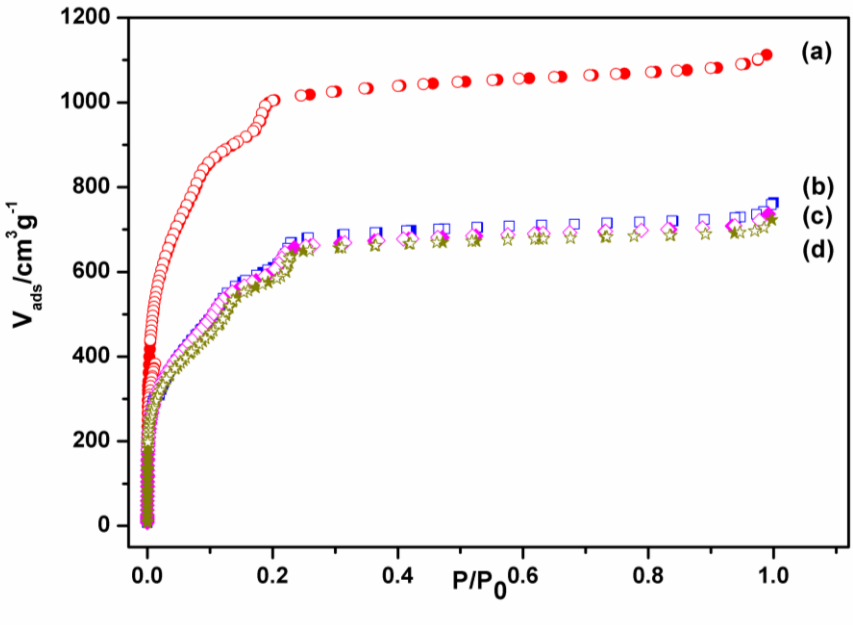

Fig. 3.2 N_2 sorption isotherms of (a) MIL-101, (b) Co@MIL-101, (c) CuCo@MIL-101 (Cu/Co = 3:7) and (d) Cu@MIL-101. Filled and open symbols represent adsorption and desorption

branches, respectively.

After the impregnation and reduction processes, there was no loss of the crystallinity in powder X-ray diffraction (PXRD) patterns for M@MIL-101, suggesting that the framework of MIL-101 was maintained[15] (Fig. 3.1). Moreover, the PXRD pattens of M@MIL-101 did not exhibit the characteristic diffractions for MNPs, indicating the formation of very small MNPs. The BET surface areas of MIL-101, Co@MIL-101, Cu@MIL-101 and CuCo@MIL-101 are 3450, 2154, 2052 and 2125 $m^2 g^{-1}$, respectively. The appreciable decreases in the amount of N_2 sorption of M@MIL-101 indicated that MNPs were highly dispersed to the framework of MIL-101 (Fig. 3.2).

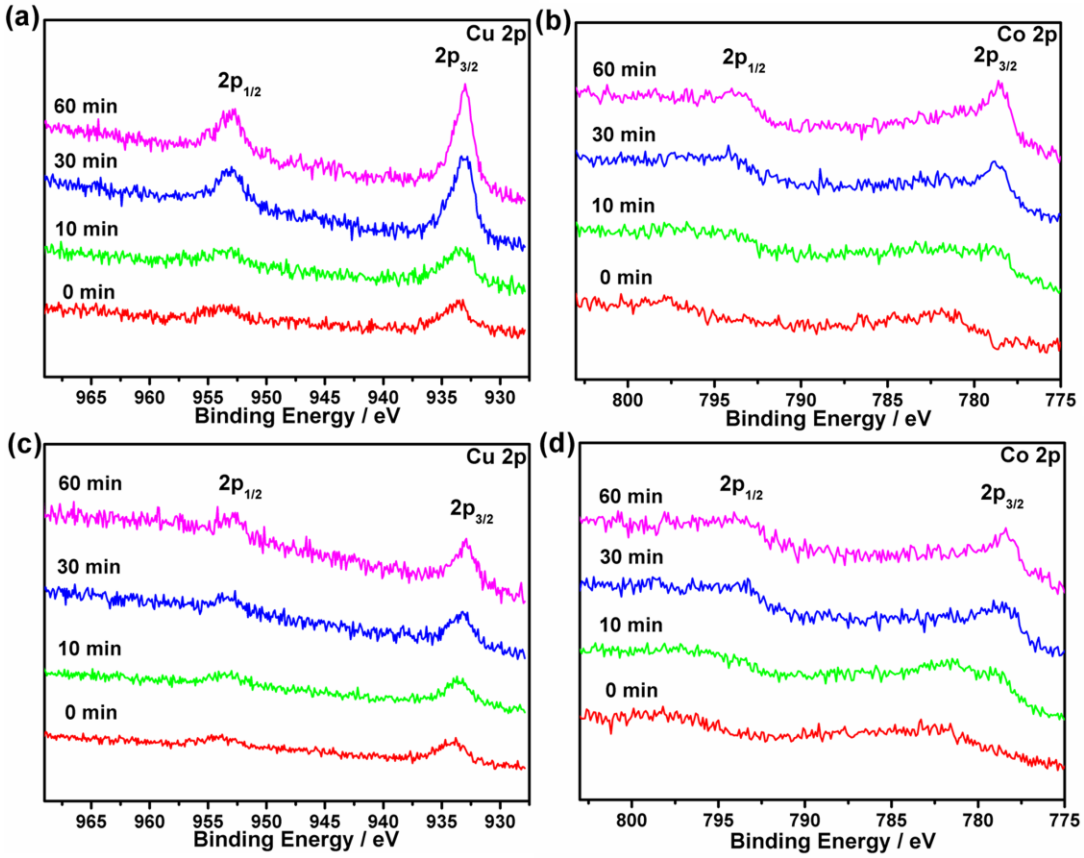

Fig. 3.3 XPS spectra for (a) Cu@MIL-101, (b) Co@MIL-101 and (c, d) CuCo@MIL-101 (Cu/Co = 3:7) before (0 min) and after (10–60 min) Ar etching (Cu $2p_{3/2}$ and $2p_{1/2}$ peaks, and Co $2p_{3/2}$ and $2p_{1/2}$ peaks).

To obtain further insights into the structure-function correlations, X-ray

photoelectron spectroscopy (XPS) with Ar etching was applied to Cu@MIL-101, Co@MIL-101 and CuCo@MIL-101 at the Cu 2p and Co 2p levels. Before Ar sputtering, broad peaks of Co $2p_{3/2}$ and Co $2p_{1/2}$ for Co@MIL-101 and CuCo@MIL-101 were observed with binding energies at 781.2 and 795.8 eV corresponding to Co 2p of CoO[16], which were caused by oxidation during the exposure of samples to air. After Ar etching for 60 min, well-defined peaks corresponding to metallic Cu and Co species both can be detected, suggesting both of two elements are in their zero-valent states. The peaks at 932.6 and 952.4 eV are attributed to Cu $2p_{3/2}$ and Cu $2p_{1/2}$ of Cu^0, and the peaks at 777.9 and 793.0 eV correspond to Co $2p_{3/2}$ and Co$2p_{1/2}$ of Co^0.[16] The metallic Cu and Co peak intensities changed synchronously during the Ar etching in CuCo@MIL-101, indicating the homogeneity of the CuCo alloy NPs and excluding the possibility of core-shells (Fig. 3.3).

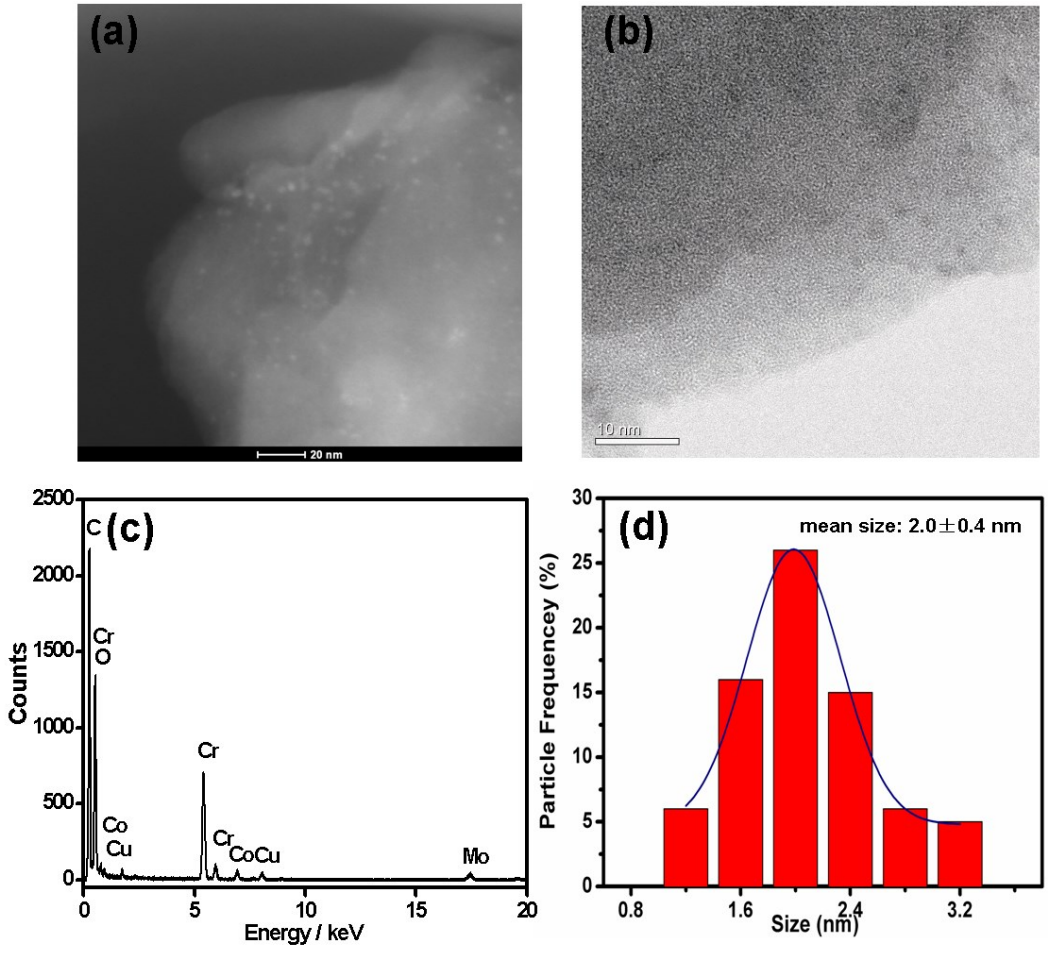

Fig. 3.4 Representative (a) HAADF-STEM and (b) TEM images, (c) EDX spectrum, and (d)

CuCo alloy nanoparticle size distribution histogram of CuCo@MIL-101 (Cu/Co = 3:7). The signal of Mo was from the TEM grid.

The morphologies of MIL-101 immobilized CuCo alloy NPs were further characterized by transmission electron microscopic (TEM), high-angle annular dark-field scanning TEM (HAADF-STEM) and energy-dispersive X-ray spectroscopy (EDX) analyses (Fig. 3.4). Both TEM and HAADF-STEM images showed that the CuCo alloy NPs were highly dispersed. The mean diameters were 2.0 ± 0.4 nm (Fig. 3.4d), which are small enough to be encapsulated in the two mesoporous cavities of MIL-101. No obvious particle aggregation occurred, which is in good agreement with the PXRD observations.

3.3.3 Catalytic activity and durability

To study the catalytic behavior, the as-synthesized M@MIL-101 composites have been applied as catalysts for hydrolysis of AB. Reaction was initiated by introducing aqueous AB solution into the reaction flask containing M@MIL-101 catalyst with vigorous shaking at room temperature. The catalytic hydrolysis of AB reaction can be briefly expressed as follows (Equation 1).

$$NH_3BH_3 + 4H_2O \rightarrow NH_4^+ + B(OH)_4^- + 3H_2 \quad (1)$$

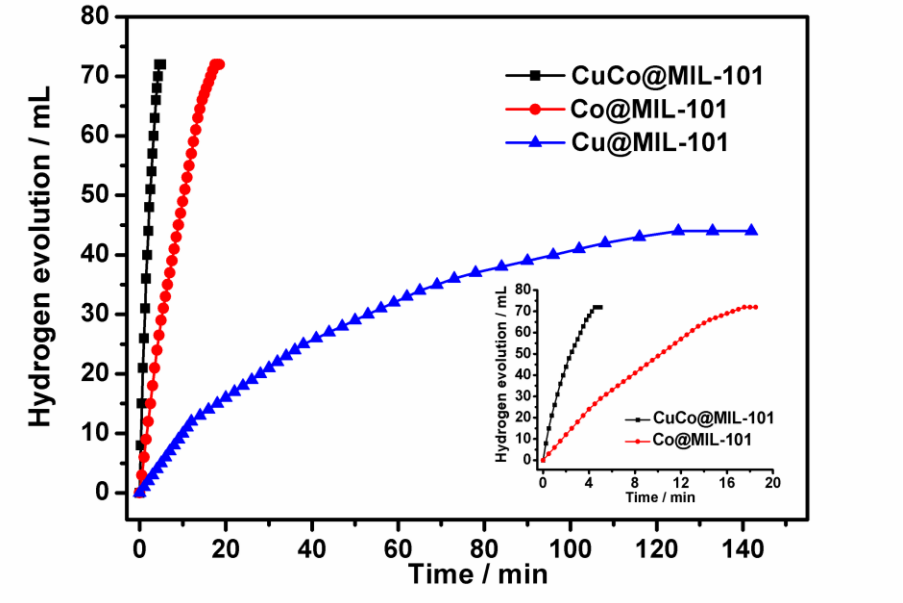

Fig. 3.5 Plots of time versus volume of hydrogen generated from AB (1 mmol in 5 mL water)

hydrolysis at room temperature catalyzed by the Cu@MIL-101, Co@MIL-101, and CuCo@MIL-101 (Cu/Co=3:7) catalysts (100 mg, (Cu+Co)/AB (molar ratio) ＝0.034).

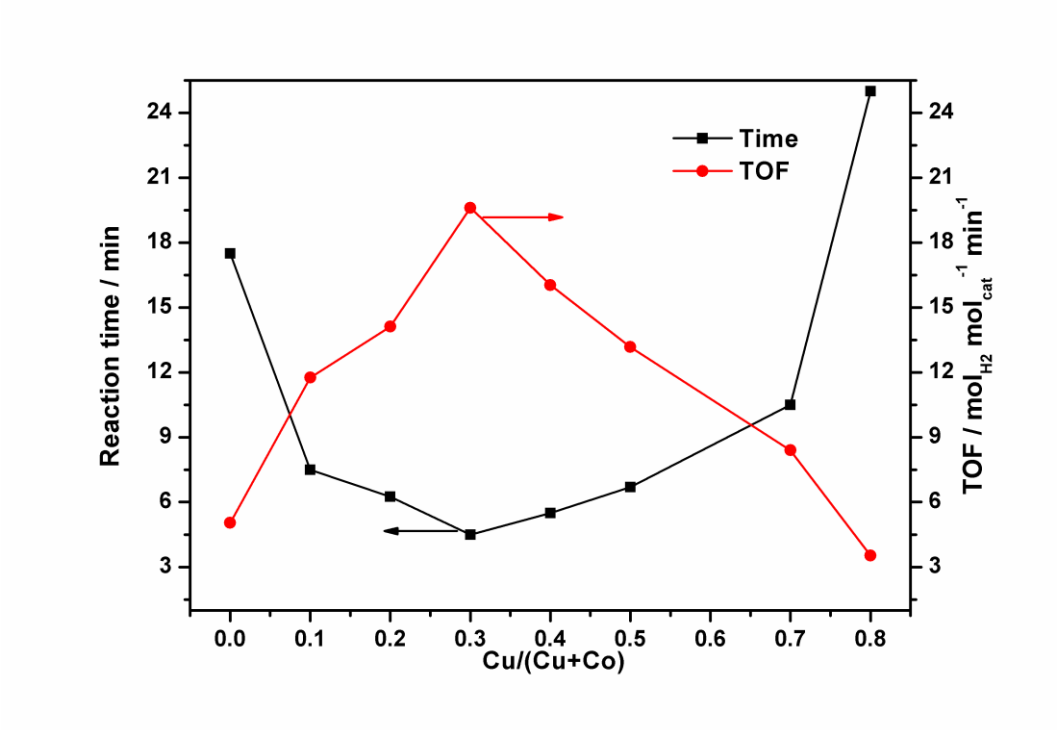

Fig. 3.6 Plots of time for reaction completion and the corresponding TOF value versus Cu molar content (Cu/(Cu+Co)) in CuCo alloy NPs ((Cu+Co)/AB＝0.034).

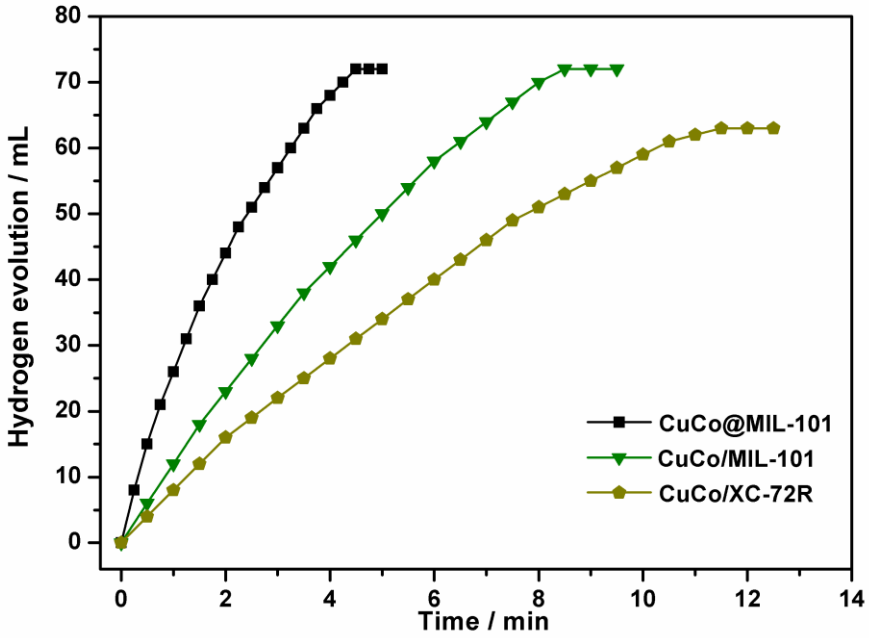

Fig. 3.7 Plots of time versus volume of hydrogen generated from AB (1 mmol in 5 mL water) hydrolysis at room temperature catalyzed by CuCo@MIL-101, CuCo/MIL-101, and CuCo/XC-72R (Cu/Co=3:7) catalysts (100 mg, (Cu+Co)/AB (molar ratio) =0.034).

As displayed in Fig. 3.5, the CuCo@MIL-101 catalyst exhibits much higher catalytic activity for hydrolysis of AB compared with its monometallic counterparts, indicating a synergetic effect between the binary components.[17] Fig. 3.6 shows the Cu content dependence of reaction times and corresponding TOF values for the dehydrogenation of AB. It is clear that, compared to pure Co, the presence of Cu can significantly improve the catalytic activity. For example, when the Cu molar ratio is as low as 0.1, the reaction time decreases from 17.5 min to 7.5 min. Moreover, with the increase in Cu molar ratio, the activity change of the CuCo system is in the shape of "V". The CuCo@MIL-101 with the Cu/Co atomic ratio of 3:7 is the most active, over which the AB hydrolysis reaction can be completed (H_2/AB = 3.0) in 4.5 min with a 72 mL H_2 release at room temperature ((Cu+Co)/AB = 0.034 in molar ratio), giving a turnover frequency (TOF) value of 19.6 mol_{H2} mol_{cat}^{-1} min^{-1}. Reasonably, the remarkably high catalytic activity is attributed to the synergetic effect between Cu and Co. For alloy nanoparticles, synergetic effects may mainly ascribed to electronic effects, which are

important when the metal atoms have significant differences in electronegativity,[18] and geometric effects. In the present case, the observed synergetic effects in catalysis might be mainly due to the geometric effects, not electronic effects, because the electronegativities of Cu (1.9) and Co (1.88) are very close. It is confirmed by the XPS measurements as no significant changes in the electronic states were observed between the CuCo alloy NPs and the monometallic Cu or Co NPs.[18] As a control experiment, CuCo/MIL-101 and CuCo/XC-72R (Cu/Co=3:7) were prepared by a conventional impregnation-reduction method, over which the evolution of 72 mL and 63 mL of hydrogen was completed in 8.5 min and 11.5 min, respectively, under the same reaction conditions (Fig. 3.7). Moreover, it is noteworthy that the TOF (19.6 mol_{H2} mol_{cat}^{-1} min^{-1}) for CuCo@MIL-101 (Cu/Co=3:7) is the highest one among the MOF supported non-noble metal catalysts ever reported for this reaction.[4a,19]

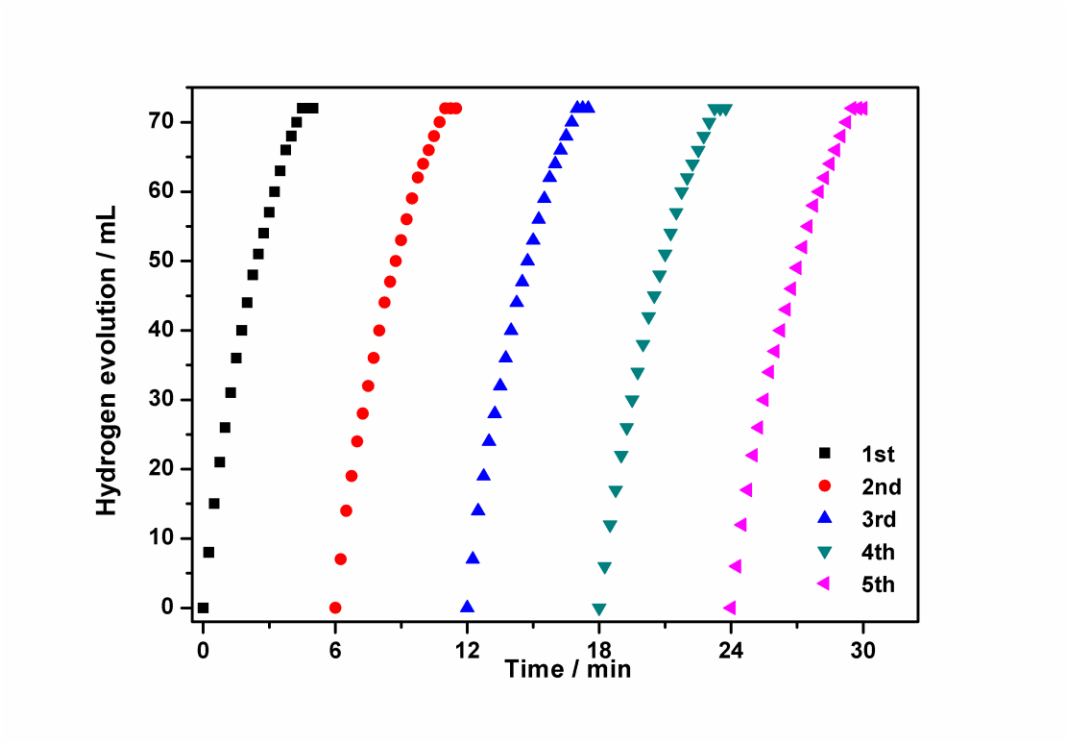

Fig. 3.8 Durability characterization of CuCo@MIL-101 in five runs for hydrogen generation from hydrolysis of aqueous AB solution (1.0 mmol, Cu/Co = 3:7, (Cu+Co)/AB＝0.034).

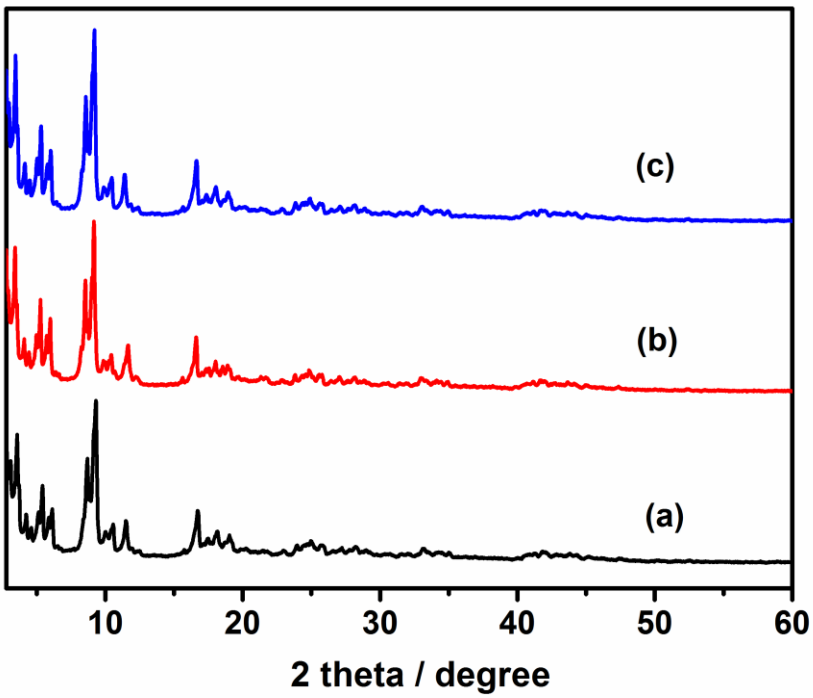

Fig. 3.9 Powder XRD patterns of (a) as-synthesized MIL-101 and CuCo@MIL-101 (Cu/Co = 3:7) (b) before and (c) after the catalytic hydrolysis of AB (Cu/Co = 3:7).

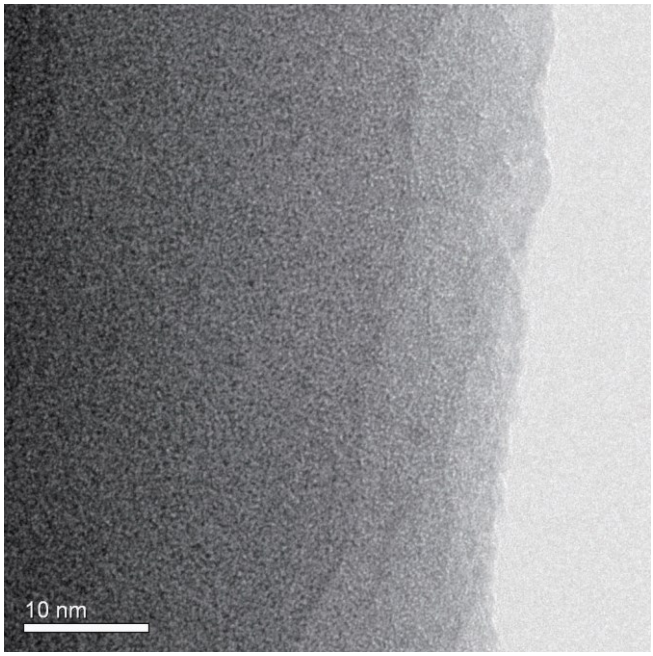

Fig. 3.10 TEM image of CuCo@MIL-101 after AB hydrolysis (Cu/Co = 3:7).

The durability/stability is the key point for the practical application of catalysts. In this sense, the durability of CuCo@MIL-101 catalyst was tested by adding additional aliquots (1.0 mmol, 200 μL) of AB under ambient atmosphere. As shown in Fig. 3.8, the activity of the as-prepared CuCo@MIL-101 catalyst has no significant decrease after a five-time recycle test, which denotes its high durability in AB hydrolysis. The long durability of the catalyst should be attributed to the fact that the ultrafine CuCo alloy NPs have been effectively encapsulated in the pores of MIL-101 for avoiding aggregation. PXRD and TEM measurements of CuCo@MIL-101 after catalysis revealed no obvious changes in the morphologies of CuCo NPs with retention of the MIL-101 framework (Fig. 3.9 and Fig. 3.10), which further confirms the advantage of the confinement effect of the MOF matrices.

3.4 Conclusion

In summary, the ultrafine CuCo alloy NPs have been successfully encapsulated in the pores of MIL-101 by using the DSM in combination with the OWR approach, which display excellent catalytic activity for hydrolytic dehydrogenation of aqueous AB, surpassing over their monometallic Cu and Co counterparts. This is the first example of MOF-supported non-noble bimetallic catalysts for hydrogen generation from hydrolysis of AB. The highly efficient catalyst represents a promising step toward the practical applications of MOF-supported non-noble metal catalysts in the catalytic hydrolysis reaction system.

References

1 (a) P. P. Edwards, V. L. Kuznetsov, W. I. David and N. P. Brandon, *Energy Policy*, **2008**, *36*, 4356; (b) C. W. Hamilton, R. T. Baker, A. Staubitzc and I. Manners, *Chem. Soc. Rev.,* **2009**, *38*, 279; (c) H. M. Chen, C. K. Chen, R.-S. Liu, L. Zhang, J. Zhang and D. P. Wilkinson, *Chem. Soc. Rev.*, **2012**, *41*, 5654.

2 (a) L. Schlapbach and A. Züttel, *Nature,* **2001**, *414*, 353; (b) R. J. Keaton, J. M. Blacquiere and R. T. Baker, *J. Am. Chem. Soc.*, **2007**, *129*, 1844; (c) Z.-G. Huang and

T. Autrey, *Energy Environ. Sci.*, **2012**, *5*, 9257; (d) Q.-L. Zhu, N. Tsumori and Q. Xu, *Chem. Sci.*, **2014**, *5,* 195.

3 (a) A. Gutowska, L. Li, Y. Shin, C.-M. Wang, X.-S. Li, J. C. Linehan, R. S. Smith, B. D. Kay, B. Schmid, W. Shaw, M. Gutowski and T. Autrey, *Angew. Chem., Int. Ed.*, **2005**, *44*, 3578; (b) M. Chandra and Q. Xu, *J. Power Sources*, **2006**, *156*, 190; (c) Q. Xu and M. J. Chandra, *J. Alloys Compd*., **2007**, *446*, 729; (d) S.-K. Kim, W.-S. Han, T.-J. Kim, T.-Y. Kim, S. W. Nam, M. Mitoraj, L. Piekos, A. Michalak, S. J. Hwang and S. O. Kang, *J. Am. Chem. Soc.*, **2010**, *132*, 9954; (e) U. Sanyal, U. B. Demirci, B. R. Jagirdar and P. Miele, *ChemSusChem*, **2011**, *4*, 1731; (f) S.-K. Kim, T.-J. Kim, T.-Y. Kim, G. Lee, J. T. Park, S. W. Nam and S. O. Kang, *Chem. Commun*., **2012**, *48*, 2021; (g) M. Yadav and Q. Xu, *Energy Environ. Sci.*, **2012**, *5*, 9698.

4 (a) H.-L. Jiang and Q. Xu, *Catal. Today*, **2011**, **170**, 56; (b) Q. Xu and M. Chandra, *J. Power Sources*, **2006**, *163*, 364.

5 (a) N. Mohajeri, A. T-Raissi and O. Adebiyi, *J. Power Sources*, **2007**, *167*, 482; (b) S. Basu, A. Brockman, P. Gagare, Y. Zheng, P. V. Ramachandran, W. N. Delgass and J. P. Gore, *J. Power Sources*, **2009**, *188*, 238; (c) F. Durap, M. Zahmakiran and S. Ökar, *Int. J. Hydrogen Energy*, **2009**, *34*, 7223; (d) S. Karahan, M. Zahmakiran and S. Özkar, *Chem. Commun*., **2012**, *48*, 1180; (e) D.-C. Zhong, K. Aranishi, A. K. Singh, U. B. Demirci and Q. Xu, *Chem. Commun.*, **2012**, *48*, 11945; (f) A. Aijaz, A. Karkamkar, Y. J. Choi, N. Tsumori, E. Rönnebro, T. Autrey, H. Shioyama and Q. Xu, *J. Am. Chem. Soc*., **2012**, *134*, 13926.

6 (a) J.-M. Yan, X.-B. Zhang, S. Han, H. Shioyama and Q. Xu, *Angew. Chem., Int. Ed.*, **2008**, *47*, 2287; (b) T. Umegaki, J.-M. Yan, X.-B. Zhang, H. Shioyama, N. Kuriyama and Q. Xu, *Int. J. Hydrogen Energy*, **2009**, *34*, 3816; (c) Ö. Metin, V. Mazumder, S. Özkar and S. H. Sun, *J. Am. Chem. Soc*., **2010**, *132*, 1468; (d) P.-Z. Li, A. Aijaz and Q. Xu*, Angew. Chem., Int. Ed.*, **2012**, *51*, 6753.

7 (a) J.-M. Yan, X.-B. Zhang, H. Shioyama and Q. Xu, *J. Power Sources*, **2010**, *195*, 1091; (b)T. Umegaki, J.-M. Yan, X.-B. Zhang, H. Shioyama, N. Kuriyama and Q. Xu, *J. Power Sources*, **2010**, *195*, 8209.

8 (a) X. H. Zhou, Z. X. Chen, D. H. Yan and H. B. Lu, *J. Mater. Chem*., **2012**, *22*, 13506; (b) K. Aranishi, A. K. Singh and Q. Xu, *ChemCatChem*, **2013**, *5*, 2248.

9 (a) J.-M. Yan, X.-B. Zhang, S. Han, H. Shioyama and Q. Xu, *J. Am. Chem. Soc.,* **2009**, *131*, 2778; (b) H.-L. Jiang, T. Akita and Q. Xu, *Chem. Commun.*, **2011**, *47*, 10999.

10 (a) N. Patel, R. Fernandes, G. Guella, A. Kal, A. Miotello, B. Patton and C. Zanchetta, *J. Phys. Chem. C*, **2008**, *11*, 6968; (b) N. Patel, R. Fernandes, G. Guella and A. Miotello, *Appl. Catal. B*, **2010**, *95*, 137.

11 (a) M. Eddaoudi, J. Kim, N. Rosi, D. Vodak, J. Wachter, M. O'Keeffe and O. M. Yaghi, *Science*, **2002**, *295*, 469; (b) S. Kitagawa, R. Kitaura and S. Noro, *Angew. Chem., Int. Ed.*, **2004**, *43*, 2334; (c) J.-P. Zhang, X.-C. Huang and X.-M. Chen, *Chem. Soc. Rev.*, **2009**, *38*, 2385; (d) G. Férey and C. Serre, *Chem. Soc. Rev.*, **2009**, *38*, 1380; (e) B. Chen, S. Xiang and G. Qian, *Acc. Chem. Res.,* **2010**, *43*, 1115; (f) H.-L. Jiang and Q. Xu, *Chem. Commun*., **2011**, *47*, 3351; (g) D. Zhao, D. J. Timmons, D. Yuan and H.-C. Zhou, *Acc. Chem. Res*., **2011**, *44*, 123.

12 (a) A. Henschel, K. Gedrich, R. Kraehnert and S. Kaskel, *Chem. Commun.*, **2008**, 4192; (b) S. Proch, J. Herrmannsdörfer, R. Kempe, C. Kern, A. Jess, L. Seyfarth and J. Senker, *Chem.—Eur. J*., **2008**, *14*, 8204; (c) H.-L. Jiang, T. Akita, T. Ishida, M. Haruta and Q. Xu, *J. Am. Chem. Soc*., **2011**, *133*, 1304; (d) X. Gu, Z.-H. Lu, H.-L. Jiang, T. Akita and Q. Xu, *J. Am. Chem. Soc.*, **2011**, *133*, 11822; (e) G. Lu, S. Li, Z. Guo, O. K. Farha, B. G. Hauser, X. Qi, Y. Wang, X. Wang, S. Han, X. Liu, J. S. DuChene, H. Zhang, Q. Zhang, X. Chen, J. Ma, S. C. J. Loo, W. D. Wei, Y. Yang, J. T. Hupp and F. Huo, *Nat. Chem.*, **2012**, *4*, 310; (f) A. Dhakshinamoorthy and H. Garcia, *Chem. Soc. Rev.,* **2012**, *41*, 5262; (g) C. Wang, K. E. deKrafft and W. Lin, *J. Am. Chem. Soc.*, **2012,** *134*, 7211; (h) S.-L. Li and Q. Xu, *Energy Environ. Sci.*, **2013**, *6*, 1656; (i) Q.-L. Zhu and Q. Xu, *Chem. Soc. Rev.*, **2014**, *43*, 5468.

13 (a) S. Hermes, M.-K. Schröter, R. Schmid, L. Khodeir, M. Muhler, A. Tissler, R. W. Fischer and R. A. Fischer, *Angew. Chem., Int. Ed.*, **2005**, *44*, 6237; (b) M. Müller, O. I. Lebedev and R. A. Fischer, *J. Mater. Chem*., **2008**, *18*, 5274; (c) F. Schröder, S. Henke, X. Zhang and R. A. Fischer, *Eur. J. Inorg. Chem.*, **2009**, 3131; (d) Y. K. Park, S. B. Choi, H. J. Nam, D. Jung, H. C. Ahn, K. Choi, H. Furukawa and J. Kim, *Chem. Commun*., **2010**, *46*, 3086; (e) M. Meilikhov, K. Yusenko, D. Esken, S. Turner, G. Van Tendeloo and R. A. Fischer, *Eur. J. Inorg. Chem.*, **2010**, 3701; (f) J.

Hermannsdörfer, M. Friedrich, N. Miyajima, R. Q. Albuquerque, S. Kümmel and R. Kempe, *Angew. Chem., Int. Ed*., **2012**, *51*, 11473; (g) H. R. Moon, D.-W. Limb and M. P. Suh, *Chem. Soc. Rev.*, **2013**, *42*, 1807; (h) A. Aijaz and Q. Xu, *J. Phys. Chem. Lett*., **2014**, *5*, 1400.

14 (a) Q.-L. Zhu, J. Li and Q. Xu, *J. Am. Chem. Soc*., **2013**, *135*, 10210; (b) J. Li, Q.-L. Zhu and Q. Xu, *Chem. Commun*., **2014**, *50*, 5899.

15 G. Férey, C. Mellot-Draznieks, C. Serre, F. Millange, J. Dutour, S. Surblé and I. Margiolaki, *Science*, **2005**, *309*, 2040.

16 C. D. Wagner, W. N. Riggs, L. E. Davis and J. F. Moulder, Handbook of X-Ray Photoelectron Spectroscopy: A Reference Book of Standard Spectra for Use In X-Ray Photoelectron Spectroscopy (Ed.: G. E. Muilenberg), Physical Electronics Division Perkin-Elmer Corp., Minnesota, 1978.

17 (a) H.-L. Jiang and Q. Xu, *J. Mater. Chem*., **2011**, *21*, 13705; (b) A. K. Singh and Q. Xu, *ChemCatChem*, **2013**, *5*, 652.

18 (a) B. Hammer and J. K. Nørskov, *Adv. Catal.*, **2000**, *45*, 71; (b) R. Ferrando, J. Jellinek and R. L. Johnston, *Chem. Rev.*, **2008**, *108*, 845.

19 P.-Z. Li, K. Aranishi and Q. Xu, *Chem. Commun.*, **2012**, *48*, 3173.

Chapter 4

Pd nanoparticles supported on hierarchically porous carbon derived from assembled nanoparticles of zeolitic imidazolate framework (ZIF-8) for methanol electrooxidation

Hierarchically porous carbons with both micro- and mesopores have been synthesized by direct carbonization of assembled nanoparticles of zeolitic imidazolate framework (ZIF-8) at different temperatures (800, 900, 1000 and 1100 °C). At the carbonization temperature of 1000 °C, the highest surface area (1105 m^2 g^{-1}) and the largest pore volume (0.95 cm^3 g^{-1}) of ZIF-8-derived carbon (ZC) were achieved. The resultant porous ZCs have been used as supports for Pd electrocatalysts for methanol electrooxidation in alkaline media for the first time. Pd/ZC-1000 catalyst is the most active and electrochemically stable among the Pd catalysts supported on ZCs prepared at 800-1100 °C. Moreover, the catalytic activity of Pd/ZC-1000 is 5 times higher than that of Pd supported on the commercial carbon black Vulcan XC-72R at the same Pd loading.

4.1 Introduction

In recent years, enormous attention has been paid to the development of the direct methanol fuel cell (DMFC) as a promising power source for portable devices and electric vehicles due to its low-cost, high power density and low operating temperature.[1-4] Up to date, Pt and Pt-based catalysts are generally considered to be the most common electrocatalysts for methanol electrooxidation reaction (MOR).[1-3] However, Pt-based catalysts suffer from some disadvantages such as high cost, readily CO poisoning and still slow kinetics of methanol electrooxidation, which severely restrict their commercial applications for DMFCs.[1-3] Therefore, it is urgent to develop low-cost electrocatalysts with highly improved kinetics toward MOR. Recently, Pd is considered to be a promising alternative to Pt since Pd or Pd-based electrocatalysts exhibit extremely high activity for electrooxidation of alcohols (e.g. methanol and ethanol) with low CO poisoning in alkaline medium.[4,25] Moreover, Pd is much cheaper and is at least 50 times more

available in the earth than Pt.[5]

In the view of the electrocatalysts used in the fuel cells, the high surface areas and large pore volumes of the support materials are required due to the fact that higher surface areas and larger pore volumes allow a better dispersion for the metal catalysts and provide an open network around the active catalysts for facile diffusion of fuels and products.[6-8] Recently, highly nanoporous carbons (NPCs) have attracted considerable attention due to their high surface area, large pore volume and good electrochemical properties.[9-11] Generally, NPCs can be prepared via several methods, such as carbonization of polymeric aerogels, activation (physical or chemical) of carbon materials, nanocasting with hard-templates, and so on.[9-12] Owing to the highly ordered porous structures with abundant organic struts, and high surface areas and large pore volumes,[13-15] metal-organic frameworks (MOFs) would be promising candidates for applications as templates/precursors to prepare porous carbon materials through thermal conversion. Currently, several MOF-derived carbons have been reported, which present large surface area and high porosity, and show outstanding properties especially in the applications of gaseous or liquid adsorptions, catalyst supports, and electrode materials for electric double layer capacitors (EDLCs) and fuel cells.[16-19]

In this work, we report the synthesis of hierarchically porous carbons with both micro- and mesopores through direct carbonization of assembled nanoparticles of zeolitic imidazolate framework (ZIF-8) at different temperatures (800, 900, 1000 and 1100 °C), which have been used as supports for Pd electrocatalysts for methanol electrooxidation in alkaline media for the first time. The Pd catalyst supported on the ZIF-8-derived carbon (ZC) prepared by carbonization at 1000 °C was found to display an extremely high catalytic activity and electrochemical stability for methanol electrooxidation.

4.2 Experimental section

4.2.1 Materials and general methods

Methanol (CH_3OH, Tokyo Chemical Industry Co., Ltd., >99.8%), ethanol (C_2H_5OH, Kishida Chem. Co., >99.8%), hydrochloric acid (Wako Pure Chemical Industries, Ltd., 35.0-37.0%), triethylamine (EA, Chameleon reagent), 2-methylimidazole (MeIM, Tokyo

Chemical Industry Co., Ltd.), 5% Nafion® Dispersion solution DE 520 CS type (Wako Pure Chemical Industries, Ltd.), Vulcan XC-72R (Carbon, specific surface area = 240 $m^2 g^{-1}$, Cabot Corp., USA), zinc nitrate ($Zn(NO_3)_2 \cdot 6H_2O$, Wako Pure Chemical Industries, Ltd.), sodium hydroxide (NaOH, Chameleon Reagent, >98%), potassium hydroxide (KOH, Kishida Chem. Co., >85.0%), sodium borohyride ($NaBH_4$, Sigma-Aldrich, 99%), potassium tetrachloropalladate (K_2PdCl_4, Wako Pure Chemical Industries, Ltd., >97%) were used as received. All reagents were commercial and used without further purification. De-ionized water with a resistivity of 18.2 MΩ·cm was obtained by reverse osmosis followed by ion-exchange and filtration (RFD 250NB, Toyo Seisakusho Kaisha, Ltd., Japan). Powder X-ray diffraction (PXRD) measurements were carried out on a Rigaku UItima IV X-ray diffractometer with Cu Kα source (40 kV, 40 mA, λ= 0.154 nm). The surface area measurements were performed with N_2 adsorption/desorption isotherms at liquid nitrogen temperature (77 K) after dehydration under vacuum at 150 °C for 12 h using automatic volumetric adsorption equipment (Belsorp-max). The pore volume was calculated by a single point method at $P/P_0 = 0.99$. Scanning electron microscopic (SEM) analyses were carried with a Hitachi S-5000 field emission scanning electron microscope. Transmission electron microscope (TEM, TECNAI G^2 F20) equipped with energy dispersed X-ray detector (EDX) was applied for the detailed microstructure and composition information for the prepared samples. X-ray photoelectron spectroscopic (XPS) measurements were performed on a Shimadzu ESCA-3400 X-ray photoelectron spectrometer using an Mg Kα source (1253.6 eV) operating at 10 kV and 10 mA.

4.2.2 Synthesis of ZIF-8

A methanolic solution (500 mL) of zinc nitrate ($Zn(NO_3)_2 \cdot 6H_2O$, 7.4350 g) was added into a methanolic solution (500 mL) of 2-methylimidazole (4.1040 g) and triethylamine (9 mL) with ultrasonication for 30 min at room temperature. After that, the turbid solution was centrifuged to give a white solid, which was washed carefully with methanol and then dried at 80 °C for 12 h.

4.2.3 Preparation of ZIF-8-derived carbon (ZC)

The ZIF-8 sample (2.0 g) was transferred into a ceramic boat and placed into a temperature-programmed furnace under flowing Ar for 3 h to exclude air. Subsequently, the sample was heated from room temperature to 800, 900, 1000, or 1100 °C in 1.5 h, and then kept at the temperature for 8 h. After cooled down to room temperature under an argon flow, the resultant black materials were washed several times with a HCl (10 vol % in water) solution, then washed with de-ionized water and dried at 80 °C for 12 h to afford ZIF-8-derived carbon (denoted as ZC-800, ZC-900, ZC-1000, and ZC-1100).

4.2.4 Syntheses of Pd/ZC and Pd/XC-72R catalysts

The Pd catalyst supported by ZC or XC-72R was synthesized by a facile sodium hydroxide-assisted reduction method reported recenty.[20] Generally, 50 mg of ZC or XC-72R carbon powder dispersed in 1.25 mL of water was mixed with an aqueous solution of K_2PdCl_4 (0.30 M, 0.15 mL) and subsequently the aqueous suspension was further homogenized under ultrasonication for 30 min. Then 10 mg of $NaBH_4$ dissolved in 0.25 mL of 2.0 M NaOH solution was added into the above obtained suspension with vigorous shaking. In order to fully deposit the metallic nanoparticles onto the support, the mixture was shaken for another half an hour. Finally, the desired catalyst Pd/ZC or Pd/XC-72R was collected by centrifuging and washed with de-ionized water for several times and then dried under vacuum at 80 °C.

4.2.5 Electrode preparation and electrochemical performance test

Electrochemical properties of the catalysts were measured on a Solartron electrochemical workstation (SI1287) using a conventional three-electrode system with a catalyst modified glassy carbon (GC, Φ = 3 mm) working electrode, a platinum wire counter electrode and a saturated calomel reference electrode (SCE). Before the surface coating, the GC electrode was polished with 0.5 and 0.05 μm alumina suspensions, followed by washing ultrasonically with HNO_3-H_2O (1:1, v/v ratio) solution, ethanol and deionizer water sequentially. 15 mg of carbon-supported Pd catalyst, 0.8 mL of H_2O, 0.2

mL of ethanol and 24 μL of Nafion solution (5 wt%) were mixed under ultrasonication for 1 h. Then 3 μL of the homogeneously mixed catalyst ink was dropped on the surface of the GC electrode by using a micropipette and dried at room temperature for 4 h. The Pd loading on the electrode was controlled at 0.054 mg cm^{-2}. Before measurement, the electrolyte (1 M KOH or 1 M KOH + 1 M CH_3OH solution) was first de-aerated with highly pure N_2 for half an hour. All electrochemical measurements were performed at ambient temperature (~25 °C).

4.3 Results and discussion

4.3.1 ZIF-8 template/precursor

The highly porous zeolite-type MOF, ZIF-8, was chosen as both precursor and template in this work to afford the porous carbon by carbonization. The ZIF-8 framework [$Zn(MeIM)_2$; MeIM = 2-methylimidazole],[21] involving the N-containing methylimidazole ligand, may effectively functionalizes the resultant carbon with the N element, which is beneficial to the improvement of adsorption and electrochemical catalysis performance.[22]

Considering the fact that the pore texture of the resultant porous carbon is crucially determined by the pore characteristics of a MOF template, in this work we used ultrasonication to prepare assembled nanoparticles of ZIF-8, between which the voids correspond to mesopores.[23] In this method, methanolic solutions of precursors zinc nitrate, MeIM and triethylamine were mixed under ultrasonication for 30 min to give a white ZIF-8, which has well-defined XRD patterns with sharp peaks characteristic of a crystalline solid (Fig. 4.1). The nitrogen sorption isotherms of ZIF-8 exhibit a BET specific surface area of 1378 m^2 g^{-1} and a pore volume of 1.14 cm^3 g^{-1} (Fig. 4.2). The pore size distribution (PSD) derived by using the non-local density functional theory (NL-DFT) method displays the presence of both micropores (1.2 nm) and mesopores (3-20 nm) (Fig. 4.3). The scanning electron microscopic (SEM) images (Fig. 4.4) display that the particle size of ZIF-8 is 30-50 nm.

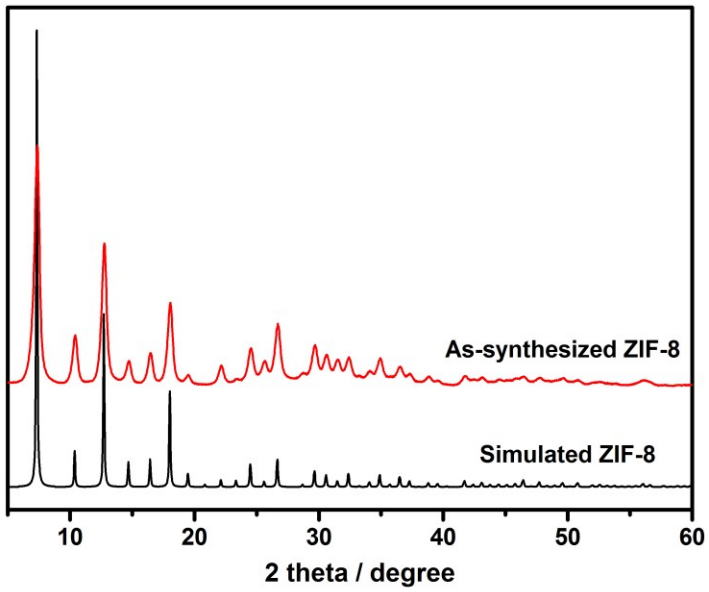

Fig. 4.1 Powder XRD patterns of ZIF-8.

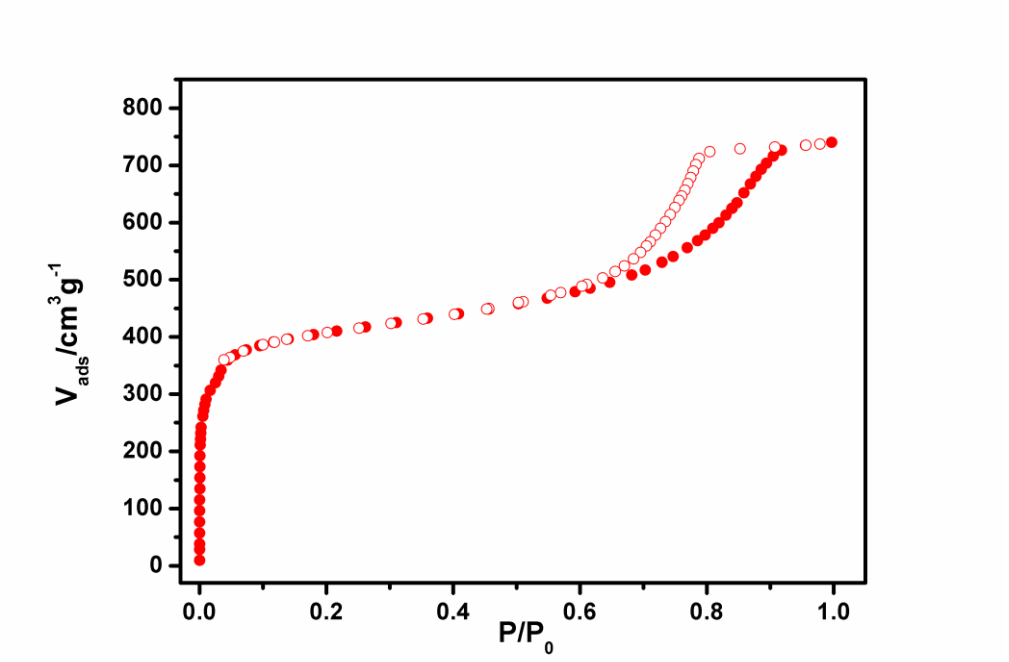

Fig. 4.2 N_2 sorption isotherms of the assembled nanoparticles of ZIF-8 at 77 K. Filled and open symbols represent adsorption and desorption branches, respectively.

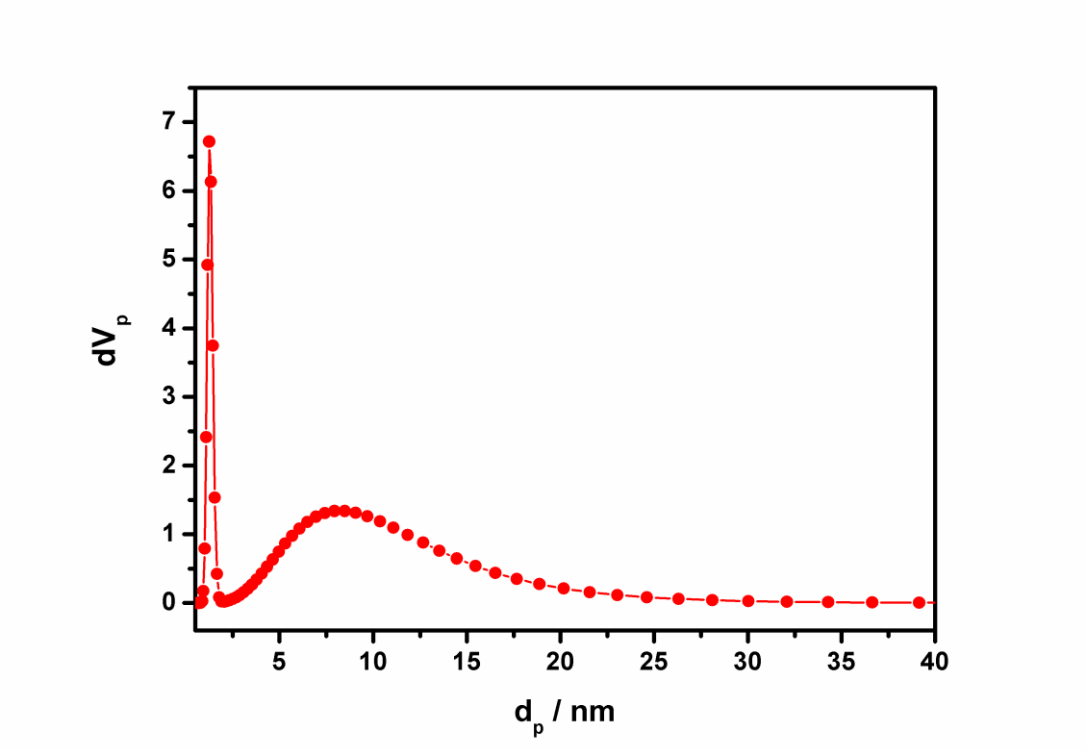

Fig. 4.3 The NL-DFT pore size distribution of the assembled nanoparticles of ZIF-8.

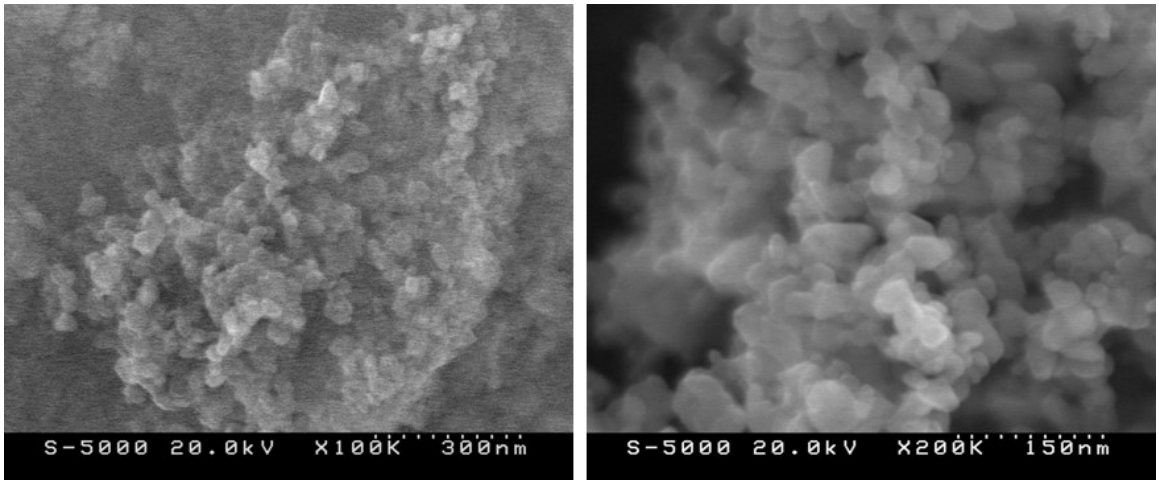

Fig. 4.4 The SEM images of the assembled nanoparticles of ZIF-8.

4.3.2 ZIF-8-derived carbon

Interestingly, hierarchically porous carbons are obtained with high yields by direct carbonization of the synthesized assembled nanoparticles of ZIF-8 at different temperatures (800, 900, 1000 and 1100 °C) in an argon flow. Fig. 4.5 shows the PXRD patterns of the carbon samples prepared at various carbonization temperatures. Two broad diffraction peaks located at around 25 and 44º, corresponding to (002) and (101) diffractions of graphitic carbon, can be observed. The broad nature of the diffraction bands suggests that the ZIF-8-derived carbon (ZC) materials are essentially amorphous. The increase in the intensity of the diffraction band at 2θ = 44º with increasing carbonization temperature indicates that more graphitic carbons can be generated at higher carbonization temperatures.

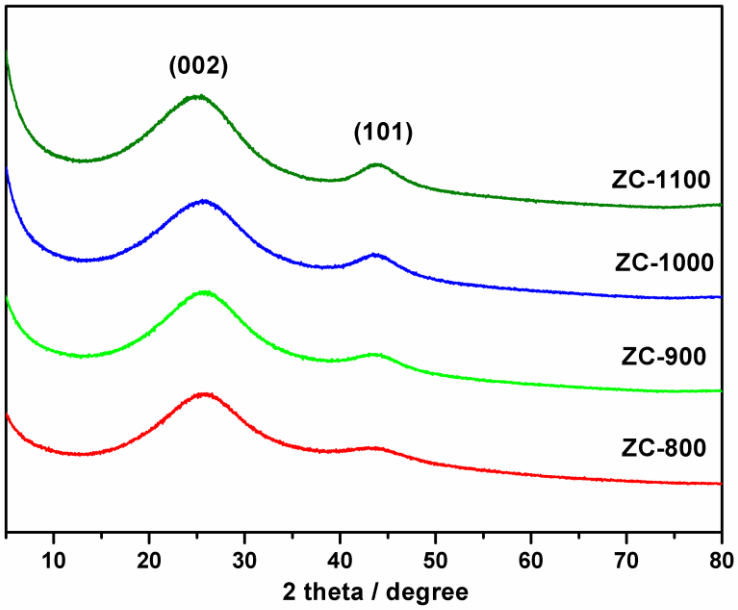

Fig. 4.5 Powder XRD patterns of carbon materials prepared by carbonization of assembled nanoparticles of ZIF-8 at various temperatures.

Nitrogen sorption experiments were performed to examine the surface areas and pore size distribution of these carbon materials. As shown in Fig. 4.6a, all of ZCs exhibit combined-characteristics of type I and IV isotherms, indicating that there are mesopores

in addition to micropores. Moreover, the ZCs have relatively comparable porosity with the BET surface areas in the range of 914-1105 m^2 g^{-1} and pore volumes between 0.73 and 0.95 cm^3 g^{-1} (Fig. 4.6a, Table 4.1). When the carbonization temperature increases to 1000 °C, the highest surface area (1105 m^2 g^{-1}) and the largest pore volume (0.95 cm^3 g^{-1}) were achieved, which are much higher than those of carbon black Vulcan XC-72R (240 m^2 g^{-1}, 0.28 cm^3 g^{-1}). The PSD of all ZIF-derived carbon materials demonstrates their hierarchical pore structure with both micro (1-2 nm) and mesopores (10-25 nm) (Fig. 4.6b), which is associated with the pore size distribution of their parent ZIF-8. The carbonization temperature appears to have some effect on the pore size distribution; with the increase of the temperature from 800 to 1000 °C, the higher proportion of the mesopore and higher surface area can be obtained. However, when the temperature increased from 1000 to 1100 °C, the surface area of ZC decreased, which may be due to the high degree of graphiticity at this high temperature (Fig. 4.5). The TEM images further confirm the uniqueness of the hierarchical pore structure of ZC-1000, which possesses 3D frameworks with micro (≤ 2 nm) and mesopores (10-25 nm) (Fig. 4.7). The PSD of carbon Vulcan XC-72R displays the presence of micro- and mesopores; the voids between the aggregated nanosized (30-60 nm) carbon particles, as observed by TEM (*vide infra*), account for the observed mesopores in PSD (Fig. 4.6b, Table 4.1).[24]

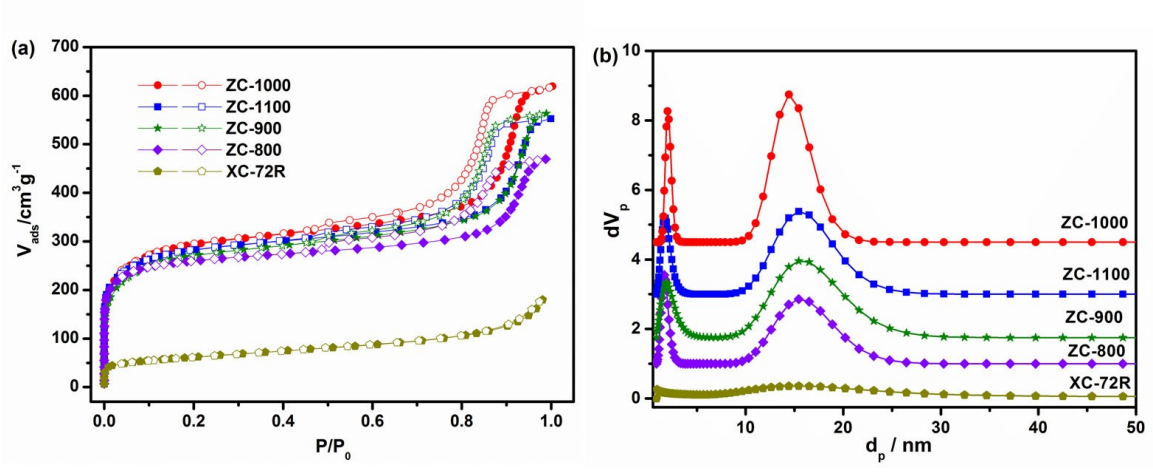

Fig. 4.6 (a) Nitrogen sorption isotherms at 77 K (Filled and open symbols represent adsorption and desorption branches, respectively), and (b) NL-DFT pore size distribution of ZCs and XC-72R.

Table 4.1. Summary of the surface areas and pore volume distributions for the carbons

Sample	Specific surface area[a] ($m^2\ g^{-1}$)	Total pore volume[b] ($cm^3\ g^{-1}$)	Mesopore volume[c] ($cm^3\ g^{-1}$)	Micropore volume[d] ($cm^3\ g^{-1}$)
ZC-1100	1029	0.8512	0.4872	0.3640
ZC-1000	1105	0.9524	0.5832	0.3692
ZC-900	1020	0.8715	0.5314	0.3401
ZC-800	914	0.7259	0.3763	0.3496
XC-72R	240	0.2781	0.2257	0.0524

[a] Calculated from the BET surface area analysis.

[b] Calculated by a single point method at $P/P_0 = 0.99$.

[c] Calculated using a t-plot method.

[d] Calculated by subtracting the total pore volume with the mesopore volumes.

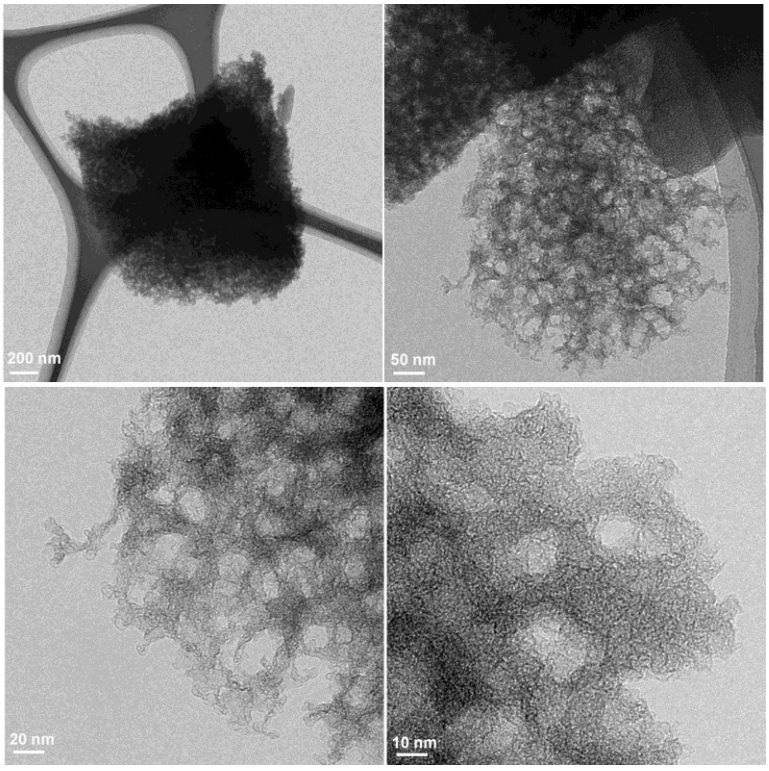

Fig. 4.7 TEM images of ZC-1000 at different magnifications.

4.3.3 Pd catalyst supported on carbons

Due to its unique structure, ZC-1000 offers high surface area, large mesopore volume, and highly graphitic degree, which make it a potential candidate as the support material for fuel cell electrocatalysts. We, for the first time, loaded the Pd nanoparticles on ZC-1000 as electrocatalyst for methanol oxidation. For comparison, Pd nanoparticles were also supported on the well-used commercial carbon black Vulcan XC-72R with the same loading. Fig. 4.8 shows the XRD patterns of catalysts Pd/ZC-1000 and Pd/XC-72R. It should be noted that the two broad peaks are located at around 25 and 44º, corresponding to (002) and (101) diffractions of graphitic carbon (Fig. 4.9). The diffraction peaks at the 2θ of 39.78º, 46.26º and 67.58º correspond to the (111), (200) and (220) facets of Pd nanocrystals. The BET surface areas of ZC-1000 and Pd/ZC-1000 are 1105 and 953 m^2 g^{-1}, respectively. The decreases in the amount of N_2 sorption of Pd/ZC-1000 indicate that the pores of the host framework of ZC-1000 are partially occupied by highly dispersed Pd NPs and/or blocked by the NPs located on surface (Fig. 4.10).

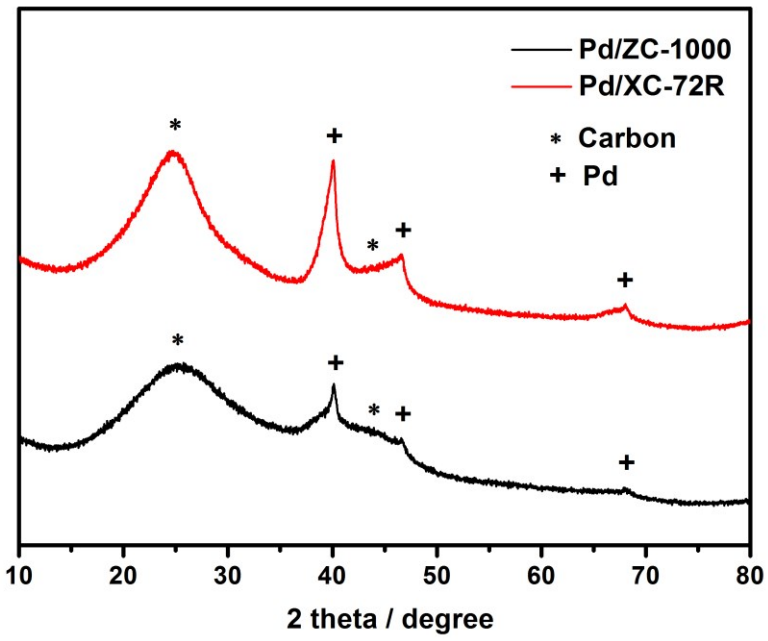

Fig. 4.8 Powder XRD patterns of Pd/ZC-1000 and Pd/XC-72R.

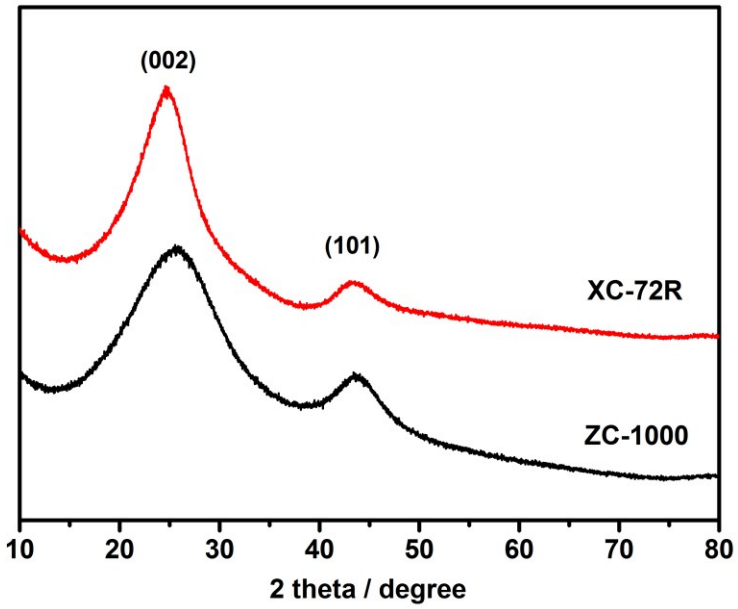

Fig. 4.9 Powder XRD patterns of ZC-1000 and XC-72R.

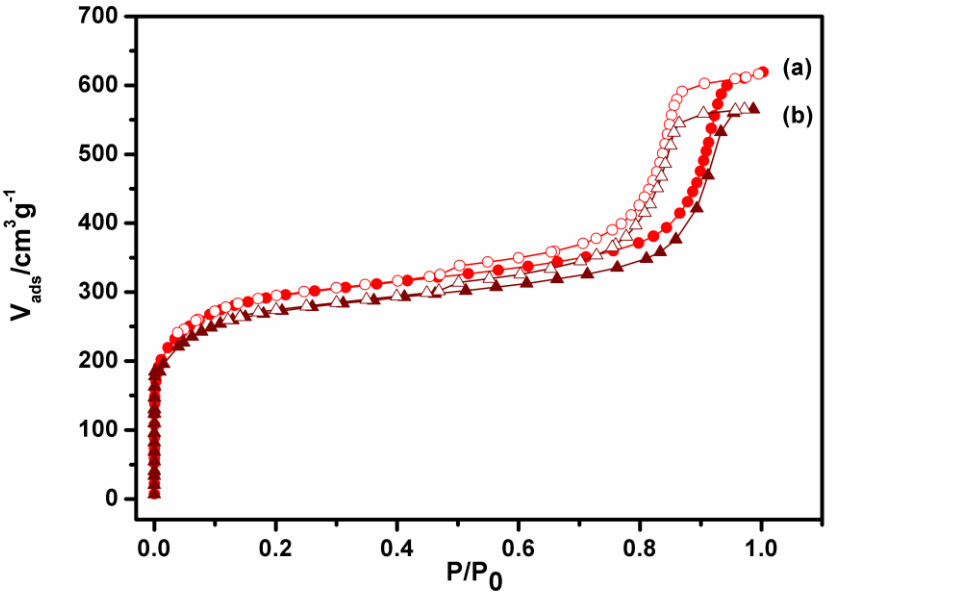

Fig. 4.10 Nitrogen sorption isotherms of (a) ZC-1000 and (b) Pd/ZC-1000. Filled and open symbols represent adsorption and desorption branches, respectively.

The Pd/ZC-1000 catalyst was further characterized by transmission electron microscopic (TEM), high-angle annular dark-field scanning TEM (HAADF-STEM) and energy-dispersive X-ray spectroscopy (EDX) analyses (Fig. 4.11). Compared to the Pd NPs (average particle size, 3.0 nm) immobilized on the surface of XC-72R carbon particles (30-60 nm) (Fig. 4.12), the Pd NPs are uniformly dispersed into the highly porous framework of ZC-1000 with a smaller average particle size of 2.4 nm (Fig. 4.11), which will lead to a higher surface area of the Pd catalysts and subsequently a better electrocatalytic activity (*vide infra*).

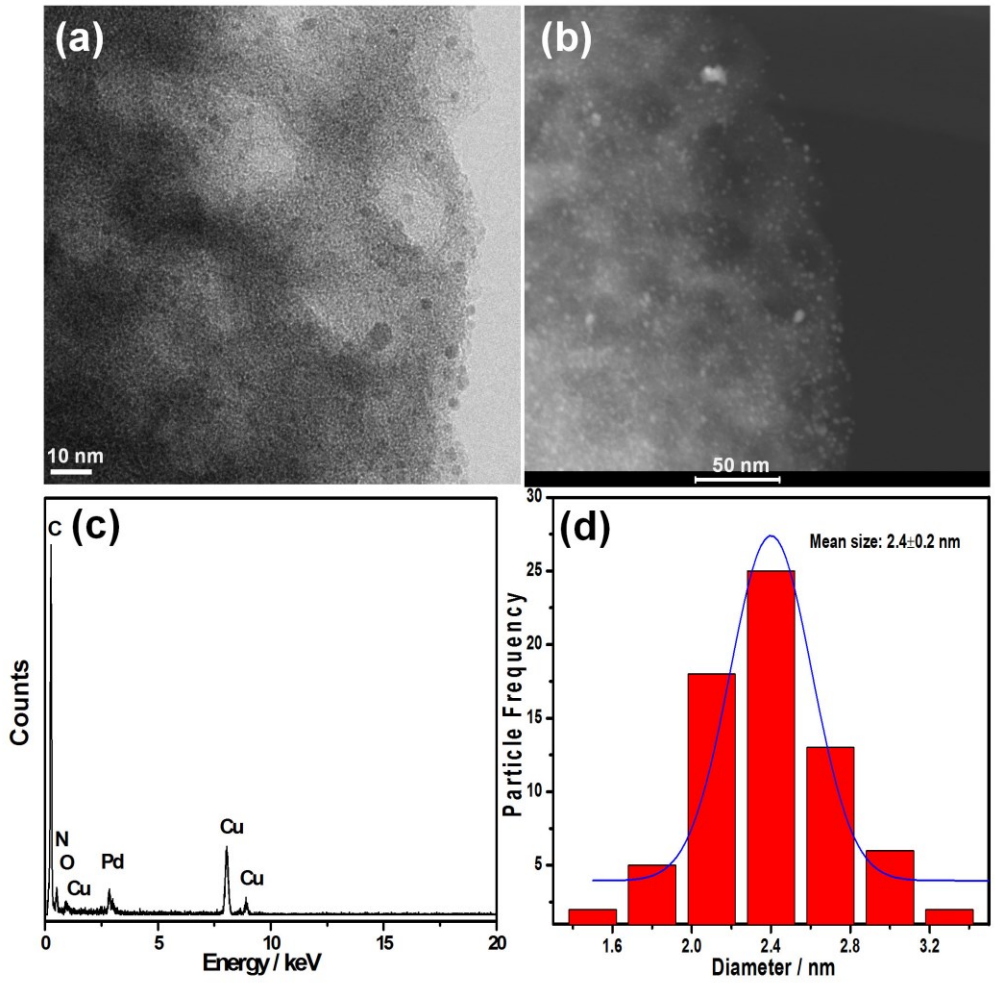

Fig. 4.11 Representative (a) TEM and (b) HAADF-STEM images, (c) EDX spectrum, and (d) Pd nanoparticle size distribution histogram of Pd/ZC-1000. The signal of Cu in (c) was from the TEM grid.

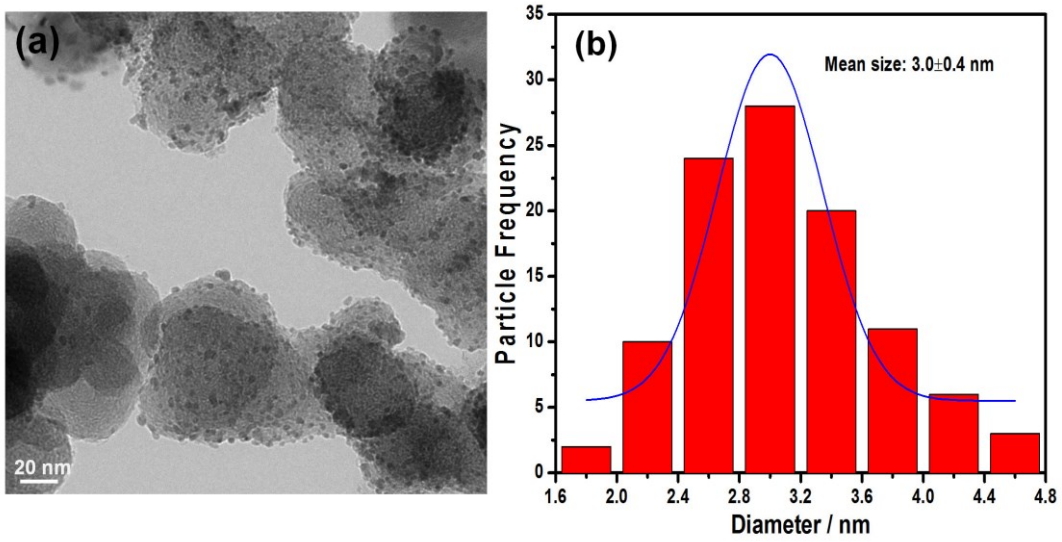

Fig. 4.12 (a) TEM image and (b) the corresponding particle size distribution histogram of Pd/XC-72R.

To obtain further insights into the structure-function correlations, X-ray photoelectron spectroscopy (XPS) was applied to Pd/ZC-1000 at the Pd 3d and N 1s levels (Fig. 4.13). Well-defined peaks are observed at 335.5 and 341.0 eV for Pd $3d_{3/2}$ and $3d_{5/2}$, corresponding to metallic Pd^0. In addition, the N 1s spectrum of Pd/ZC-1000 (Fig. 4.13b) suggests the incorporation of nitrogen into the carbon material, which further confirms that the N-doped carbon has been derived from ZIF-8.

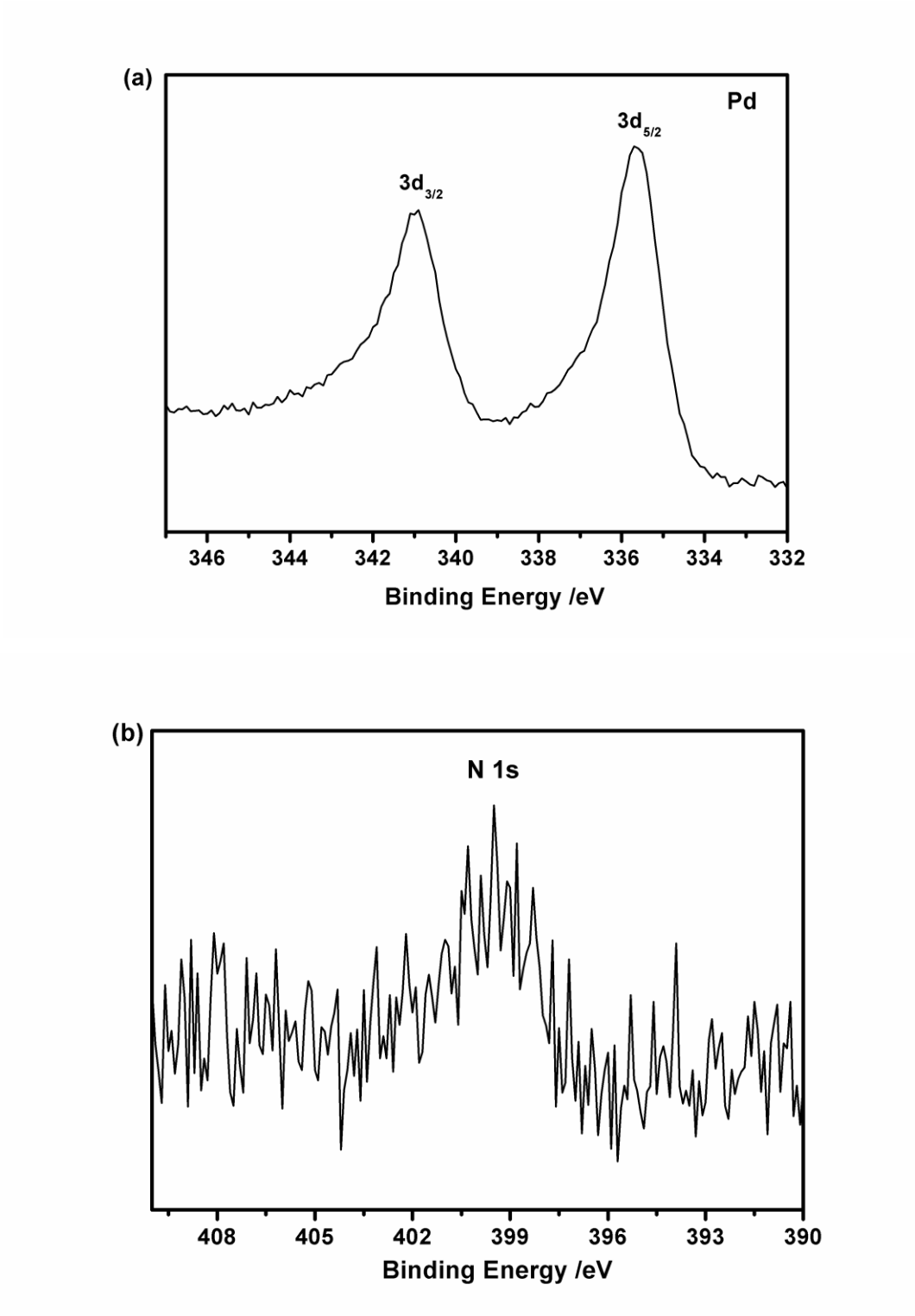

Fig. 4.13 XPS spectra for Pd/ZC-1000 at (a) Pd $3d_{3/2}$ and $3d_{5/2}$ and (b) N 1s levels.

4.3.4 Electrooxidation of methanol over Pd catalyst supported on carbons

The electrochemical activities of the catalysts were tested by cyclic voltammogram (CV) for the methanol electrooxidation reaction (MOR) as the anodic half-cell reaction in DMFCs. The corresponding CV curves of catalysts Pd/carbons are shown in Fig. 4.14, where the current density has been defined as the current for the specific area of the working electrode. The electrooxidation of methanol is characterized by two well-defined current peaks: one in the forward scan corresponds to the oxidation of freshly chemsorbed methanol species, and the other one in the reverse scan is primarily associated with the removal of carbonaceous species that have not been completely oxidized in the forward scan.[25] Therefore, the higher oxidation peak current density in the forward scan (I_f) indicates the higher electrocatalyic activity of the catalysts for the methanol oxidation reaction. It is obvious that after excluding the double layer currents, Pd/ZC-1000 displays much higher I_f for methanol oxidation compared to Pd/ZC-800, Pd/ZC-900 and Pd/ZC-1100 under the same conditions (Fig. 4.14, Fig. 4.15 and Table 4.3), which may be contributed by the combined total effects of the high graphitic degree (Fig. 4.5) and high surface area (Fig. 4.6) of ZC-1000. Specifically, the increase in the graphitic degree of carbon can not only enhance the conductivity but also decrease the carbon corrosion at the high potential and oxidizing environment.[26] In addition, a large surface area can improve the dispersion of the catalyst with a narrow size distribution.

It is noteworthy that the catalytic activity of Pd/ZC-1000 (45.20 mA cm^{-2}) is 5 times higher than that of Pd/XC-72R (9.36 mA cm^{-2}) at the same Pd loading (Fig. 4.14, Fig. 4.15 and Table 4.3). This significantly enhanced electrocatalytic activity of Pd/ZC-1000 can be attributed to the higher surface area and the hierarchically porous network of ZC-1000. The higher surface area can facilitate the dispersion of Pd catalyst on the surface or in the pores of the support with a small size, as confirmed by the TEM observations (Fig. 4.11 and 4.12). The hierarchically porous 3-dimensional (3D) network of ZC-1000 is favorable for the good conductivity compared with the aggregation of carbon particles of Vulcan XC-72R, which are poorly connected.[24] In addition, the nitrogen atoms doped in the ZC-1000 structure (Fig. 4.13b) may interact with the

methanol molecules via hydrogen bonds, which can accelerate the charge transfer kinetics of the methanol at Pd/ZC-1000 as previously reported.[22] To the best of our knowledge, the mass activity (j_f) of Pd/ZC-1000 in this work is the highest among those of Pd NPs supported on other carbon materials for methanol electrooxidation in alkaline media in previous work (Table 4.2). Therefore, ZC-1000 is a promising catalyst support for the direct methanol fuel cell applications.

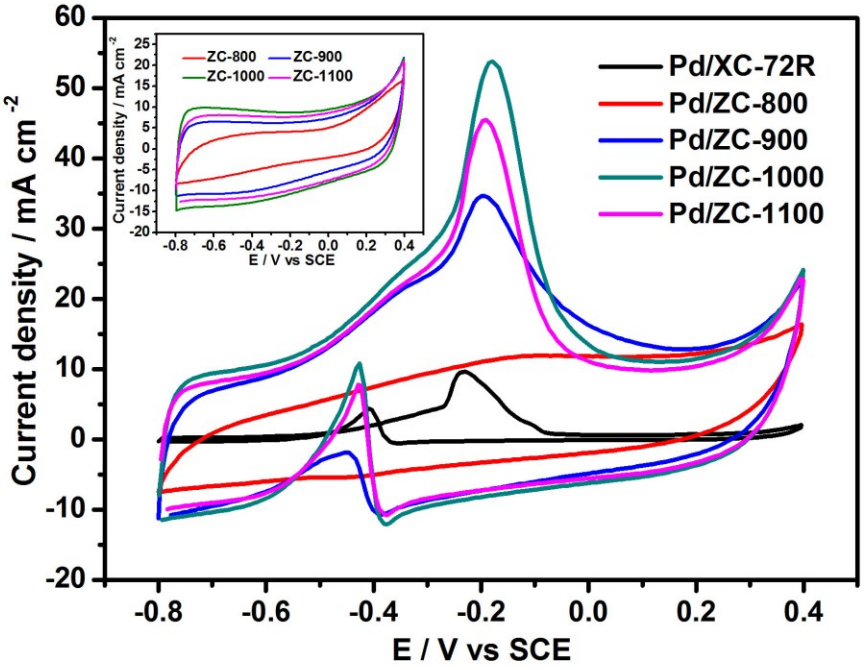

Fig. 4.14 Cyclic voltammograms of Pd/ZC and Pd/XC-72R electrodes in 1 M KOH solution containing 1 M CH_3OH with sweep rate of 50 mV s^{-1} at room temperature. Pd loading: 0.054 mg cm^{-2}. Inset is the CVs of ZC electrodes in 1 M KOH solution containing 1 M CH_3OH with sweep rate of 50 mV s^{-1} at room temperature.

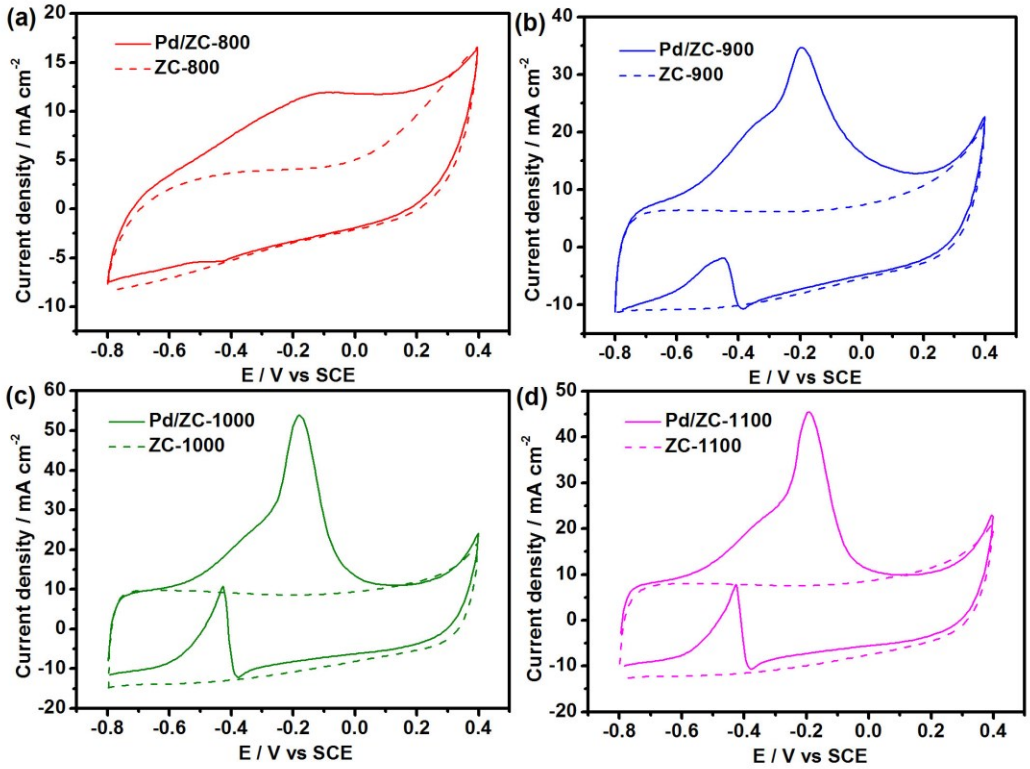

Fig. 4.15 Cyclic voltammograms of Pd/ZC and ZC electrodes in 1 M KOH solution containing 1 M CH_3OH with sweep rate of 50 mV s^{-1} at room temperature. Pd loading: 0.054 mg cm^{-2}.

Table 4.2. The forward anodic peak current density (mass activity j_f) in CVs of the Pd catalyst supported on different carbon materials for methanol electrooxidation in alkaline media

Catalyst electrodes	Solutions	Scan rate (mV s^{-1})	j_f (mA mg^{-1})	Ref.
Pd/CMS[a]/CRE[b]	1.0 M MeOH + 1.0 M KOH	5	500	25a
Pd/graphite block	1.0 M MeOH + 0.5 M NaOH	50	80	25b
Pd/PVP-graphene/GCE[c]	0.5 M MeOH + 1.0 M NaOH	100	250	25c
Pd/CNTs[d]/GCE	0.5 M MeOH + 1.0 M KOH	50	274.5	25d
Pd/VrGO[e]/GCE	1.0 M MeOH + 1.0 M KOH	50	620.1	25e
Pd/ZC-1000/GCE	1.0 M MeOH + 1.0 M KOH	50	837.0	This work
Pd/XC-72R/GCE	1.0 M MeOH + 1.0 M KOH	50	173.3	This work

[a] carbon microspheres. [b] carbon rod electrode. [c] glassy carbon electrode. [d] carbon naotubes.
[e] vertically oriented reduced graphene oxide.

The electrochemical stability of Pd-based catalysts for methanol oxidation was then investigated by chronoamperometric experiments at -0.25 V. As displayed in Fig. 4.16, Pd/ZC-1000 exhibits a slower current decay over time and the highest current at the time of 3000 s in comparison with other Pd/carbon catalysts (Table 4.3), proving a higher tolerance to the carbonaceous species generated during methanol oxidation.

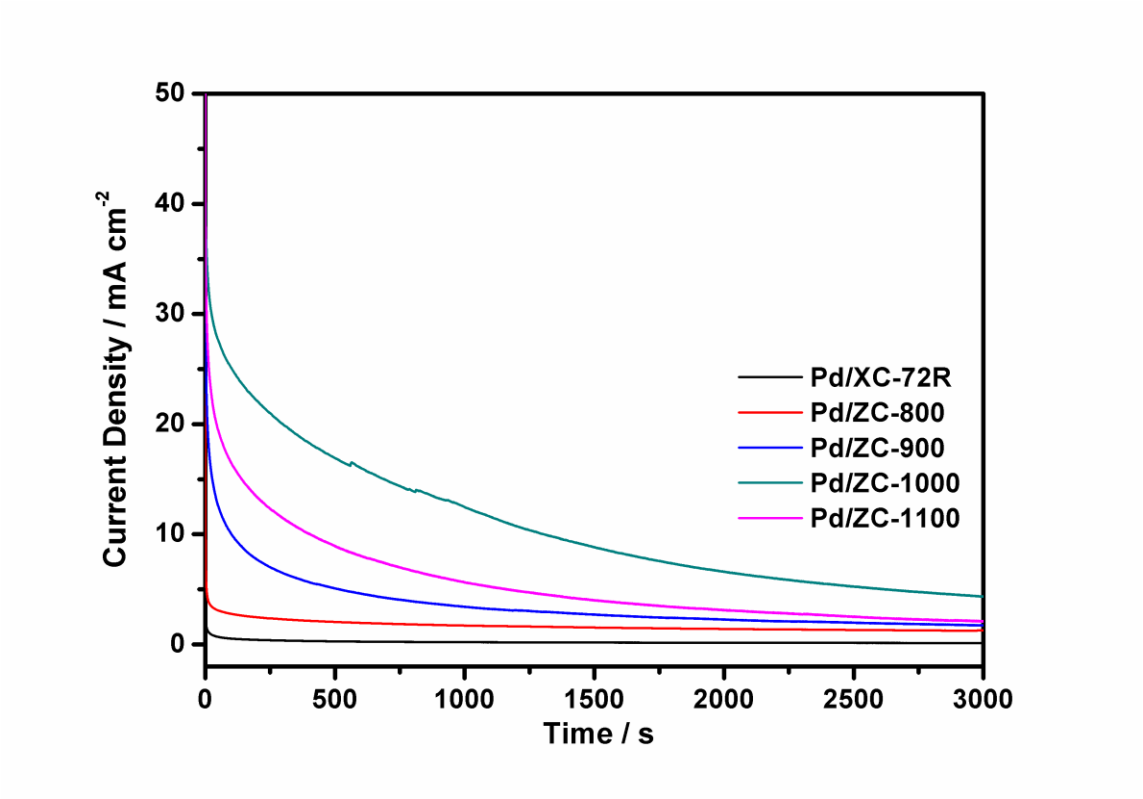

Fig. 4.16 Chronoamperometric curves of methanol oxidation on Pd/ZC electrodes and Pd/XC-72R electrode in 1 mol KOH containing 1 M CH_3OH at -0.25 V.

Table 4.3. The forward anodic peak current density in CVs (specific activity I_f and mass activity j_f) and the current density at the time of 3000 s in chronoamperometry (I_s) for the methanol electrooxidation over different catalysts

Catalysts	Specific activity I_f (mA cm^{-2})	Mass activity j_f (mA mg^{-1})	I_s (mA cm^{-2})
Pd/ZC-1100	37.86	701.1	2.09
Pd/ZC-1000	45.20	837.0	4.36
Pd/ZC-900	28.42	526.3	1.75
Pd/ZC-800	7.64	141.5	1.28
Pd/XC-72R	9.36	173.3	0.13

4.4 Conclusion

The hierarchically porous carbons with both micro- and mesopores have been synthesized by direct carbonization of assembled nanoparticles of ZIF-8 at different temperatures (800, 900, 1000 and 1100 °C). At the carbonization temperature of 1000 °C, the highest surface area (1105 m^2 g^{-1}) and the largest pore volume (0.95 cm^3 g^{-1}) of ZIF-8-derived carbon (ZC) can be achieved. For the first time, the porous ZCs have been used as supports for Pd electrocatalyst for methanol electrooxidation in alkaline media. Pd/ZC-1000 catalyst shows the highest electrochemical activity and stability among the ZC-supported Pd catalysts. Furthermore, the catalytic activity of Pd/ZC-1000 is 5 times higher than that of Pd/XC-72R at the same Pd loading. The unique performance of Pd/ZC-1000 represents a promising step toward the practical applications of MOF-derived carbons as support materials for electrocatalysts in fuel cells.

References

1 (a) Y. X. Chen, A. Miki, S. Ye, H. Sakai and M. Osawa, *J. Am. Chem. Soc*., **2003**, *125*, 3680; (b) Y. L. Hsin, K. C. Hwang and C. Yeh, *J. Am. Chem. Soc*., **2007**, *129*, 9999.

2 (a) H. Qiao, T. Kasajima, M. Kunimatsu, N. Fujiwara and T. Okada, *J. Electrochem. Soc.,* **2006**, *153*, A42; (b) J. N. Tiwari, R. N. Tiwari, G. Singh and K. S. Kim, *Nano Energy,* **2013**, *2*, 553.

3 (a) H.-J. Huang and X. Wang, *J. Mater. Chem. A,* **2014**, *2*, 6266; (b) A. B. A. A. Nassr, I. Sinev, M.-M. Pohl, W. Grünert and M. Bron, *ACS Catal.,* **2014**, *4*, 2449.

4 (a) C. Bianchini and P. K. Shen, *Chem. Rev*., **2009**, *109*, 4183; (b) E. Antolini, *Energy Environ. Sci.,* **2009**, *2*, 915; (c) M. Sawangphruk, A. Krittayavathananon and N. Chinwipas, *J. Mater. Chem. A,* **2013**, *1*, 1030.

5 (a) O. Savadogo, K. Lee, K. Oishi, S. Mitsushima, N. Kamiya and K.-I. Ota, *Electrochem. Commun.*, **2004**, *6*, 105; (b) P. K. Shen and C.-W. Xu, *Electrochem. Commun.*, **2006**, *8*, 184.

6 (a) J. M. Planeix, N. Coustel, B. Coq, V. Brotons, P. S. Kumbhar, R. Duatartre, P. Ganestes, P. Bernier and P. M. Ajayan, *J. Am. Chem. Soc*., **1994**, *116*, 7935; (b) M. C.

R. Román-Martinez, D. Cazorla-Amorós, A. Linares-Solano, C. Salinas-Martïnez De Lecea, H. Yamashida and M. Anpo, *Carbon*, **1995**, *33*, 3.

7 (a) G.-G. Park, T.-H. Yang, Y.-G. Yoon, W.-Y. Lee and C. S. Kim, *Int. J. Hydrogen Energy*, **2003**, *28*, 645; (b) V. Raghuveer and A. Manthiram, *Electrochem. Solid-State Lett.,* **2004**, *7*, A336.

8 H. T. Zheng, Y.-L. Li, S.-X. Chen and P. K. Shen, *J. Power Sources*, **2006**, *163*, 371.

9 (a) S. Flandrois and B. Simon, *Carbon*, **1999**, *37*, 165; (b) T. Kyotani, *Carbon*, **2000**, *38*, 269; (c) Z. Hu, M. P. Srinivasan and Y. Ni, *Adv. Mater.*, **2000**, *12*, 62; (d) R. Ryoo, S. H. Joo, M. Kruk and M. Jaroniec, *Adv. Mater.*, **2001**, *13*, 677; (e) J. Lee, J. Kim and T. Hyeon, *Adv. Mater.*, **2006**, *18*, 2073.

10 (a) C. G. Wu and T. Bein, *Science*, **1994**, *266*, 1013; (b) S. H. Joo, S. J. Choi, I. Oh, J. Kwak, Z. Liu, O. Terasaki and R. Ryoo, *Nature*, **2001**, *412*, 169; (c) S. Tanaka, N. Nishiyama, Y. Egashira and K. Ueyama, *Chem. Commun.*, **2005**, 2125.

11 (a) S. A. Johnson, E. S. Brigham, P. J. Ollivier and T. E. Mallouk, *Chem. Mater.*, **1997**, *9*, 2448; (b) K. Matsuoka, Y. Yamagishi, T. Yamazaki, N. Setoyama, A. Tomita and T. Kyotani, *Carbon*, **2005**, *43*, 855; (c) P.-X. Hou, T. Yamazakia, H. Orikasa and T. Kyotani, *Carbon*, **2005**, *43*, 2624; (d) Z. Yang, Y. Xia and R. Mokaya, *J. Am. Chem. Soc*., **2007**, *129*, 1673.

12 (a) T. Horikawa, J. Hayashi and K. Muroyama, *Carbon*, **2004**, *42*, 1625; (b) K. Lozano, S.-Y. Yang and R. E. Jones, *Carbon*, **2004**, *42*, 2329; (c) H. Chang, S. H. Joo and C. Park, *J. Mater. Chem.*, **2007**, *17*, 3078.

13 (a) M. Eddaoudi, J. Kim, N. Rosi, D. Vodak, J. Wachter, M. O'Keeffe and O. M. Yaghi, *Science*, **2002**, *295*, 469; (b) J.-P. Zhang, X.-C. Huang and X.-M. Chen, *Chem. Soc. Rev.*, **2009**, *38*, 2385; (c) G. Férey and C. Serre, *Chem. Soc. Rev*., **2009**, *38*, 1380; (d) J. Lee, O. K. Farha, J. Roberts, K. A. Scheidt, S. T. Nguyen and J. T. Hupp, *Chem. Soc. Rev*., **2009**, *38*, 1450; (e) B.-L. Chen, S. Xiang and G. Qian, *Acc. Chem. Res.,* **2010**, *43*, 1115.

14 (a) S. Ma and H.-C. Zhou, *J. Am. Chem. Soc*., **2006**, 128, 11734; (b) S. K. Ghosh, S. Bureekaew and S. Kitagawa, *Angew. Chem., Int. Ed.*, **2008**, 47, 3403; (c) X. L. Yang, M.-H. Xie, C. Zou, Y. He, B.-L. Chen, M. O'Keeffe and C.-D. Wu, *J. Am. Chem. Soc*., **2012**, *134*, 10638.

15 (a) J. S. Seo, D. Whang, H. Lee, S. I. Jun, J. Oh, Y. J. Jeon and K. Kim, *Nature*, **2000**, *404*, 982; (b) S. Motoyama, R. Makiura, O. Sakata and H. Kitagawa, *J. Am. Chem. Soc.*, **2011**, *133*, 5640; (c) M. M. Wanderley, C. Wang, C.-D. Wu and W. Lin, *J. Am. Chem. Soc*., **2012**, *134*, 9050.

16 (a) B. Liu, H. Shioyama, T. Akita and Q. Xu, *J. Am. Chem. Soc.*, **2008**, *130*, 5390; (b) H.-L. Jiang and Q. Xu, *Chem. Commun.*, **2011**, *47*, 3351; (c) S.-L. Li and Q. Xu, *Energy Environ. Sci.*, **2013**, *6*, 1656; (d) J.-K. Sun and Q. Xu, *Energy Environ. Sci.,* **2014**, *7*, 2071.

17 (a) F. Afsahi, H. V.-Thang, S. Mikhailenko and S. Kaliaguine, *J. Power Sources*, **2013**, *239*, 415; (b) J. Liu, H. Wang, C. Wu, Q.-L. Zhao, X.-Y. Wang and L.-H. Yi, *Int. J. Hydrogen Energ.*, **2014**, *39*, 6729.

18 (a) P. Pachfule, B. P. Biswal and R. Banerjee, *Chem.–Eur. J.*, **2012**, *18*, 11399; (b) S. Lim, K. Suh, Y. Kim, M. Yoon, H. Park, D. N. Dybtsev and K. Kim, *Chem. Commun*., **2012**, *48*, 7447; (c) S. J. Yang and C. R. Park, *Adv. Mater.*, **2012**, *24*, 4010.

19 (a) H.-L. Jiang, B. Liu, Y.-Q. Lan, K. Kuratani, T. Akita, H. Shioyama, F. Zong and Q. Xu, *J. Am. Chem. Soc.*, **2011**, *133*, 11854; (b) W. Chaikittisilp, M. Hu, H. Wang, H.-S. Huang, T. Fujita, K. C.-W. Wu, L.-C. Chen, Y. Yamauchi and K. Ariga, *Chem. Commun.*, **2012**, *48*, 7259; (c) A. Almasoudi and R. Mokaya, *J. Mater. Chem.*, **2012**, *22*, 146; (d) J.-K. Sun and Q. Xu, *Chem. Commun*., **2014**, *50*, 13502.

20 Q.-L. Zhu, N. Tsumoria and Q. Xu, *Chem. Sci.*, **2014**, *5*, 195.

21 K. S. Park, Z. Ni, A. P. Côté, J. Y. Choi, R. Huang, F. J. Uribe-Romo, H. K. Chae, M. O'Keeffe and O. M. Yaghi, *Proc. Natl. Acad. Sci*. U. S. A., **2006**, *103*, 10186.

22 (a) X. Xu, Y. Li, Y.-T. Gong, P.-F. Zhang, H.-R. Li and Y. Wang, *J. Am. Chem. Soc.*, **2012**, *134*, 16987; (b) P. Zhang, Y. Gong, H. Li, Z. Chen and Y. Wang, *Nat. Commun.*, **2013**, *4*, 1593; (c) P. Chen, L. M. Chew, A. Kostka, M. Muhler and W. Xia, *Catal. Sci. Technol.*, **2013**, *3*, 1964; (d) P.-B. Gai, H.-J. Zhang, Y.-S. Zhang, W. Liu, G.-B. Zhu, X.-H. Zhang and J.-H. Chen, *J. Mater. Chem. B*, **2013**, *1*, 2742.

23 A. J. Amali, J.-K. Sun and Q. Xu, *Chem. Commun.*, **2014**, *50*, 1519.

24 (a) M. Uchida, Y. Aoyama, M. Tanabe, N. Yanagihara, N. Eda and A. Ohta, *J. Electrochem. Soc.,* **1995**, *142*, 2572; (b) K. Wikander, H. Ekström, A. E. C. Palmqvist, A. Lundblad, K. Holmberg and G. lindbergh, *Fuel Cells,* **2006**, *6*, 21; (c) E. Antolini,

Appl. Catal. B Environ., **2009**, *88*, 1.

25 (a) C. Xu , Y.-L. Liu and D.-S. Yuan, *Int. J. Electrochem. Sci.,* **2007**, *2*, 674; (b) S. S. Mahapatra and J. Datta*, Int. J. Electrochem.,* **2011**, *2011*, 1; (c) Y.-T. Zhang, H.-H. Shu, G. Chang, K. Ji, M. Oyama, X. Liu and Y.-B. He, *Electrochimica Acta*, **2013**, *109*, 570; (d) F.-C. Zhu, G.-S. Ma, Z.-C. Bai, R. Q. Hang, B. Tang, Z.-H. Zhang and X.-G.Wang, *J. Power Sources*, **2013**, *242*, 610; (e) L.-M. Yang, Y.-H. Tang, S.-L. Luo, C.-B. Liu, H.-J. Song and D.-F. Yan, *ChemSusChem,* **2014**, *7*, 2907.

26 (a) T.-W. Kim, I.-S. Park and R. Ryoo, *Angew. Chem., Int. Ed*., **2003**, *42*, 4375; (b) C. H. Kim, D.-K. Lee and T. J. Pinnavaia, *Langmuir*, **2004**, *20*, 5157; (c) D.-S. Yuan, S.-Z. Tan, Y.-L. Liu, J.-H. Zeng, F.-P. Hu, X. Wang and P.-K. Shen, *Carbon*, **2008**, 46, 531.

Chapter 5

Conclusion

Research on metal-organic frameworks (MOFs) is a rapidly developing field. The purpose of the research work presented in this dissertation is exploring the applications of MOF materials based on their high porosity, large surface area and chemical tunability. Especially, MOF was used as a host matrice for immobilizing metal nanoparticals (MNPs) and the fabricated MNP@MOF composites were used as catalysts for catalytic hydrogen generation from ammonia borane (AB). In addition, MOF was used as template/precursor for nanoporous carbon material synthesis and the MOF-derived carbons were employed as supports of Pd electrocatalyst for methanol electrooxidation for the first time. The main research results of this dissertation are summarized as follows.

(i) Highly active AuCo alloy nanoparticles encapsulated in the pores of metal-organic frameworks for hydrolytic dehydrogenation of ammonia borane

Ultrafine AuCo alloy nanoparticles were successfully encapsulated in the pores of MIL-101 without aggregation on the external surfaces of the host framework by using the double solvents method combined with the overwhelming reduction approach, as demonstrated by transmission electron microscopic (TEM) and high-angle annular dark-field scanning TEM (HAADF-STEM) analyses. The ultrafine AuCo alloy NPs inside the mesoporous MIL-101 exhibit much higher catalytic activity for hydrolytic dehydrogenation of AB in comparison with their monometallic Au and Co counterparts. To the best of our knowledge, this obtained activity is the highest for supported Co and Co-based catalysts ever reported for hydrolytic dehydrogenation of aqueous AB.

(ii) Non-noble bimetallic CuCo nanoparticles encapsulated in the pores of metal-organic frameworks: synergetic catalysis in the hydrolysis of ammonia borane for hydrogen generation

Non-noble bimetallic CuCo alloy nanoparticles were successfully encapsulated in the pores of MIL-101 by using the double solvents method combined with the overwhelming reduction approach, which display remarkably enhanced catalytic activity

for hydrolytic dehydrogenation of AB to generate a stoichiometric amount of hydrogen at room temperature for chemical hydrogen storage, which presents the first example of MOF-supported non-noble bimetallic catalysts for the hydrogen generation from hydrolysis of AB. The synergetic effect between copper and cobalt species plays an important role for the improved performance in the catalytic hydrolysis of AB.

(iii) Pd nanoparticles supported on hierarchically porous carbon derived from assembled nanoparticles of zeolitic imidazolate framework (ZIF-8) for methanol electrooxidation

We, for the first time, use the hierarchically porous carbons with both micro- and mesopores obtained from direct carbonization of assembled nanoparticles of ZIF-8 [$Zn(MeIM)_2$; MeIM = 2-methylimidazole] as support for Pd electrocatalysts for methanol electrooxidation in alkaline media. At the carbonization temperature of 1000 °C, the highest surface area (1105 m^2 g^{-1}) and the largest pore volume (0.95 cm^3 g^{-1}) of ZIF-8-derived carbon (ZC) are achieved. The Pd/ZC-1000 catalyst is the most active and electrochemically stable among the Pd catalysts supported on ZCs prepared at 800-1100 °C. Moreover, the catalytic activity of Pd/ZC-1000 is 5 times higher than that of Pd supported on the commercial carbon black Vulcan XC-72R at the same Pd loading. The ZC-1000 with unique physical properties and high electrochemical performance will be a promising catalyst support for the application of direct methanol fuel cell.

In summary, this dissertation focuses on the fabrication of a series of MOF-based materials, that is, the composites of metal nanoparticles with MOFs and MOF-derived carbons, and their applications as heterogeneous catalysts for hydrolytic dehydrogenation of ammonia borane and methanol electrooxidation.

List of Publications

Journal Publications

1. “Highly active AuCo alloy nanoparticles encapsulated in the pores of metal-organic frameworks for hydrolytic dehydrogenation of ammonia borane”.

Jun Li, Qi-Long Zhu and Qiang Xu*

Chemical Communications, **2014**, *50*, 5899-5901.

2. “Non-noble bimetallic CuCo nanoparticles encapsulated in the pores of metal-organic frameworks: synergetic catalysis in the hydrolysis of ammonia borane for hydrogen generation”.

Jun Li, Qi-Long Zhu and Qiang Xu*

Catalysis Science & Technology, **2015**, *5*, 525-530.

3. “Pd nanoparticles supported on hierarchically porous carbon derived from assembled nanoparticles of zeolitic imidazolate framework (ZIF-8) for methanol electrooxidation”.

Jun Li, Qi-Long Zhu and Qiang Xu*

Submitted

Conference Presentations

1. “Highly active AuCo alloy nanoparticles immobilized inside the pores of metal-organic framework for hydrolytic dehydrogenation of ammonia borane”.

Jun Li and Qiang Xu*

The 63rd Japan Society of Coordination Chemistry (JSCC) Symposium, Oral presentation, No. 2If-05, Okinawa, Japan, November 2-4, **2013**.

2. “Highly-dispersed AuNi alloy nanoparticles encapsulated in MIL-101 as high-performance catalyst for hydrolytic dehydrogenation of ammonia borane”.

Jun Li, Qi-Long Zhu and Qiang Xu*

The 94th Chemical Society of Japan (CSJ) Annual Meeting, Poster, No. 2PB-142, Nagoya, Japan, March 27-30, **2014**.

3. “Highly active AuCo alloy nanoparticles immobilized inside the pores of metal-organic framework for hydrolytic dehydrogenation of ammonia borane”.

Jun Li and Qiang Xu*

4th International Conference on Metal-Organic Frameworks & Open Framework Compounds, Poster, No. P1-128, Kobe, Japan, September 28-October 1, **2014**.

Doctoral Dissertation, Kobe University
“Application of Functional Metal-Organic Frameworks to Catalysis”, 88 pages
Submitted on January, 23, 2015
The date of publication is printed in cover of repository version published in Kobe University Repository Kernel.